Elsevier Editorial System(tm) for Journal of Structural Geology
Manuscript Draft

Manuscript Number: SG-D-17-00002R1

Title: Assessing interaction of extensional active faults from structural and paleoseismological analysis: the Teruel and Concud faults (eastern Spain)

Article Type: Full Length Article

Keywords: fault linkage, fault relay, intraplate extension, paleoseismicity, seismic hazard, Teruel Basin

Corresponding Author: Dr. Jose Luis Simon,

Corresponding Author's Institution: Universidad de Zaragoza

First Author: Jose Luis Simon

Order of Authors: Jose Luis Simon; Luis E Arlegui, Lecturer; Lope Ezquerro, Researcher; Paloma Lafuente, Researcher; Carlos L Liesa, Lecturer; Aránzazu Luzón, Lecturer

Abstract: The relationship of independence, interaction or linkage between two neighbouring intraplate active extensional faults, the Teruel and Concud faults, are investigated from structural and paleoseismological data, and the results are discussed to improve seismic hazard assessment for the region. This paper provides the structural and paleoseismological characterization of the almost unknown Teruel Fault from detailed mapping and trench analysis, and discusses its kinematic and kinematic relationships with the Concud Fault. Four individual events occurred between 76.0 ka and 9.2 ka BP have been recorded at two branches of the Teruel Fault. Unfortunately, these only represent a small fraction of its overall activity during such time lapse, and their time constraints do not allow correlating them with those at the Concud Fault. The Teruel and Concud faults are independent structures from the geometric and kinematic point of view, as evinced by their distinct (i) transport directions (N275°E and N220°E, respectively), and (ii) average coseismic displacements (0.5 m and 1.9 m, respectively). These displacements are consistent with their respective lengths (9.0 km and 14.2 km) and significantly smaller than those expected for a hypothetically joint Concud-Teruel, 23 km-long fault. However, their displacement gradients close to the relay zone indicate that both faults undergo dynamic interaction, thus suggesting a transient stage from independence to linkage. We hypothesize that slip on both structures occurred, at the scale of the seismic cycle, in a broadly alternating maner, which induced strain partitioning between them and allowed accommodating bulk biaxial extension in the region. Such deformation pattern would have increased the earthquake frequency with respect to the scenario of a hypothetically linked Concud-Teruel Fault, but diminished the potential seismic magnitude.

COVER LETTER Paper SG-D-17-00002

Dear Editor:

Herewith, we send the revised version of our work entitled "Assessing interaction of active extensional faults from structural and paleoseismological analysis: the Teruel and Concud faults (eastern Spain)", according to suggestions made by the reviewers Drs. Nicol and Caputo.

Two versions of the manuscript are uploaded. One of them is a clean version with the changes already in place. The second one (marked version) details the changes done, with the following colour code:
- Yellow background: changes made according to referees' comments.
- Blue background: changes aimed to reduce the length of the manuscript, as required by the Editor. The main text has been shortened from 58,824 to 52,866 characters (10.1%), bibliography from 13,692 to 13339 (2.6%), and Appendix 1 from 6661 to 5649 (15.2%).

Most suggestions annotated on the manuscript by both reviewers have been considered. This has greatly improved the text; we are very grateful to them for their intense work with this respect.

Next we add some comments to a number of referees' suggestions. Some of them refer to proposals that we have not assumed; in such cases, we explain our reasons for keeping the original text. Line numbers in the first version of the manuscript have been used for reference.

Answers to comments by Reviewer 1 (A. Nicol):

- Lines 270-282. In our opinion, relay ramps are a geometrical result of fault relay arrangement, independently on the kinematics of each individual fault. Therefore, it does not involve kinematic interdependence between faults, and the opening sentence of this paragraph can be kept.

- Line 308. We substitute 'Overall' by 'Preliminary' in the title, but we cannot write just 'Paleoseismicity of the Concud Fault' because only preliminary paleoseismological assessing is included in this section.

- Lines 322-324. We prefer to keep this paragraph in its present location, as it deals with an aspect of the preliminary paleoseismological characterization, and it refers to numerical results also shown in Table 1.

- Lines 390-392: We cannot follow the suggestion by the reviewer because it would produce a longer and somehow ambiguous sentence (the ambiguity concerns the timing of the six mentioned units).

- Lines 498-499: O.K., we remove the argument of cross-cut relationships, which was not quite solid and was very laxly stated.

- Lines 546-554: It is true that our estimates of coseismic slip values are minimums, but all of them are significantly lower than that provided by Stirling's empirical correlation. We believe that the essential of the sentence should be kept, although minor changes to text style are accepted.

- Line 619: We believe that such transport direction is anomalous, but not 'inconsistent' with connection of the Las Ramblillas faults to the Teruel fault. Indeed, we describe a case in the Concud fault surface where a second striation oriented towards NW overprints the SW-oriented prevailing striation, therefore recording such an 'anomalous' movement on the main fault.

- Line 622: We prefer to write 'striation' as a singular name (an striation is a set of parallel striae or slickenlines), in order to avoid confusion when we refer to two or more sets of striae exhibiting distinct rakes on the fault surface. In this second case we talk about several 'striations' (plural).

Answers to comments by Reviewer 2 (R. Caputo):

- Lines 194-200: Rephrasing as suggested by the reviewer and removing the reference to *stress partitioning* change the sense of the sentence. We believe that such changes are not adequate, hence we prefer to keep the original text. Nevertheless, we find opportune referring here to a publication (suggested by R. Caputo for being included in Section 8.6, but useful as well for this one) that deals with a similar stress setting in the Italian Alps.

- Abstract and lines 206, 256-257, 303: the 'transport direction' (trend of the slip vector on a fault or shear zone, as usual in Structural Geology) is conceptually different from the 'stretching direction' (trend of the X axis of the strain ellipsoid). In our case, we deal with transport directions *s.s.* on faults and we should kept this term.

- Line 326 (and others throughout the manuscript): 'mid Pliocene' means 'approximately in the middle of the Pliocene'. We avoid 'Middle Pliocene' since this division does not officially exist.

- Lines 325-329: It is true that a very long-term average slip-rate as that calculated since 3.6 Ma B.P. is not the optimum in this case. Nevertheless, it is the only reliable rate available for the fault prior to the present research, therefore the only one that should be used for this 'preliminary characterization'.

- Line 422: In the same way as discussed for the transport direction on a fault, the 'movement plane' of a fold (plane orthogonal to the fold axis) is conceptually different from 'shortening direction'. We keep 'movement plane'.

- Lines 435-441: We agree with Dr. Caputo's comment about the computed number of paleoseismic events. We minimize the importance of event(s) previous to Pleistocene sediments in trenches Pitraque 1 and Pitraque 2; we explain that it (they) could actually represent a succession of several seismic episodes, either Pleistocene or even Pliocene in age; we denote it as ‘Event 0’ in Section 8.1; and we do not use it when the average recurrence period is estimated.

- Lines 451-453 (also 430-432): Concerning bending of units 4-5 in trench Pitraque 1, we have smoothed the inference of a relationship with fault Fδ, and we generically refer to ‘a hypothetical underlying, blind fault’.

- 483-484: We explain in more detail our interpretation of reactivation of a previous structure from analysis of splay faults liked to a fault tip.

Highlights:

Teruel and Concud faults: independent structures, but undergoing dynamic interaction

Four paleoseismic events recorded at the Teruel Fault since 70.7 to 9.9 ka BP

Hypothetical alternating slip on both faults would involve strain/stress partitioning

Higher earthquake frequency, but lower seismic magnitude than a full linked fault

• Assessing interaction of active extensional faults from structural and paleoseismological analysis: the Teruel and Concud faults (eastern Spain)

José L. Simón[1,2,*], Luis E. Arlegui[1,3], Lope Ezquerro[1,4], Paloma Lafuente[1,5], Carlos L. Liesa[1,6], Aránzazu Luzón[1,7]

[1] Dep. Ciencias de la Tierra, Universidad de Zaragoza, C/ Pedro Cerbuna 12, 50009 Zaragoza, Spain.
[2] jsimon@unizar.es
[3] arlegui@unizar.es
[4] lope@unizar.es
[5] palomalaf@gmail.com
[6] carluis@unizar.es
[7] aluzon@unizar.es
* Corresponding author: tel: +34 976 76 10 95; fax: +34 976 86 11 06.

Key words: fault linkage, fault relay, intraplate extension, paleoseismicity, seismic hazard, Teruel Basin.

Abstract

The relationship of independence, interaction or linkage between two neighbouring intraplate active extensional faults, the Teruel and Concud faults, are investigated from structural and paleoseismological data, and the results are discussed to improve seismic hazard assessment for the region. This paper provides the structural and paleoseismological characterization of the almost unknown Teruel Fault from detailed mapping and trench analysis, and discusses its kinematic and kinematic relationships with the Concud Fault. Four individual events occurred between 76.0 ka and 9.2 ka BP have been recorded at two branches of the Teruel Fault. Unfortunately, these only represent a small fraction of its overall activity during such time lapse, and their time constraints do not allow correlating them with those at the Concud Fault. The Teruel and Concud faults are independent structures from the geometric and kinematic point of view, as evinced by their distinct (i) transport directions (N275ºE and N220ºE, respectively), and (ii) average coseismic displacements (0.5 m and 1.9 m, respectively). These displacements are consistent with their respective lengths (9.0 km and 14.2 km) and significantly smaller than those expected for a hypothetically joint Concud-Teruel, 23 km-long fault. However, their displacement gradients close to the relay zone indicate that both faults undergo dynamic interaction, thus suggesting a transient stage from independence to linkage. We hypothesize that slip on both structures occurred, at the scale of the seismic cycle, in a broadly alternating maner, which induced strain partitioning between them and allowed accommodating bulk biaxial extension in the region. Such deformation pattern would have increased the earthquake frequency with respect to the scenario of a hypothetically linked Concud-Teruel Fault, but diminished the potential seismic magnitude.

1. Introduction

In the last few decades, great efforts have been made to improve our understanding of the geometric interaction and linkage of segments of extensional fractures and normal faults showing overlapping or en-échelon arrays (e.g., Gibbs 1984; Childs et al., 1995; Nicol et al., 1996; Ferrill et al., 1999; Peacock, 2002; Walsh et al., 2003; Fossen and Rotevatn, 2016). Recognition of linked en-échelon fault systems in the early stages of development is critical in seismic hazard assessment because seismic hazard analyses rely also on the ability to predict whether an earthquake will terminate at a fault tip or propagate onto adjacent faults (Ferrill et al., 1999; Wesnousky, 2008; Biasi and Wesnousky, 2016).

In moderately active intraplate areas, the historical seismic record is not long enough to include large earthquakes, owing to their large average recurrence intervals. Therefore, to reconstruct the true seismic history of faults, it is necessary to rely on paleoseismological studies (McCalpin, 1996; Caputo et al., 2008). Paleoseismology also provides additional information about fault kinematics: the pattern of incremental or ‘infinitesimal’ slip on individual faults, and hence the possibility of approaching the progressive bulk deformation of a tectonically active area.

This study assesses the state of geometric, kinematic and dynamic interaction of two neighbouring active faults, the Teruel and Concud faults, and discusses its influence on seismic hazard assessment for the region. These faults are located at the junction of the Teruel and Jiloca grabens (Fig. 1), which represent the largest Neogene-Quaternary extensional basins in the intraplate Iberian Chain (eastern Spain). The west-dipping Concud and Teruel faults strike NW-SE and N-S, respectively, and show a right-stepping arrangement with a 1.3 km-wide relay zone (Fig. 2a). The Concud Fault, the best documented active structure in the region, is expressed in the relief by a prominent scarp. It is located in the southern sector of the Jiloca Graben, and shows paleoseismological evidence of recurrent activity during Late Pleistocene (Lafuente, 2011; Lafuente et al., 2011a, 2014; Simón et al., 2012, 2016).

While the paleoseismological behaviour of the Concud Fault is reasonably established, the Teruel Fault remain almost unknown. Most of the Teruel Fault trace, somehow “invisible” through the local landscape, mainly crosses Neogene units, while Quaternary deposits along its trace are very scarce. Such differences between the Concud and Teruel faults are due to their distinct morpho-sedimentary setting during Pleistocene times. Sedimentary aggradation dominated at the hanging-wall block of the Concud Fault (alluvial fans making the piedmont of the Concud mountain front); on the contrary, downcutting of the drainage network (Alfambra and Turia rivers) in both the footwall and hanging-wall blocks of the Teruel Fault caused the lack of deposition. Therefore, the geological record of its Quaternary activity is expected to be much poorer than that of the Concud Fault.

Based on the proximity of the Teruel and Concud faults (Fig. 2a), Gutiérrez et al. (2012) have suggested that they make a single seismogenic structure (Concud-Teruel Fault), which would therefore involve the possibility of larger earthquakes than those generated by each separate structure. However, previous macro and mesostructural data indicate that they are independent structures from the geometric and kinematic point of view (Lafuente, 2011;

Lafuente et al., 2011b), therefore our hypothesis is that they are also seismically independent.

This paper presents the paleoseismological characterization of the Teruel Fault based on the results obtained in three trenches, together with a comprehensive structural study. The paleoseismic data will contribute both to evaluate seismic hazard and to discern the kinematic and kinematic relationships between the Concud and Teruel faults on short time scales. Our specific objectives are:

(1) Characterizing the structure and kinematics of the Teruel Fault, estimating its slip rates for different time intervals.

(2) Reconstructing the paleoseismological record of the Teruel Fault, and comparing it with that of the nearby Concud Fault. Additionally, analysing the representativeness of such paleoseismic record taking into account the morpho-sedimentary framework.

(3) Understanding the geometric, kinematic and dynamic interactions between the Concud and Teruel faults. In particular, examining their hypothetical structural linkage (and hence their potential joint activity as a single seismogenic structure) vs. hypothetical strain partitioning through independent, commonly alternating slip events on both of them.

(4) Discussing the implications for seismic hazard assessment.

2. Methodology

In order to evaluate Quaternary activity of the Teruel Fault, three explorative trenches were excavated across the fault. Ideal trench locations are those where recent sediments are affected by the fault, so that a geological record is present at least in the hanging-wall block enabling us to identify the sequence and timing of seismic events. Following a general survey of the fault, a study area (Pitraque-Valdelobos area; Fig. 2a) was selected in the central-southern sector, where the main fault splits into distinct branches. This area contains the only remnants of Quaternary sediments extending across the fault zone.

A detailed geological map of this area was made, based on field survey and orthoimage analysis, complemented with low-height aerial photographs taken from a drone. We also acquired topographic data: GPS coordinates (using a Garmin Oregon 450 device); height measurements for controlling the position of critical markers (Nikon hypsometer Forestry 550 pro); a laser-level (Leica Sprinter 100) profile along the Rambla de Valdelobos talweg across the Teruel fault zone, in order to check the hypothesis of a topographic drop.

Once selected the location of the trenches, we applied the classical methodology (e.g., McCalpin, 1996), which includes: excavating the trench; cleaning and gridding the selected walls; identifying, interpreting and marking sedimentary units and structures; taking a photograph and drawing a detailed log of each cell; analysing the relationship between units and faults to identify individual events; and collecting samples for absolute dating, especially those that pre- and post-date seismic events. Owing to clastic lithology of sediments, the dating method was that based on Optically Stimulated Luminescence (OSL); the samples were analysed in the Laboratorio de Datación y Radioquímica of Universidad Autónoma de Madrid (Spain).

3. Geological setting

The Neogene-Quaternary, NNW-SSE to NNE-SSW trending extensional basins of the eastern Iberian Chain (Fig. 1) cut in an oblique direction, and postdate the Alpine contractional structures (Vegas et al., 1979). The extensional faults represent the onshore deformation linked to rifting of the Valencia Trough, which is accommodated by a listric extensional fault system detached at a depth of 11-14 km (Roca and Guimerà, 1992).

The Teruel Basin, where the Teruel Fault is located, is a N-S to NNE-SSW trending half graben (Fig. 1). Its active, eastern boundary shows prominent mountain fronts separating the floor of the graben (usually at 800-1000 m a.s.l.) from El Pobo and Javalambre massifs (around 1700 and 2000 m, respectively). The graben is filled with Neogene alluvial deposits that grade basinwards into lacustrine carbonates and evaporites. Several units based on either lithostratigraphy (Weerd, 1976; Godoy et al., 1983) or changes in allocyclic factors (Alcalá et al., 2000; Ezquerro et al., 2014) have been defined, their ages being constrained by mammal ages and magnetostratigraphy (Alcalá et al., 2000). The informal units proposed by Godoy et al. (1983) are commonly used in maps of the Neogene Teruel Basin: Rojo 1 (red clastics; Vallesian); Páramo 1 (white carbonates, Turolian); Rojo 2 (red lutites, Upper Turolian-Ruscinian); Páramo 2 (white carbonates, Ruscinian); and Rojo 3 (red lutites, Ruscinian-Villafranchian).

During the Late Pliocene-Quaternary the graben infill was excavated by the Alfambra and Turia rivers and their tributaries. Four main fluvial terrace levels developed (Peña, 1981; Godoy et al., 1983), some of them locally splitting into several sublevels (Sánchez Fabre, 1989; Moissenet, 1993; Simón et al., 2016).) Table 1 compiles the available information on the height and age of these terrace levels.

During graben development, the tectonic stress field evolved from: (i) triaxial extension with minimum stress (σ_3) trajectories oriented WNW-ESE, prevailing during the first, Late Miocene rift episode, to (ii) almost radial extension (σ_1 vertical, $\sigma_2 \approx \sigma_3$) with nearly WSW-ENE trending σ_3, prevailing during the second, Pliocene to Quaternary rift episode (Simón, 1982, 1989; Capote et al., 2002; Arlegui et al., 2005). The latter has remained active up to the present-day (Herraiz et al., 2000), although both WSW-ENE and WNW-ESE σ_3 directions are recorded by fracture systems formed during the Pliocene and Quaternary. In summary, this regional 'multidirectional' extensional stress field has been partitioned (in the sense of Simón et al., 2008) into two stress systems, with S_{Hmax} (maximum horizontal stress axis) nearly parallel to trends of the Jiloca and Teruel grabens, respectively, and directly linked to the main tectonic stress sources during the Neogene-Quaternary in eastern Spain: the intraplate NNW-SSE compression produced by Africa-Iberia convergence, and the WNW-ESE extension induced by rifting at the Valencia trough (Simón, 1989; Herraiz et al., 2000; Capote et al., 2002; Arlegui et al., 2005). A similar 'time dissociation' of the overall stress field into distinct genetic stress systems (although in a compressional setting) has been described in the Italian Alps as *Twist Tectonics* by Caputo et al. (2010). Moreover, minor-order stress heterogeneities (deflection of stress trajectories, veering to become either parallel or perpendicular to major faults; swapping between σ_2 and σ_3 axes) are also frequent within this complex stress field (Simón, 1989; Arlegui et al., 2005, 2006).

The Concud Fault is a NW-SE trending, west-dipping fault, which shows an average transport direction N220ºE, has been active since the mid Pliocene, and totalizes a net slip of 255-300 m. Paleoseismological studies have been carried out on the Concud Fault based on analysis of five trenches (Lafuente, 2011; Lafuente et al., 2011a, 2014; Simón et al., 2016). The results indicate that the fault underwent eleven events since ca. 74 ka BP, with an average recurrence period of 7.1 to 8.0 ka (according to different hypotheses on the age of the youngest recorded event; Simón et al., 2016). Timing of paleoearthquakes on the fault has been constrained by a total of 37 OSL ages. The net accumulated slip during this time interval was 20.5 m, with average coseismic slip of 1.9 m. The displacement pattern shows alternating 'fast periods' (up to 0.53 mm/a) and 'slow periods' (0.13 mm/a), resulting in an average slip rate of 0.29 mm/a. A potential moment magnitude up to Mw = 6.8 has been estimated by Lafuente et al. (2011a) based on the empirical correlation proposed by Wells and Coppersmith (1994), Stirling et al. (2002) and Pavlides and Caputo (2004). Recent calculations made by Ezquerro et al. (2015) using the equation by Hanks and Kanamori (1979), considering (i) a hypothetical rupture of the total length (14.2 km) up to a 14 km-deep detachment level with an assumed dip angle of 60º, and (ii) the average coseismic slip inferred from paleoseismological studies, renders Mw = 6.6.

Historic and instrumental seismicity of the Teruel Graben and the surrounding region is low to moderate. There exists a moderate epicentre clustering along the Teruel Fault (see e.g. Simón et al., 2016, fig. 2). Measured magnitudes (Mb) usually range from 1.5 to 3.5, with maximum Mb = 4.4 in the Teruel Graben (data from Instituto Geográfico Nacional, 2010). Before the instrumental period, intensities up to VIII were recorded in the Teruel Basin, and IV-V in the Jiloca Graben. Focal depths typically range from 5 to 15 km, at the brittle layer above the basal detachment level identified by Roca and Guimerà (1992). Most of the available focal mechanisms correspond to normal faults, and are consistent with the regional recent stress field (Herraiz et al., 2000).

4. Structure and kinematics

4.1. The Teruel Fault

The Teruel Fault is a N-S striking, 9.0 km-long normal fault that offsets the Neogene infill of the Teruel basin (Fig. 2a). In detail, it shows a single, N170ºE trending trace in its northern sector, while southwards it branches into two main fault traces trending N-S and NNW-SSE, respectively. The latter, together with additional minor faults, progressively die out in the red lutites of Rojo 2 unit and the coeval Castralvo gypsum succession.

The hanging-wall block shows a rollover structure reflected by tilting of the Páramo 2 unit (Figs. 2b, 3a). This unit exhibits an average dip of 2ºE, its base decreasing in height from 1010 m a.s.l. at the highest point to less than 880 m a.s.l. west of Teruel city. In the footwall block, the base of the Páramo 2 unit lies at about 1130 m a.s.l., from which a cumulative throw of ca. 250 m can be estimated. This displacement has been partially accommodated by bending (perhaps, a monocline above a blind fault in a previous evolutionary stage), with dips up to 17º at the east of the Teruel city. The combination of rollover and monocline gives rise to a synformal sag parallel to the fault (Figs. 2b, 3a,b).

Field measurements of rupture surfaces within the Teruel Fault show average strike close to N-S and dip ranging from 60º to 80º W (average: 68º; Fig. 2c,d). Striations observed on the main fault surfaces indicate an almost-pure normal movement with average transport direction towards N275ºE.

Considering (i) the above calculated throw, (ii) the average fault dip, and (iii) a pure normal movement, a net slip of ca. 270 m can be inferred for the base of the Páramo 2 unit. Given an age of ~ 3.6 Ma (latest Ruscinian, Godoy et al., 1983; Opdyke et al., 1997; Alcalá et al., 2000) for this stratigraphic marker, the long-term slip rate is ca. 0.075 mm/a.

4.2. The relay zone between Teruel and Concud faults

Surface structural information, together with results of geophysical (magnetic, electromagnetic and georadar) surveys, suggest that the Teruel and Concud faults are geometrically and kinematically independent structures (Lafuente et al., 2011b). These faults do not show any evidence of a physical link: the northern tip of the Teruel Fault is located at a distance of 1.3 km from the Concud Fault (Fig. 2a), and both have distinct hanging-wall transport directions (N275ºE and N220ºE, respectively). They exhibit a right-stepping relay geometry, their displacement being transferred by means of a relay ramp dipping towards N or NNW, which can be clearly identified in Fig. 3a,b. Their displacement-length (D-L) profiles show high displacement gradients approaching the relay zone (Fig. 3c), indicating sharp slip transference between the faults. Further structural complexity at the relay zone occurs due to the presence of a transverse faulted syncline (Mansuetos-Valdecebro syncline; Fig. 2a, 3a,b).

Although the northern tip of the fault is apparently located to the north of Teruel city, there exist two sites aligned with the main trace where deformation structures affecting the fluvial terrace T2b are exposed. These could hypothetically reveal a prolongation of the Teruel Fault to the north, either at surface or as a blind fault (Figs. 2a, 3a). At Las Ramblillas site, T2b is offset by two synthetic faults decametre-scale throw, and separated into two tilted blocks where bedding dips up to 10º E and 18º E, respectively (Fig. 4). The western synthetic fault has an average orientation 157, 48 W and striations that pitch 70ºS. The measured fault plane is nearly parallel to that of the southern Concud Fault, as well as to the northern Teruel Fault (Fig. 2a). Cuesta de la Bajada site shows two main rupture surfaces striking NNW-SSE, with minimum offsets of 7 m and 2.5 m, and associated rollover monoclines that tilt T2b beds up to 28º E and 10º E, respectively (Peiro, 2016). If the described deformation features actually represent the northwards propagation of the Teruel Fault parallel to the adjacent Concud Fault after the Middle Pleistocene, its total length would be more than 11 km.

The only misfit concerns the kinematics of Las Ramblillas faults. The transport direction (N 218ºE, inferred from a single striation measure) closely approaches the average calculated for the Concud Fault (N220ºE; Lafuente et al., 2011a,b), and clearly differs from that recorded for the entire Teruel Fault (N275ºE; Fig. 2e). Nevertheless, the possibility of occasional slip of one of these faults following the typical transport direction of the other fault cannot be ruled out. Indeed, Lafuente et al. (2014) describe striations recording two distinct movements along transport directions SW and WNW superposed on a single rupture plane of the Concud fault zone. This issue will be examined later when discussing strain partitioning between these structures.

5. Preliminary paleoseismological characterization of the Teruel Fault

Several empirical relationships allow the expected maximum moment magnitude (M_w) of a fault and its associated coseismic displacement to be estimated. Those proposed by Wells and Coppersmith (1994), Stirling et al. (2002), Pavlides and Caputo (2004), and Mohammadioun and Serva (2001) have been applied in this study. Considering a length of 9.0 km for the Teruel Fault and applying the mentioned relationships, values of M_w ranging from 6.1 to 6.6 are obtained (Table 2). For the coseismic displacement. Wells and Coppersmith (1994) and Pavlides and Caputo (2004) correlations yield values of 0.40 m and 0.65 m, respectively, while that by Stirling et al. (2002) attains 1.32 m (Table 2). These estimates will be later compared with real offsets measured in trenches. As mentioned above, there exists the possibility of a prolongation of the Teruel Fault to the north, reaching a total length of at least 11 km. If this length was considered, the inferred M_w values and coseismic displacements would be a little higher (Table 2).

Combining the potential coseismic displacement based on empirical relationships (0.37 m to 1.28 m, considering a 9 km-length fault) with the long-term slip rate calculated since mid Pliocene times (0.075 mm/a; only reliable rate available for the fault prior to the present research), a recurrence interval between 4.9 ka and 17.1 ka is tentatively approached. If the fault were 11 km long, the recurrence periods would slightly increase (5.3-17.6 ka).

6. Detailed structure of the Pitraque-Valdelobos area

In the Pitraque-Valdelobos area the Teruel Fault cuts Quaternary deposits, so it has been selected for trenching study. Puntal del Pitraque is a conical hill located 1.2 km south of

Teruel city, in the area where the Teruel Fault splits southwards into several synthetic fault branches (M, N, P, Q, R, S in Fig. 5a; see location in Fig. 2a). A remnant of the lower sublevel of the Middle Terrace (T2a) occupies the top of the hill. A larger remnant of the same terrace appears on a horizontal platform some 100 m westwards. T2a unconformably overlies Neogene units (Rojo 2 and Páramo 2), and had previously provided an OSL age of 76.0 ± 5.0 ka (Simón et al., 2012). The Rambla de Valdelobos is a gully transverse to the Teruel Fault that drains westwards into the Turia River, and shows a relatively wide bottom filled with Holocene clastic sediments.

The main Teruel Fault branch (M) crops out north of Puntal del Pitraque site (Fig. 5b), where it has an average strike N033ºE and juxtaposes the Páramo 2 (hanging-wall block) and Rojo 2 (footwall block) units. The other macro-scale faults are also clustered around NNE-SSW (N024ºE in average) and show westwards dip ranging from 52º to 84º (68ºW in average) (Fig. 5c,d). Each individual fault offsets several metres to several tens of metres the Neogene beds. Together with the main fault and the monocline visible at the footwall block, the total displacement accommodated across this transect is estimated at 190 m (Figs. 2b, 3a).

The top of Middle Terrace (T2a) at Puntal del Pitraque lies 8.2 m higher than that at the western, horizontal platform (Fig. 5e). Such a height difference can be attributed to displacement on fault branches M and N. The corresponding net slip, assuming the average dip of the rupture surface (68º) and the inferred transport direction (N275ºE), is ca. 8.8 m. If the younger OSL age provided in the present work (46.5 ± 3.2 ka; Table 3) is assigned to the terrace top, a slip rate of 0.19 ± 0.01 mm/a is obtained. Since the displacement is only recorded at two (among five) synthetic branches within the fault zone, the total slip rate for the overall structure should exceed this value. The absence of Quaternary deposits displaced by the eastern branches of the fault makes impossible to test such hypothesis.

The primary target for our paleoseismological study was the M fault branch west of Puntal del Pitraque. Two paleoseismological trenches (Pitraque 1 and Pitraque 2) were excavated at this site, exposing Neogene lacustrine limestones and lutites unconformably overlain by the Pleistocene materials. Detailed inspection after trench digging showed that, within the M branch, the main observed fault surface (Fμ), locally striking N020ºE to N030ºE, is cut by a second fault (Fα) striking N050ºE, which is exposed in Pitraque 2 trench and apparently extends below Pitraque 1 (Fig. 6a). In addition, a third fault striking N019ºE is exposed in Pitraque 2 (Fβ) as well as at the natural terrace scarp. Fβ constitutes the prolongation of Fμ, but their physical linkage could not be observed in the field. The described structural relationships suggest local segmentation of the main NNE-SSW fault surfaces, these being articulated with (and their displacement being locally transferred to) NE-SW striking faults. Fracture patterns observed at a mesostructural scale, both in trenches and on natural outcrops (Fig. 6b,c,d,e), are consistent with the general structure of the Pitraque-Valdelobos area, although the range of strike values (from NNE-SSW to ENE-WSW) is wider than that expressed at macroscale (Fig. 5d).

7. Trench study at the Pitraque-Valdelobos area

7.1. Pitraque 1 trench

The Pitraque 1 trench was excavated for studying deformation associated to the main branch of the Teruel fault zone (M in Fig. 5a,c). This trench trends N148ºE, is 12.5 m long and 4.5 m deep; its western wall was selected for detailed logging and analysis (Fig. 7a). Neogene sedimentary units (Rojo 2 and Páramo 2) crop out in the lower part of the trench, overlain by Pleistocene coarse clastic, materials that have been subdivided into six units (1 to 6 in Fig. 7a; see description in Appendix 1).

The largest deformation structure exposed in this trench is a gentle bending fold that occupies most of the logged section shown in Fig. 7a. The geometry of the fold is continuous along both the Pliocene and Pleistocene beds (units 2 to 5), which suggests that folding essentially occurred after sedimentation of unit 5. The boundary between both lithological successions represents an erosional discontinuity, not an angular unconformity.

The Páramo 2 unit is also deformed by a number of normal, NE-SW striking faults (domain 4 in Fig. 7a) that make a rough conjugate system (Fig. 7e). The overlying Pleistocene units in the northwestern sector are affected by numerous fractures also with an average NE-SW strike (domain 2; Fig. 7a,c). These fractures include a few small faults with centimetre-scale offsets, small closed joints, and a large tensile crack filled with carbonate (C1 in Fig. 7a) that attains about 2 m in length and 20 cm in thickness. The fracture systems affecting domains 2 and 4 are disconnected from each other; indeed, the only Pleistocene fracture that could be rooted in a Neogene fault does not clearly show any physical linkage with it (see cell 10c in Fig. 7a). Domain 1 shows the same types of faults and fractures as in domain 2 (although in domain 1 these are mostly close to vertical; Fig. 7b), as well as a second large open crack filled with carbonate (C2 in Fig. 7a). Finally, domain 3 contains a number of small faults close to the Neogene-Pleistocene boundary. One of them (Fγ), oriented NE-SW, produces an offset of about 0.1 m and propagates within the lower part of Unit 2. The others are oriented NNW-SSE (Fig. 7d) and do not produce any visible displacement.

Most fractures in the lower structural domains (3 and 4) express the prevailing extensional fracture pattern in the region, represented by sets oriented NNW-SSE and NNE-SSW. In contrast, most fractures within domains 1 and 2 seem to be induced by local deformation conditions, i.e. the bending fold. This interpretation is based on two pieces of evidence: (i) most of the fractures are concentrated within the outer arc at the hinge zone (cells 9d and 10d in Fig. 7a); (ii) the movement plane of the bending fold, as defined by poles of bedding (Fig. 7f), is nearly orthogonal to NE-SW fractures of domains 1 and 2 (including cracks C1 and C2, which accommodate an important part of stretching affecting units 3, 4 and 5 in the outer arc). Although at present most of these fractures dip towards SE, they probably originated as nearly vertical fractures, as can be inferred by restoring bed tilting. The genetic dependence of these fractures with respect to local bending, as well as the rheological contrast between Pleistocene cemented clastic deposits and Neogene carbonates, could explain why the fracture systems affecting domains 2 and 4 appear to be independent from each other. Bending, and hence the associated tensional fractures, could be related to movement on an underlying blind fault.

Considering the structural relationships between faults and sedimentary units, as well as their OSL ages (Fig. 7a; Table 3), three paleoseimic events have been identified:

- Event(s) X_{P1}. Interpreted by the rupture and displacement (not quantified) of Neogene materials along fault Fα, and maybe other faults in domain 4, prior to local sedimentation of the Pleistocene terrace. More than one paleoearthquake could have resulted in such faulting, but they cannot be distinguished. This event (or events) occurred before 70.7 ± 5.3 ka BP (earliest OSL age obtained in the lower part of Unit 1). From the geologic record in the trench, it is not possible to estimate the associated displacement.

- Event Y_{P1}. Interpreted by the rupture along a small fault (Fγ), which produces a throw of 0.1 m at the base of the Pleistocene Unit 2. Predated by the upper part of Unit 1 (OSL age of 70.7 ± 5.3 ka BP) and postdated by overlying materials of Unit 2 (OSL age of 71.8 ± 5.1 ka BP).

- Event Z_{P1}. Represented by bending of Neogene (R2, P2) and Pleistocene (2, 3, 4, 5) units and development of associated tensional fractures, including opening of cracks (C1 and C2) subsequently filled with carbonate. This event is predated by the youngest available OSL age (48.5 ± 3.8 ka BP; middle-upper part of Unit 5), and postdated by the regolith (Unit 4, probably Holocene in age). Considering the amplitude of the bending fold, a mimimum coseismic throw of 1.0 m is estimated on a hypothetical underlying, blind fault (coseismic net slip >1.1 m for a 70º dipping plane).

7.2. Pitraque 2 trench

Pitraque 2 trench also exposes the main branch of the Teruel fault zone (M in Fig. 5a,c). It trends N133ºE, is 7.5 m long and 2.5 m deep, the southwest wall being selected for study (Fig. 8a). As in Pitraque 1 trench, Rojo 2 and Páramo 2 Pliocene units underlie Pleistocene conglomerates and sandstones, which have been subdivided into four units (1 to 4 in Fig. 8a); see description in Appendix 1).

Two main normal faults are exposed in Pitraque 2 trench. To the northwest, fault Fα (domain 2; Fig. 8a,d), locally striking N035ºE, offsets the Neogene units sinking its NW block and being responsible for erosion of Páramo 2 unit at the SE one; then Fα is overlain by non-affected Pleistocene deposits. To the southeast, Fβ (N019ºE) offsets Pleistocene units 1, 2 and 3, producing the same throw (0,5 m) on each of them, and splits upwards into several splay faults (domain 1, Fig. 8a,b,c). The association of splay faults to the main fault makes a *horse tail* structure (as defined by Granier, 1985), which is interpreted to be the product of local stretching close to the fault tip while fault Fβ was activated and propagated through the overlying Pleistocene deposits. This fracture system is also exposed on the opposite trench wall, with the same NNE-SSW to NE-SW strike and exhibiting pure-normal striations on the main fault Fβ (Fig. 8e). Finally, a tensile crack filled with carbonate (C3), similar to C1 and C2 of Pitraque 1 trench, overprints this system of splay faults. Although included within the main fault zone, C3 represents a kinematically distinct deformation pattern. Its opening vectors, with homogeneous length about 2-3 cm, are nearly orthogonal to the crack walls (Fig. 8a,b). Such a displacement pattern does not fit slip parallel to fault Fβ, and instead is consistent with tangential stretching at the outer arc of an accommodation monocline.

Three paleoseismic events have been interpreted (Fig. 8a; Table 3):

Event(s) X_{P2}. As in the case of Event $X_{P1,}$ deformation previous to deposition of the observed Pleistocene units is attributed to a first local event, although it may represent more than one paleoearthquake. Two inferred fault movements can be assigned to such a 'composite' X_{P2} event: (i) movement of Fβ that cut the Neogene Rojo 2 unit previously to deposition of Unit 1, therefore before 78.3 ± 5.2 ka BP; its associated *horse tail* structure (a fracture pattern typically found at extensional fault tips) involves activation of a blind, pre-existent fault through the overlying Pleistocene deposits; (ii) rupture and displacement of Rojo 2 and Páramo 2 units along fault Fα, as well as northwards tilting, previous to 50.0 ± 3.4 ka BP (age of the base of Unit 2, not affected). Since Fα is also exposed in Pitraque 1 trench, where it is postdated by OSL 70.7 ± 5.3 ka BP, we can assume this time constrain for it. These two fault movements cannot be chronologically distinguished and their associated displacements remain unknown.

Event Y_{P2}. Rupture and displacement of Pleistocene units 1, 2, and 3 along fault Fβ and its associated splay faults. Predated by the youngest OSL age available in the trench, at the base of Unit 3 (46.5 ± 3.1 ka). The associated coseismic slip along fault Fβ can be estimated at 0.5 m.

Event Z_{P2}. Represented by opening of tensile crack C3, which was subsequently filled with carbonate. As with the previous event, this one is predated by the youngest available OSL age (46.5 ± 3.1 ka), and postdated by the regolith (Unit 4, probably Holocene in age). We infer that the Z_{P2} event is distinct from the former event based on the kinematic differences between the tensile crack and the structures linked to Event Y_{P2}. The geometry of deformation does not permit measurement of coseismic slip.

7.3. Valdelobos trench

This N100ºE trending trench was excavated in the T0 terrace of Rambla de Valdelobos south of Puntal del Pitraque, where the gully apparently crosses the fault branch P (Fig. 5a), and its talweg exhibits a discrete gradient anomaly inferred from the laser-levelling profile (Fig. 5f). An exposure of around 5 m long and 2.5 m deep along the southern wall of the trench was studied in detail. The trench shows massive red Neogene lutites (Rojo 2) at its base, which are covered by Quaternary clastic deposits subdivided into five units (1 to 5 in Fig. 9; see description in Appendix 1).

The Neogene materials are displaced by a normal fault (Fε) striking N155ºE (Fig. 9). This fault also affects the lowermost Quaternary deposits (Units 1 and 2), and is covered by Unit 3. The minimum fault throw is 0.3 m, but it could be much larger since the fault scarp was eroded below the base of Unit 2. A single event has been interpreted in this case, referred to as **Event Z_{VL}**, occurred between 26.7 ± 1.9 ka BP (age of Unit 2) and 9.9 ± 0.7 ka BP (age of Unit 3).

8. Interpretation and discussion

8.1. Paleoseismic record of the Teruel Fault: correlation of events

Correlation of events between the Pitraque and Rambla de Valdelobos trenches (Table 4; Fig. 10) has been accomplished on the basis of geological judgement and OSL ages. It can be conventionally assumed that Event(s) X is common to both Pitraque 1 and Pitraque 2 trenches and inferred to be the same event (now renamed as Event 0): this event only affects Neogene materials, exhibiting upper time limits 70.7 ± 5.3 and 78.3 ± 5.2 ka BP, respectively, for each trench. We are aware that this event could actually represent a succession of several seismic episodes, either Pleistocene or even Pliocene in age. Considering the OSL ages that constrain their timing, Y_{P1} and Y_{P2} are interpreted as being two independent events: Event 1, with absolute time brackets 76.0 and 66.7 ka BP (central, most probable age: 70-71 ka BP), and Event 2, younger than 49.6 ka BP. Z_{P1} and Z_{P2} are interpreted as a single event (renamed Event 3, younger than 49.6 ka BP), taking into account their postdating OSL ages, the style of deformation (crack opening, subsequent carbonate filling) and the orientation of coseismic fractures (around NE-SW in both cases). Finally, Event Z_{VL}, only recorded at the Rambla de Valdelobos trench and therefore at a different fault branch, represents the youngest event (renamed Event 4, with absolute time brackets 28.6 and 9.2 ka BP).

In summary, the trench study has yielded one (or several) uncertain event prior to 73.1 ka BP, and four events occurred between 76.0-66.7 ka and 28.6-9.2 ka BP. This four-event-succession yields an average recurrence period in the range of 9.5-16.7 ka. Nevertheless, the individual interseismic periods remain unknown, as only the timing of events 1 and 4 are constrained (quite widely in the case of the second one).

8.2. Representativeness of the paleoseismic record of the Teruel Fault

Events 1, 2 and 3 occurred on the western, main branch (M) of the Teruel Fault, while

Event 4 occurred on a minor branch (P; see map in Fig. 5a). Events 1, 2 and 3 represent a minimum accumulated net slip of 1.7 m on branch M. The average coseismic slip for these three events (0.57 m) lies close to the estimates made from the empirical correlations of Wells and Coppersmith (1994) and Pavlides and Caputo (2004) (see section 5 and Table 2). This suggests that (i) these correlation models better describes our data than that of Stirling et al. (2002), and (ii) the recorded paleoseismic single event displacements approach the *characteristic earthquake* of the Teruel Fault (in the sense of Schwartz and Coppersmith, 1984). If Event 4 is incorporated, the results do not change substantially: minimum net slip on branches M+P (as recorded in trenches) will attain 2.0 m, with average coseismic slip of 0.50 m, and local slip rate of 0.04 ± 0.01 mm/a (Fig. 11d).

This paleoseismic succession only represents a fraction of the total activity on the western branches of the fault system during the sampled time interval. It should be reminded that the total offset of the fluvial terrace T2a represents a net slip of 8.8 m, with slip rate = 0.19 ± 0.01 mm/a for the last 46.5 ± 3.2 ka (Fig. 11d; see Section 6 and Table 5). Therefore, only a small part of the paleoseismic history of the Teruel Fault during the studied time window has been recorded in the studied trenches, and the calculated average recurrence period (9.5 to 16.7 ka) has little meaning. Assuming the average coseismic slip of 0.57 m and the accumulated net slip of 8.8 m, the total number of paleoseismic events on branches M+N since 76.0 ± 5.0 ka BP could attain fifteen, with a shorter average recurrence period of 5.1 ± 0.3 ka (close to the minimum estimated from empirical correlation, 4.9 ka).

8.3. Comparison with the paleoseismic record of the Concud Fault

The paleoseismic results for the Teruel Fault can be compared with those previously obtained on the neighbouring Concud Fault (Lafuente, 2011; Lafuente et al., 2011a, 2014; Simón et al., 2016) in order to analyse the seismogenic dependence or independence between them. At first glance, the recorded paleoseismic activity of the Teruel Fault seems significantly lower than that of the Concud Fault during a similar time period (76 ka vs. 74 ka BP; Fig. 10; Table 5): four events with average coseismic slip of ca. 0.6 m vs. eleven events with average coseismic slip of 1.9 m. Nevertheless, we should remind that the paleoseismic record obtained for the Teruel fault zone only includes the seismic events occurred on two fault branches (M and P). With this respect, it would be more realistic a comparison with the paleoseismic record obtained at a single fault branch in the the central sector of the Concud Fault (Fig. 11b,d; Table 5). Two trenches excavated across its southern branch (El Hocino site) provided a sequence of five events occurred since 74 ka BP, with an accumulated net displacement of 3.9 m, average coseismic slip close to 0.8 m, and slip rate of 0.05 mm/a (Fig. 11b) (Lafuente et al., 2014). These results are closer to those obtained for the Teruel Fault in the present work, which allows us to estimate that the likely degree of activity of both faults has been similar. Unfortunately, due to the poor time constraint on individual events interpreted for the Teruel Fault, comparing and correlating events recorded on the Teruel and Concud faults is impractical (Fig. 10).

8.4. Structural and seismotectonic relationships between the Teruel and Concud faults

As stated above, surface and shallow subsoil information does not support the hypothesis of full structural link between the Teruel and Concud faults (hard linkage in the sense of Walsh and Watterson, 1991). Moreover, their distinct transport directions (N275ºE vs. N220ºE) indicate that they behave as two independent structures from the kinematic point of view. Their separate displacement-length profiles at the relay zone (Fig. 3c) are also consistent with such independence, although the sharp gradients of these profiles close to the fault tips suggest some dynamic interaction between them.

Our paleoseismological study provides further evidence for autonomous activity on each fault. Time constraints of events in the Teruel Fault do not allow us to either confirm or disprove that some events ruptured both faults (Fig. 10). Nevertheless, coseismic displacements observed at the Teruel Fault helps us to suggest that the Teruel and Concud faults behave as two independent seismogenic sources instead of as a single seismogenic structure. Displacement values of the Teruel Fault (0.1 to 1.1 m; average = 0.5-0.57 m): (i) are consistent with those expected for a 9.0 km-long fault according to empirical correlation; (ii) are significantly smaller than those actually recorded on the 14.2 km-long Concud Fault (1.9 m, in average); and (iii) are less consistent with a hypothetically joint Concud-Teruel, 23 km-long fault (expected coseismic slip ranging from 0.7 m to 2.4 m, according to empirical correlation; see section 5 and Table 2). Moreover, the difference between their prevailing transport directions, previously noticed from overall kinematic data at both faults, has been confirmed from faults exposed in paleoseismological trenches (Fig. 11a,c).

Another different issue concerns the location of the true northern tip, and hence the true length of the Teruel Fault and its distance to the Concud Fault. Faults and associated tilted beds observed in Middle Pleistocene deposits at two sites (Cuesta de la Bajada and Las Ramblillas; see location in Fig. 2a) suggest a prolongation of the Teruel Fault some 2 km northwards from the mapped tip point located north of Teruel city. As in the case of the Concud Fault, no trace can be identified through the flood plain of the Alfambra River

(Holocene, T0 terrace), but the Teruel Fault could cut the underlying Neogene and Pleistocene units.

The transport direction inferred at Las Ramblillas (N218ºE) differs from that of the Teruel Fault (N275ºE) and is approximately parallel to that of the Concud Fault (N220ºE). This observation plays against the full connection of the Las Ramblillas structure to the Teruel Fault, and points to two alternative hypothesis: (i) the outcropping Las Ramblillas fault is a smaller, recent synthetic rupture kinematically associated with the Concud Fault, although it could play a role within an eventual linkage process with the Teruel Fault; (ii) the striation measured on the Las Ramblillas fault is not representative of its prevailing transport direction: in the same way that a second striation exists on the Concud Fault surface at El Hocino site, oriented towards NW and overprinting the SW-oriented prevailing striation (Fig. 11a; Lafuente et al., 2014), an 'anomalous' movement towards SW could have been recorded on the Teruel Fault.

In any case, the tentative propagation and linkage of the Teruel Fault with the Las Ramblillas structure would represent a recent, incipient process, as suggested by the pronounced bell-shape of its D-L profile. In this profile a high D-L gradient at the relay zone (around the abscise 14 km in Fig. 3c) is followed by a sharp reduction of the gradient near the northern tip (frictional breakdown zone; Cowie and Sholz, 1992; Cowie and Shipton, 1998).

8.5. Dynamic interaction and future linkage?

Although the Teruel and Concud faults remain two independent structures, future linkage is possible, as proposed by Ezquerro et al. (2012) and Lafuente et al. (2012). Linkage would be consistent with the mechanical state inferred for the relay zone. The steep gradients of their displacement-length (D-L) profiles in the relay zone indicate that both faults undergo dynamic interaction, according to theoretical models. The elastic strain fields of two adjacent faults interfere close to their tip lines, which tends to hinder propagation while displacement increases, resulting in anomalously high displacement gradients (Huggins et al., 1995; Nicol et al., 1996; Cartwright and Mansfield, 1998; Gupta y Scholz, 2000; Peacock, 2002).

According to this hypothesis, the relay zone between the Teruel and Concud faults is in a transient stage from independence to linkage. It cannot be anticipated how such full connection would happen. The coalescence of Las Ramblillas fault with both the Teruel and Concud faults could be the most probable one, the southernmost, NNW-SSE trending segment of the Concud Fault probably remaining as an inactive splay fault (Childs et al., 1995). Alternatively, transverse faults of the Mansuetos-Valdecebro structure could cut the relay ramp, resulting in hard linkage.

8.6. A scenario of strain and stress partitioning at the scale of the seismic cycle

Owing to their dynamic interaction, it is expected that displacement on one fault results in stress perturbation of the rock volume surrounding the other fault, and vice versa. At the scale of individual earthquakes, static Coulomb stress changes could trigger seismic events on segments of the other fault that were approaching critical conditions for rupture (Freed, 2005; King et al.,1994).

This suggests a scenario of slip on both structures taking place in a broadly alternating manner: stress release on one fault after a seismic event, and stress instability induced in the surrounding volume, will favour the next event to occur in the other fault (Fig. 12). Indeed, the average recurrence period may be similar for both structures during the Late Pleistocene times, with 7.1 ± 3.5 to 8.0 ± 3.3 ka on the Concud fault (Simón et al., 2016), and 10-15 ka on the Teruel Fault, as estimated from empirical correlation proposed by Villamor and Berryman (1999) using the average slip rate. This scenario involves local strain partitioning between the Teruel and Concud faults at the scale of the seismic cycle, representing a small incremental deformation episode within overall strain partitioning between NNW-SSE and NNE-SSW normal faults.

It is known that conjugate fault systems formed according to Mohr-Coulomb's failure criterium only accommodate plane strain (λ_2 = 1). In order to accommodate 3D finite strain, movement on multiple-set fault patterns (such as those typically made of four sets with orthorhombic symmetry) is necessary (Reches, 1978; Krantz, 1989; Nieto-Samaniego, 1999). Therefore, the biaxial extensional deformation that characterizes the recent tectonic setting of eastern Iberian Chain (Simón, 1982, 1989; Capote et al., 2002) could not be accommodated by a single fault set, or by a single conjugate normal fault system; progressive slip on diversely orientated fault planes and along diverse transport directions is needed.

However, this does not occur as a linear, steady process, but as a non-linear sequence of rupture episodes, during discontinuous deformation. The bulk 3D deformation is partitioned into a number of slip events on individual faults, which in their turn involve a sequence of episodic, systematic (not chaotic) stress changes that Simón et al. (2008) define as *stress partitioning*. Each failure event is compatible with stress-based models, while the finite 3-D strain fits kinematic boundary conditions.

The described process can occur at any spatial scale between e.g. tensile joints up to intraplate regions, and also at a wide range of time scales. In our study region, the long-term, Neogene-Quaternary tectonic evolution of eastern Iberia is characterized by both spatial transition and time shifting between regional stress systems with NNW-SSE and NNE-SSW S_{Hmax} trajectories, coexisting with local switching to orthogonal, either ENE-WSW or ESE-WNW trending ones (Simón, 1989; Cortés et al., 1996; Herraiz et al., 2000; Arlegui et al., 2005). At a much shorter time scale, it is known that earthquake focal mechanisms frequently reveal stress instabilities during aftershock sequences, some fault mechanisms being representative of the regional stress field while others represent second-order stresses including episodes of stress axis swapping (Mercier et al., 1989; Bowman et al., 2003; Caputo, 2005). Similar outcomes arise from laboratory experiments carried out by Reches and Dieterich (1983), which describe how fracture patterns made of four sets with orthorhombic symmetry (needed for accommodating 3D finite strain) developed through two yielding events with swapping of the two major stress axes between them.

Our hypothesis is that strain/stress partitioning also occurs at an intermediate time scale, i.e. the scale of seismic cycle (as postulated as well for the notion of *Twist Tectonics* by Caputo et al., 2010) giving rise to broadly alternating slip on the Teruel and Concud faults. Dynamic interaction between neighbouring faults (described in the previous section) provides the way for that process to come about. In this way, our scenario: (i) is consistent with the structural and dynamic relationships between faults, (ii) is consistent with the intrinsic stress changes in the complex regional stress field, and (iii) allows accommodation of bulk biaxial extension in the Teruel region.

8.7. Implications for seismic hazard assessment

The relationship interpreted for the Teruel and Concud faults has undeniable implications for seismic hazard assessment of the Teruel region. In general, an intermediate, transient stage (structural decoupling but dynamic interaction) implies a different seismic hazard level than that involved by the alternative, extreme options: (i) full independence, or (ii) linkage.

A hypothetically linked Concud-Teruel fault, with a total length of 23 km, would represent a seismogenic structure able to produce larger earthquakes than those generated by each separate structure. Their characteristic earthquake would show maximum moment magnitude Mw ≈ 6.6-7.0, while Mw ≈ 6.1-6.6 and Mw ≈ 6.6-6.8 for the single Teruel and Concud faults, respectively (Table 2). In the case of two independent seismic sources, with each having a similar recurrence period to that of the hypothetical linked structure, the probability of occurrence of such characteristic earthquakes in a given term would be significantly increased.

On the other hand, dynamic interaction between both faults involves shortening of the seismic cycle. Local stress perturbations induced by movement on one fault can trigger movement on the other one, which is found to be most evident within short distances (up to ≈ 5 km), although only for events that are relatively late in their respective earthquake cycle (Chen et al., 2010).

9. Conclusions

(1) Surface and shallow subsoil information indicates that the Teruel and Concud faults are not structurally linked. They also behave as kinematically independent structures, with distinct transport directions: N275ºE and N220ºE, respectively.

(2) The Pleistocene paleoseismic record of the Teruel Fault includes four events (Events 1, 2, 3, and 4) occurred between 76.0 and 9.2 ka BP (Table 4, Fig. 10). Since timing of individual events is poorly constrained, the duration of interseismic periods remains unknown. The recorded paleoseismic activity only represents a limited succession of slip events in two fault branches (therefore far from embodying the total activity of the Teruel fault zone).

(3) This paleoseismic record is significantly lower than that of the overall Concud Fault during a similar studied time lapse (76 ka BP vs. 74 ka), but comparable to that obtained in the southern branch of the Concud Fault at its central sector (Fig. 11). Hence we estimate that the overall degree of activity of both faults could be similar. The most representative slip rates obtained from morpho-sedimentary markers (see Table 5) are ≈ 0.075 mm/a for the last ~ 3.6 Ma on the overall Teruel fault zone, and 0.19 ± 0.01 mm/a for the last 46.5 ± 3.2 ka on two branches at Pitraque site. Strictly considering the events recorded at trenches, such slip rate is reduced to 0.04 ± 0.01 mm/a. These values are comparable to those previously obtained at the Concud Fault: 0.07-0.08 mm/a for the last ~ 3.6 Ma, and 0.29 mm/a since ~74 ka BP on the entire fault zone; 0.05 mm/a since ~74 ka BP on a single branch (Lafuente, 2011; Lafuente et al., 2011a, 2014; Simón et al., 2016).

(4) Owing to the poorly constrained timing of events identified at the Teruel Fault, comparing and correlating them with those on the Concud Fault is not feasible, neither discerning whether some rupture event have simultaneously occurred on both faults. Nevertheless, the observed coseismic displacements on the 9.0 km-long Teruel Fault (average = 0.5-0.57 m) are consistently smaller than those previously measured on the 14.2 km-long Concud Fault (average = 1.9 m), and unsuitable for a hypothetically joint Concud-Teruel, 23 km-long fault. We therefore interpret that the Teruel and Concud faults behave as two independent seismogenic sources.

(5) In spite of their geometric and kinematic independence, both structures undergo dynamic interaction (i.e. stress perturbation at the rock volume surrounding one fault subsequent to activation of the other one). This could have induced broadly alternating slip on both faults along their distinctive transport directions, which would involve a certain type of strain partitioning at the scale of the seismic cycle (Fig. 12): combining multiple slip events on both fault surfaces would allow accommodation of bulk 3D deformation in the Teruel region, within the framework of a biaxial extensional stress regime. The described scenario represents a transient stage from independence to linkage; future connection (probably through coalescence with an intermediate fault, Las Ramblillas fault) is a potential process.

(6) Structural relationships between the Teruel and Concud faults clearly influences seismic hazard. Two independent seismic sources will produce smaller, although more frequent earthquakes than those generated by a hypothetically linked Concud-Teruel fault. Dynamic interaction between both faults probably involves shortening of the seismic cycle, therefore increasing the probability of seism occurrence, but distributing the total released energy into smaller events.

Acknowledgements

The research has been financed by project CGL2012-35662 of Spanish Ministerio de Economía y Competitividad-FEDER, as well as by the Aragón regional government (E27, Geotransfer research group). L. Ezquerro benefited from a FPI grant (BES-2010-031339) of Spanish Ministerio de Economía y Competitividad. We thank Laboratorio de Datación y Radioquímica de la Universidad Autónoma de Madrid for OSL dating, and Gabinete Geológico de la Diputación Provincial de Teruel for technical assistence in trenching works. I. Casado, A. Peiro and G. Simón helped us in field surveys.

References

Alcalá, L., Alonso-Zarza, A.M., Álvarez, M.A., Azanza, B., Calvo, J.P., Cañaveras, J.C., van Dam, J.A., Garcés, M., Krijgsman, W., van der Meulen, A.J., Morales, J., Peláez, P., Pérez-González, A., Sánchez, S., Sancho, R., Sanz, E., 2000. El registro sedimentario y faunístico de las cuencas de Calatayud-Daroca y Teruel. Evolución paleoambiental y paleoclimática durante el Neógeno. Revista de la Sociedad Geológica de España 13, 323-343.

Arlegui, L.E., Simón, J.L., Lisle, R.J., Orife, T., 2005. Late Pliocene-Pleistocene stress field in the Teruel and Jiloca grabens (eastern Spain): contribution of a new method of stress inversion. Journal of Structural Geology 27, 693-705.

Arlegui, L.E., Simón, J.L., Lisle, R.J., Orife, T., 2006. Analysis of non-striated faults in a recent extensional setting: the Plio-Pleistocene Concud fault (Jiloca graben, eastern Spain). Journal of Structural Geology 28, 1019-1027.

Biasi, G.P, Wesnousky, S.G., 2016. Steps and Gaps in Ground Ruptures: Empirical Bounds on Rupture Propagation. Bulletin of the Seismological Society of America 106, 1110-1124.

Bowman, D., King, G., Tapponnier, P., 2003. Slip partitioning by elastoplastic propagation of oblique slip at depth. Science 300, 1121-1123.

Capote, R., Muñoz, J.A., Simón, J.L., Liesa, C.L., Arlegui, L.E., 2002. Alpine tectonics I: The Alpine system north of the Betic Cordillera. In: Gibbons, W., Moreno, T. (Eds), Geology of Spain. The Geological Society, London, 367-400.

Caputo, R., 2005. Stress variability and brittle tectonic structures. Earth Sciences Reviews 70, 103-127.

Caputo, R., Mucciarelli, M., Pavlides, S., 2008. Magnitude distribution of linear morphogenic earthquakes in the Mediterranean region: Insights from paleoseismological and historical data. Geophysical Journal International 174, 930-940.

Caputo, R., Poli, M.E., Zanferrari, A. 2010. Neogene-Quaternary tectonic stratigraphy of the eastern Southern Alps, NE Italy. Journal of Structural Geology 32, 1009-1027.

Cartwright, J.A., Mansfield, C.S., 1998. Lateral displacement variation and lateral tip geometry of normal faults in the Canyonlands National Park, Utah. Journal of Structural Geology 20, 3-19.

Chen, K.H., Bürgmann, R., Nadeau, R.M., 2010. Triggering Effect of M 4–5 Earthquakes on the Earthquake Cycle of Repeating Events at Parkfield, California. Bulletin of the Seismological Society of America 100, 522–531.

Childs, C., Watterson, J., Walsh, J.J., 1995. Fault overlap zones within developing normal fault systems. Journal of the Geological Society, London 152, 535-549.

Cortés, A.L., Liesa, C.L., Simón, J.L., Casas. A.M., Maestro, A., Arlegui, L.E., 1996. El campo de esfuerzos compresivo neógeno en el NE de la Península Ibérica. Geogaceta 20, 806-809.

Cowie, P.A., Scholz, C.H., 1992. Physical explanation for the displacement-length relationship of faults using a post-yield fracture mechanics model. Journal of Structural Geology 14, 1133-1148.

Cowie, P.A., Shipton, Z.K., 1998. Fault tip displacement gradients and process zone dimensions. Journal of Structural Geology 20, 983-997.

Ezquerro, L,. Lafuente, P., Pesquero, M.D., Alcalá, L., Arlegui, L.E., Liesa, C.L., Luque, L., Rodríguez-Pascua, M.A., Simón, J.L., 2012. Una cubeta endorreica residual del Pleistoceno inferior en la zona de relevo entre las fallas neógenas de Concud y Teruel, Cordillera Ibérica: implicaciones paleogeográficas. Revista de la Sociedad Geológica de España 25, 157-175.

Ezquerro, L., Luzón, A., Navarro, M., Liesa, C.L., Simón, J.L., 2014. Climatic vs. tectonic signal in the Neogene extensional Teruel basin (NE Spain), based on stable isotope (δ18O) and megasequential evolution. Terranova 26, 337-346.

Ezquerro, L., Moretti, M., Liesa, C.L, Luzón, A., Simón, J.L., 2015. Seismites from a well core of palustrine deposits as a tool for reconstructing the palaeoseismic record of a fault. Tectonophysics 655, 191–205.

Ferrill, A.D., Stamatakos, J.A., Sims, D., 1999. Normal fault corrugation: implications for growth and seismicity of active normal faults. Journal of Structural Geology 21, 1027-1038.

Fossen, H., Rotevatn, A., 2016. Fault linkage and relay structures in extensional settings–A review. Earth Science Reviews 154, 14-28.

Freed, A.M., 2005. Earthquake triggering by static, dynamic, and postseismic stress transfer. Annual Review of Earth and Planetary Sciences 33, 335–367.

Gibbs, A.D., 1984. Structural evolution of extensional basin margins. Journal of the Geological Society, London 141, 609–620.

Godoy, A., Ramírez, J.I., Olivé, A., Moissenet, E., Aznar, J.M., Aragonés, E., Aguilar, M.J., Ramírez del Pozo, J., Leal, M.C., Jerez-Mir, L., Adrover, R., Goy, A., Comas, M.J., Alberdi, M.T., Giner, J., Gutiérrez-Elorza, M., Portero, J.M., Gabaldón, V., 1983. Mapa Geológico Nacional 1:50.000, hoja 567 (Teruel). Instituto Geológico y Minero, Madrid.

Granier, T., 1985. Origin, damping, and pattern of development of faults in granite. Tectonics 4, 721-737.

Gupta, S., Scholz, C.H., 2000. A model of normal fault interaction based on observations and theory. Journal of Structural Geology 22, 865-880.

Gutiérrez, F., Gutiérrez, M., Gracia, F.J., McCalpin, J.P., Lucha, P., Guerrero, J., 2008. Plio-Quaternary extensional seismotectonics and drainage network development in the central sector of the Iberian Range (NE Spain). Geomorphology 102, 21-42.

Gutiérrez, F., Gracia, F.J., Gutiérrez, M., Lucha, P., Guerrero, J., Carbonel, D., Galve, J.P., 2012. A review on Quaternary tectonic and nontectonic faults in the central sector of the Iberian Chain, NE Spain. Journal of Iberian Geology 38, 145-160.

Hanks, T.C., Kanamori, H., 1979. A moment magnitude scale. Journal of Geophysical Research 84, 2348-2350.

Herraiz, M., De Vicente, G., Lindo-Ñaupari, R., Giner, J., Simón, J.L., González-Casado, J.M., Vadillo, O., Rodríguez-Pascua, M.A., Cicuéndez, J.I., Casas, A., Cabañas, L., Rincón, P., Cortés, A.L., Ramírez, M., Lucini, M., 2000. The recent (upper Miocene to Quaternary) and present tectonic stress distributions in the Iberian Peninsula. Tectonics 19, 762-786.

Huggins, P., Watterson, J., Walsh, J.J., Childs, C., 1995. Relay zone geometry and displacement transfer between normal faults recorded in coal-mine plans. Journal of Structural Geology 12, 1741-1755.

Instituto Geográfico Nacional, 2010. Servicio de Información Sísmica del Instituto Geográfico Nacional. http://www.ign.es/ign/es/IGN/SisCatalogo.jsp. Accessed December 2010.

King, G.C.P., Stein, R.S., Lin, J., 1994. Static stress changes and the triggering of earthquakes. Bulletin of the Seismological Society of America 84, 935–953.

Krantz R.W., 1989. Orthorhombic fault patterns: the odd axis model and slip vector orientations. Tectonics 8, 483-495.

Lafuente, P., 2011. Tectónica activa y paleosismicidad de la falla de Concud (Cordillera Ibérica central). Ph.D. thesis, Universidad de Zaragoza.

Lafuente, P., Rodríguez-Pascua, M.A., Simón, J.L., Arlegui, L.E., Liesa, C.L., 2008. Sismitas en depósitos pliocenos y pleistocenos de la fosa de Teruel. Revista de la Sociedad Geológica de España 21, 133-149.

Lafuente, P., Arlegui, L.E., Liesa, C.L., Simón, J.L., 2011a. Paleoseismological analysis of an intraplate extensional structure: the Concud fault (Iberian Chain, Spain). International Journal of Earth Sciences 100, 1713-1732.

Lafuente, P,. Arlegui, L.E.,, Casado, I., Ezquerro, L., Liesa, C.L., Pueyo, Ó., Simón, J.L., 2011b. Geometría y cinemática de la zona de relevo entre las fallas neógeno-cuaternarias de Concud y Teruel (Cordillera Ibérica). Revista de la Sociedad Geológica de España 24, 117-132.

Lafuente, P., Arlegui, L.E., Liesa, C.L., Pueyo, Ó., Simón, J.L., 2014. Spatial and temporal variation of paleoseismic activity at an intraplate, historically quiescent structure: the Concud fault (Iberian Chain, Spain). Tectonophysics 632, 167-187.

McCalpin, J.P., 1996. Paleoseismology. Academic Press, San Diego.

Mercier, J.L., Carey-Gailhardis, E., 1989. Regional state of stress and characteristic fault kinematics instabilities sown by aftershock sequences: the aftershock sequences of the 1978 Thessaloniki (Greece) and 1980 Campania-Lucania (Italia) earthquakes as examples. Earth and Planetary Science Letters 92, 247-264.

Mohammadioun, B., Serva, L., 2001. Stress drop, slip type, earthquake magnitude, and seismic hazard. Bulletin of the Seismological Society of America 91, 694-707.

Moissenet, E., 1993. L’age et les déformations des terrases alluviales du Fossé de Teruel. In: El Cuaternario de España y Portugal, Vol. I. Instituto Geológico y Minero de España-AEQUA, Madrid, 267-279

Nicol, A., Watterson, J., Walsh, J.J., Childs, C., 1996. The shapes, major axis orientations and displacement patterns of fault surfaces. Journal of Structural Geology 18, 235-248.

Nieto-Samaniego, A.F., 1999. Stress, strain and fault patterns. Journal of Structural Geology 21, 1065-1070.

Opdyke, N., Mein, P., Lindsay, E., Pérez-González, A., Moissenet, E., Norton, V.L., 1997. Continental deposits, magnetostratigraphy and vertebrate paleontology, late Neogene of Eastern Spain. Palaeogeography, Palaeoclimatology, Palaeoecology 133, 129-148.

Pavlides, S., Caputo, R., 2004. Magnitude versus faults´ surface parameters: quantitative relationships from the Aegean Region. Tectonophysics 380, 159-188.

Peacock, D.C.P., 2002. Propagation, interaction and linkage in normal fault systems. Earth-Science Reviews 58, 121-142.

Peiro, A. (2016). Una posible prolongación septentrional de la Falla de Teruel y su interacción con la Falla de Concud. Trabajo Fin de Grado, Universidad de Zaragoza.

Peña, J.L., 1981. Las acumulaciones cuaternarias de la confluencia de los ríos Alfambra y Guadalaviar, en las cercanías de Teruel. En: Actas VII Coloquio de Geografía, Pamplona, 255-259.

Reches, Z., 1978. Analysis of faulting in three-dimensional strain fields. Tectonophysics 47, 109-129.

Reches, Z., Dieterich, J.H., 1983. Faulting of rocks in three-dimensional strain fields. I. Failure of rocks in polyaxial, servo-control experiments. Tectonophysics 95, 111-132.

Roca, E., Guimerà, J., 1992. The Neogene structure of the eastern Iberian margin: structural constraints on the crustal evolution of the Valencia trough (western Mediterranean). Tectonophys 203, 203-218.

Sánchez Fabre, M., 1989. Estudio geomorfológico de la Depresión de Alfambra-Teruel-Landete y sus rebordes montañosos. Ph.D. thesis, Universidad de Zaragoza.

Simón, J.L., 1982. Compresión y distensión alpinas en la Cadena Ibérica Oriental. Ph.D. thesis, Universidad de Zaragoza.

Simón, J.L., 1983. Tectónica y neotectónica del sistema de fosas de Teruel. Teruel 69, 21-97.

Simón, J.L., 1989. Late Cenozoic stress field and fracturing in the Iberian Chain and Ebro Basin (Spain). Journal of Structural Geology 11, 285-294.

Simón, J.L., Arlegui, L.E., Liesa, C.L., 2008. Stress partitioning: a practical concept for analysing boundary conditions of brittle deformation. Geodinamica Acta 53, 1057-1065.

Simón, J.L., Arlegui, L.E., Lafuente, P., Liesa, C.L., 2012. Active extensional faults in the central-eastern Iberian Chain, Spain. Journal of Iberian Geology 38, 127-144.

Simón, J.L., Arlegui, L.E., Ezquerro, L., Lafuente, P., Liesa, C.L., Luzón, A., 2016. Enhaced paleoseismic succession at the Concud Fault (Iberian Chain, Spain): new insights for seismic hazard assessment. Natural Hazards 80, 1967-1993.

Stirling, M., Rhoades, D., Berryman, K., 2002. Comparison of Earthquake Scaling Relations Derived from Data of the Instrumental and Preinstrumental Era. Bulletin of the Seismological Society of America 92, 812-830.

Schwartz, D.P., Coppersmith, K.J., 1984. Fault behaviour and characteristic earthquakes: Examples form the Wasatch and San Andreas Faults, Journal of Geophysical Research 89, 5681-5698.

Vegas, R., Fontboté, J.M., Banda, E., 1979. Widespread Neogene rifting superimposed on alpine regions of the Iberian Peninsula. In: Proceedings Symposium Evolution and Tectonics of the Western Mediterranean and Surrounding Areas,Viena. Instituto Geográfico Nacional, Madrid, Special Publication 201, 109-128.

Villamor, P., Berryman, K.R., 1999. La tasa de desplazamiento de una falla como aproximación de primer orden en las estimaciones de peligrosidad sísmica. I Congreso Nacional de Ingeniería Sismica, Asociación Española de Ingeniería Sísmica, Abstracts, 1.

Walsh, J.J., Bailey, W.R., Childs, C., Nicol, A., Bonson, C.G., 2003. Formation of segmented normal faults: a 3-D perspective. Journal of Structural Geology 25, 1251–1262.

Walsh, J.J., Watterson, J., 1991. Geometric and kinematic coherence and scale effects in normal fault systems. In: Roberts, A.M., Yielding, G., Freeman, B. (Eds.), The Geometry of Normal Faults, Geological Society Special Publication No 56, 193-203.

Weerd, A. van de, 1976. Rodent faunas of the Mio-Pliocene continental sediments of the Teruel-Alfambra region, Spain. Utrecht Micropaleontology Bulletin, Special Publication 2, 1-185.

Wells, D.L., Coppersmith, K.J., 1994. New Empirical Relationships among Magnitude, Rupture Length, Rupture Width, Rupture Area, and Surface Displacement. Bulletin of the Seismological Society of America 84, 974-1002.

Wesnousky, S.G., 2008. Displacement and Geometrical Characteristics of Earthquake Surface Ruptures: Issues and Implications for Seismic-Hazard Analysis and the Process of Earthquake Rupture. Bulletin of the Seismological Society of America 98,1609-1632.

FIGURE CAPTIONS

Fig. 1. Location of the Teruel Fault within the Teruel Graben system, eastern Spain. Inset: sketch of the main Alpine chains within the Iberian Peninsula.

Fig. 2. Structure of the Teruel Fault. (a) Geological map. MVS: Mansuetos-Valdecebro syncline. (b) Cross section (see location in a). (c) Partial outcrop view of the main fault zone cutting the Rojo 2 unit within the Teruel urban area (see location in a). (d) Equal-area plot (lower hemisphere) showing orientations of measured planes and striations along the main fault. Black: data from central and southern sectors, showing an overall transport direction (red dot) towards N275ºE. Grey: Las Ramblillas fault.

Fig. 3. (a) Structural contour map of the base of Páramo 2 (youngest pre-rift unit relative to the Late Pliocene-Quaternary extensional period) at the relay zone between the Teruel and Concud faults. (b) 3D scheme of the relay structure reconstructed from the previous map. (c) Distribution of vertical displacement (throw) along fault length (D-L profiles) for the Concud and Teruel faults, obtained from the structural contour map. Modified from Lafuente et al. (2011b).

Fig. 4. Deformation at Las Ramblillas site, revealing hypothetic prolongation of the Teruel Fault. (a) Panoramic view. (b) Interpretation sketch. V: Villafranchian pediment; T2b: Middle Terrace of Alfambra River; T0: Holocene terrace; Qa: Quaternary alluvial pediment.

Fig. 5. Aspects of local geology of the Pitraque-Valdelobos area. (a) Detailed geological map (see location in Fig. 2a). (b) Outcrop view of the main Teruel Fault branch (M) north of Puntal del Pitraque (see location in Fig. 2a). (c) Overall field view. (d) Equal-area plot (lower hemisphere) of the main macroscale fault planes, and one observed striation. (e) Schematic cross section showing offset of the Middle Terrace T2a (see location on Fig. 5a). (f) Laser-levelling profile along the talweg of Valdelobos gully (sector shown in map a), showing the

location chosen for the Valdelobos trench. M, N, P, Q, R, S: fault branches referred to in the text; R1, R2, and P2: Rojo 1, Rojo 2, and Páramo 2 units, respectively; T2a: Middle Terrace of the Turia River; T0: Holocene terrace; QA: Holocene alluvium and colluvium.

Fig. 6. Meso-scale fracturing at the Pitraque 1 and Pitraque 2 site (equal-area plots, lower hemisphere). (a) Vertical, low height aerial photograph with structural sketch. (b) Fault planes and striations observed on the natural terrace scarp. (c) Idem in Pitraque 1 trench. (d) Idem in Pitraque 2 trench. (e) Synthetic rose diagram of fault strikes measured in the whole site. Fμ, Fδ, Fα, Fβ: faults referred to in the text; R2: Rojo 2 unit; P2: Páramo 2 unit; T2a: Middle Terrace of the Turia River.

Fig. 7. (a) Detailed cross section of Pitraque 1 trench. R2: Rojo 2 unit; P2: Páramo 2 unit; 1, 2, 3, 4, 5, 6: Pleistocene units described in the text; light-grey stripes: carbonate; Fγ, Fα, Fδ: faults referred to in the text; location (asterisks) and age of samples dated by OSL is indicated. (b) (c) (d) (e) Stereoplots (equal-area, lower hemisphere; symbols as in Fig. 6) of meso-scale fractures measured in domains 1, 2, 3 and 4, respectively. (f) Poles to bedding measured in all sedimentary units, and inferred movement plane (M).

Fig. 8. (a) Detailed cross section of trench Pitraque 2. R2: Rojo 2 unit; P2: Páramo 2 unit; 1, 2, 3, 4: Pleistocene units described in the text; light-grey stripes: carbonate; Fβ, Fα: faults referred to in the text; location (asterisks) and age of samples dated by OSL is indicated. (b) Detail photograph of domain 1 in (a). (c) (d) Stereoplots (equal-area, lower hemisphere; symbols as in Fig. 6) of meso-scale fractures measured in domains 1 and 2, respectively. (e) Idem in the opposite, not logged trench wall.

Fig. 9. Detailed cross section of Valdelobos trench. R2: Rojo 2 unit; 1, 2, 3, 4, 5: Quaternary units described in the text; Fε: active fault; location (asterisks) and age of samples dated by OSL is indicated.

Fig. 10. Chronological sketch of paleoseismic events recorded at the overall Concud Fault (complete paleoseismic succession reconstructed by Simón et al., 2016), its southern branch (El Hocino trenches; Lafuente et al., 2104), and the Teruel Fault (this work).

Fig. 11. Comparison between seismic succession reconstructed for the southern branch of the Concud Fault (Lafuente et al., 2014) and for the Teruel Fault (M and P branches, present work). (a) Kinematic data for the southern branch of the Concud Fault at El Hocino site: equal-area, lower hemisphere stereoplot of fault planes and striations, and prevailing transport direction. (b) Slip history of the southern branch of the Concud Fault, as inferred from the palaeosesimic succession at El Hocino trenches; slip rates inferred from that succession and from offset of a morpho-sedimentary marker (pediment cover) are expressed as dotted lines. (c) and (d): Idem as a and b, respectively, for the western branches of the Teruel Fault at Pitraque-Valdelobos site (offset marker in this case: top of fluvial terrace T2a).

Fig. 12. Proposed model of stress/strain partitioning at the scale of seismic cycle for the activity of the Teruel and Concud faults. (a) (b) (c) (d) Sketches of succesive, alternating slip on both faults favoured by stress release on each fault after a seismic event (see explanation in text); large arrows: transport directions; stereoplots: active fault (plane and prevailing striation) for each seismic event, and oriention of stress axes (σ_1, σ_2 and σ_3) of the most representative stress systems (according to palaeostress analysis by Lafuente, 2011). (e) Simplified model for the overall fracture systems in the Teruel area, and kinematic interpretation according to the model proposed by Reches (1978); X, Y, Z: virtual strain axes representing the bulk finite deformation.

TABLE 1:

Level	Age	Sublevel	Height above talweg (m)	Numerical age	Dating method	References
Upper	Early Pleistocene (?)	T3	85-90	Unknown		
Middel	Middle Pleistocene	T2b	45-65	250 (± 32) to 116 (± 4) ka	U/Th	Arlegui et al. (2005); Gutiérrez et al. (2008)
		T2a	40-45	90.5 (± 5.3) to 76.0 (± 5.0) ka	OSL	Lafuente et al. (2008); Simón et al. (2012)
Lower	Late Pleistocene	T1c	20-30	22.0 (± 1.6) ka	OSL	Lafuente (2011)
		T1b	15-20	14.9 (± 1.0) to 15.6 (± 1.3) ka	OSL	Lafuente et al. (2008); Gutiérrez et al. (2008)
		T1a	10-15	Unknown		
Subactual	Holocene	T0	3-5	3.4 (± 0.7) ka	OSL	Lafuente (2011)

Table 1. Levels of fluvial terraces defined in the Teruel area (Alfambra and Turia rivers).

TABLE 2:

Scenario Paleoseismic parameters		Wells & Coppersmith (1994)	Stirling *et al.* (2002)	Pavlides & Caputo (2004) (*) (**)	Mohammadioun & Serva (2001) (*) (***)	
Length of 9 km					100 bar	30 bar
Moment magnitude (M_w)		6.12	6.64	6.35	6.26	5.73
Coseismic slip (m)	Vertical	-	-	0.55	-	-
	Net	0.37	1.28	0.59	-	-
Length of 11 km						
Moment magnitude (M_w)		6.23	6.71	6.41	6.39	5.87
Coseismic slip (m)	Vertical	-	-	0.60	-	-
	Net	0.40	1.32	0.65	-	-
Length of 23 km (linked Concud and Teruel faults)						
Moment magnitude (M_w)		6.66	6.96	6.62	6.88	6.36
Coseismic slip (m)	Vertical	-	-	0.66	-	-
	Net	1.19	2.43	0.71	-	-

Table 2. Moment magnitude and coseismic slip for the Teruel Fault estimated from empirical relationships for three different scenarios. ([a]) Obtained M_s values have been transformed to M_w by applying the relationship of Konstantinou et al. (2005): $M_w = 0.76\ M_s + 1.53$. ([b]) Vertical displacement initially yielded by this correlation has been translated into net displacement considering an average dip of 68º and a pure normal movement of the Teruel Fault. ([c]) Moment magnitudes according to Mohammadioun and Serva (2001) have been calculated for stress drop scenarios of 100 and 30 bar.

TABLE 3:

Sample	Laboratory reference	Lithological unit	Equivalent dose (Gy)	Annual dose (mGy/yr)	Supralinearity (Gy)	K factor	OSL age (ka B.P.)
Trench: Pitraque 1							
P1-4	MAD-6076SDA	Fluvial terrace (Unit 1)	170.46	2.41	0	0.19	70.730 ± 5.259
P1-5	MAD-6077SDA	Fluvial terrace (Unit 2)	124.93	1.74	0	0.12	71.798 ± 5.059
P1-6	MAD-6078BIN	Fluvial terrace (Unit 5)	77.57	1.60	0	0.11	48.481 ± 3.801
Trench: Pitraque 2							
P2-1	MAD-6079SDA	Fluvial terrace (Unit 1)	130.05	1.66	0	0.14	78.343 ± 5.189
P2-7	MAD-6081BIN	Fluvial terrace (Unit 2)	91.95	1.84	0	0.11	49.972 ± 3.365
P2-5	MAD-6080SDA	Fluvial terrace (Unit 3)	127.80	2.75	0	0.14	46.472 ± 3.147
Trench: Valdelobos							
VL-C1	MAD-6073SDA	Fluvial terrace (Unit 2)	112.82	4.23	0	0.16	26.671 ± 1.912
VL-B2	MAD-6074SDA	Fluvial terrace (Unit 3)	16.97	1.71	0	0.23	9.923 ± 0.690

Table 3. OSL dating of samples collected from trenches at the Teruel fault.

TABLE 4:

Teruel Fault event (renamed)	Original event at individual trench	Predating OSL age (ka B.P.)	Postdating OSL age (ka B.P.)	Absolute age constraints (ka)	Coseismic net slip (m)
Event 0	X_{P1} X_{P2}		70.7 ± 5.3 78.3 ± 5.2	Pre-73.1	?
Event 1	Y_{P1}	70.7 ± 5.3	71.8 ± 5.1	76.0 – 66.7	0.1
Event 2	Y_{P2}	46.5 ± 3.1		Post-49.6	0.5
Event 3	Z_{P1} Z_{P2}	48.5 ± 3.8 46.5 ± 3.1		Post-49.6	> 1.1
Event 4	Z_{VL}	26.7 ± 1.9	9.9 ± 0.7	28.6 – 9.2	> 0.3

Table 4. Summary of paleoseismic events of the Teruel Fault interpreted and correlated from the studied trenches: Pitraque 1 (P1), Pitraque 2 (P2) and Valdelobos (VL). Absolute age constraints take into account the error bar for each OSL age.

TABLE 5:

Marker / data source	Age / time window	**Teruel Fault** (this work)			**Concud Fault (*)**		
		Net slip (m)	**Slip rate (mm/a)**		**Net slip (m) (**)**	**Slip rate (mm/a)**	
			Overall	**Partial** (In 1-2 branches among 4-5)		**Overall**	**Partial** (In 1 branches among 2-3)
Trenching information							
Compilation of coseismic slip values	since 76.0 to 9.9 ka BP	1.7 - 2.0		0.03 – 0.05			
	since ca. 74 to 3.4 ka BP				20.5 (3.9)	0.29	0.05
Stratigraphic marker							
T2b terrace top	46.5 ± 3.2 ka	8.8		0.18 – 0.20			
T2a terrace top	282 – 112 ka				39	0.14 – 0.35	
Páramo 2 unit (Latest Ruscinian)	3.6 Ma	270	0.075		255 – 290	0.07 – 0.08	

Table 5. Summary of slip rates calculated for the Teruel and Concud faults from different markers and for different time windows. (*) Data for the Concud Fault are compiled from Gutiérrez et al. (2008), Lafuente (2011), Lafuente et al. (2011a, 2014), and Simón et al. (2016). (**) In parentheses, partial net displacement measured on one fault branch.

APPENDIX 1:

Description and age of sedimentary units exposed in trenches

Pitraque 1 trench

Neogene sediments comprise: (i) pedogenized massive brown lutites (top of Rojo 2 unit); (ii) brecciated grey and white limestones interbedding black and green marls with remains of gastropods and charophytes, representing Páramo 2 carbonate unit. The Pleistocene succession has been subdivided into six units (1 to 6 in Fig. 7a):

Unit 1. Gravel with Neogene limestone angular-subrounded pebbles boulders and rip up clasts. It is grain-supported and crops out discontinuously below the erosive base of unit 2. Sample P1-4 (see location in Fig. 7a) yielded an OSL age of 70.7 ± 5.3 ka (Table 2).

Unit 2. Greyish and yellowish gravel with interbedded brown, fine- to coarse-grained sand. Gravel is grain-supported and made of angular-subangular carbonate and siliceous pebbles and cobbles up to 14 cm in diameter; it shows trough cross-bedding. Sand forms decimetre-scale, tabular levels with parallel and cross-lamination, and ripples. Sample P1-5 (see location in Fig. 7a) yielded an OSL age of 71.8 ± 5.1 ka (Table 2).

Unit 3. Grey gravel with encased brown medium-grained sand lenses with floating clasts up to 3 cm in diameter. Gravel is grain-supported and made of angular-subrounded limestone and siliceous pebbles and cobbles up to 24 cm in diameter; it shows pebble-granule cycles and trough cross-bedding.

Unit 4. Grey gravel with interbedded medium to coarse-grained brown sand. Gravel is grain-supported with subangular-subrounded limestone clasts up to 8 cm in diameter and trough cross-bedding. Sand makes laminated lensoid or tabular bodies.

Unit 5. Grey gravel with encased coarse-grained brown sand. Gravel is grain-supported, composed of angular-subangular clasts up to 6 cm in diameter. Horizontal bedding (pebble-granule cycles) merges laterally into trough cross-bedding sets. Sand makes tabular levels with parallel lamination and floating grey limestone clasts up to 1 cm in diameter. Sample P1-6 (see location in Fig. 7a) yielded an OSL age of 48.5 ± 3.8 ka (Table 2).

Unit 6. Regolith. Brown lutite with scattered centimetre-scale limestone clasts, carbonate nodules, and root traces.

Pitraque 2 trench

Neogene sediments are similar to those described in Pitraque 1 trench (Rojo 2 and Páramo 2 units). The overlying Pleistocene materials have been subdivided into four units (1 to 4 in Fig. 8a):

Unit 1. Grey and brown, grain-supported gravel with rare sand. Gravel is made of angular-subangular limestone and siliceous-pebbles and cobbles up to 18 cm in diameter; it shows planar cross-stratification and interbbedded sand levels in the lower part. Sample P2-1 (see location in Fig. 8a) has an OSL age of 78.3 ± 5.2 ka BP (Table 2).

Unit 2. Grey and brown gravel with intercalated brown very coarse-grained sand towards the top. Gravel, matrix-supported at the base and grain-supported topwards, consists of angular limestone and siliceous pebbles and cobbles up to 16 cm in diameter, and shows cross-bedding. Sand forms a slightly channelled body with angular, grey limestone floating clasts (up to 2 cm), and armoured clay balls (up to 16 cm). Sample P2-7 (Fig. 8a) yielded an OSL age of 50.0 ± 3.4 ka (Table 2).

Unit 3. Gravel with interbbeded centimetre-thick levels of fine- to coarse-grained sand. Gravel, mainly grain-supported, is made of angular limestone pebbles and cobbles. It forms a tabular body in the lower part and a channel in the upper part; the channel is composed by larger clasts (up to 15 cm) and shows planar cross-bedding. Sand makes irregular levels with horizontal and cross-lamination. Its base has an OSL age (sample P2-5) of 46.5 ± 3.1 ka (Table 2).

Unit 4. Regolith. Brown lutite with carbonate nodules, root traces and scattered centimetre-scale limestone clasts.

Valdelobos trench

Massive red Neogene lutites (Rojo 2) are covered by Quaternary alluvial deposits in which five units have been distinguished (1 to 5 in Fig. 9):

Unit 1. Massive brown lutite with grey patches, carbonate nodules and interbedded fine- to medium-grained sand with carbonate granules that grades laterally into brown silt.

Unit 2. Coarse-grained sand with white and grey carbonate and black quartzite granules in a coarsening upward channelled body close to a fault plane in the middle part of the trench. Sample VL-C1 (Fig. 9) yielded an OSL age of 26.7 ± 1.9 ka BP (Table 2).

Unit 3**.** Channeled highly erosive body with brown gravel in the lower part and medium-grained sand and lutites in the upper part. Gravel is made of subangular-subrounded white carbonate (up to 8 cm in diameter) and brown and red siliceous clasts (up to 3 cm); it shows horizontal bedding and imbricated clasts. Sand forms tabular levels with parallel lamination and low angle cross-stratification. Some mud boulders have been recognized, up to 88 cm exist. Sample VL-B2 (Fig. 9) yielded an OSL age of 9.9 ± 6.9 ka BP (Table 2).

Unit 4. Gravel (lower part) and coarse-grained sand (upper part) arranged in a dominantly red, tabular and fining-upwards erosive body with locally channelled base. Gravel, matrix-supported,- made of white, subangular-subrounded carbonate clasts, up to 15 cm in diameter. Sand shows parallel lamination, ripples, scattered clasts and rare mud boulders.

Unit 5. Greyish grain-supported gravel in a tabular body with erosive base and horizontal stratification made of fining upwards sequences. It is composed by subangular-subrounded white carbonate clasts (up to 7 cm in diameter), subrounded orange siliceous clasts (up to 4 cm), and rare mud boulders. It supplied two fragments of clay teals (historical times, post-Middle Age).

• Assessing interaction of active extensional faults from structural and paleoseismological analysis: the Teruel and Concud faults (eastern Spain)

José L. Simón[1,2,*], Luis E. Arlegui[1,3], Lope Ezquerro[1,4], Paloma Lafuente[1,5], Carlos L. Liesa[1,6], Aránzazu Luzón[1,7]

[1] Dep. Ciencias de la Tierra, Universidad de Zaragoza, C/ Pedro Cerbuna 12, 50009 Zaragoza, Spain.
[2] jsimon@unizar.es
[3] arlegui@unizar.es
[4] lope@unizar.es
[5] palomalaf@gmail.com
[6] carluis@unizar.es
[7] aluzon@unizar.es
* Corresponding author: tel: +34 976 76 10 95; fax: +34 976 86 11 06.

Key words: fault linkage, fault relay, intraplate extension, paleoseismicity, seismic hazard, Teruel Basin.

Abstract

The relationship of independence, interaction or linkage between two neighbouring intraplate active extensional faults, the Teruel and Concud faults, are investigated from structural and paleoseismological data, and the results are discussed to improve seismic hazard assessment for the region. This paper provides the structural and paleoseismological characterization of the almost unknown Teruel Fault from detailed mapping and trench analysis, and discusses its kinematic and kinematic relationships with the Concud Fault. Four individual events occurred between 76.0 ka and 9.2 ka BP have been recorded at two branches of the Teruel Fault. Unfortunately, these only represent a small fraction of its overall activity during such time lapse, and their time constraints do not allow correlating them with those at the Concud Fault. The Teruel and Concud faults are independent structures from the geometric and kinematic point of view, as evinced by their distinct (i) transport directions (N275ºE and N220ºE, respectively), and (ii) average coseismic displacements (0.5 m and 1.9 m, respectively). These displacements are consistent with their respective lengths (9.0 km and 14.2 km) and significantly smaller than those expected for a hypothetically joint Concud-Teruel, 23 km-long fault. However, their displacement gradients close to the relay zone indicate that both faults undergo dynamic interaction, thus suggesting a transient stage from independence to linkage. We hypothesize that slip on both structures occurred, at the scale of the seismic cycle, in a broadly alternating maner, which induced strain partitioning between them and allowed accommodating bulk biaxial extension in the region. Such deformation pattern would have increased the earthquake frequency with respect to the scenario of a hypothetically linked Concud-Teruel Fault, but diminished the potential seismic magnitude.

1. Introduction

In the last few decades, great efforts have been made to improve our understanding of the geometric interaction and linkage of segments of extensional fractures and normal faults showing overlapping or en-échelon arrays (e.g., Gibbs 1984~~, Faulds et al., 1990~~; Childs et al., 1995; Nicol et al., 1996; Ferrill et al., 1999; Peacock, 2002; Walsh et al., 2003; Fossen and Rotevatn, 2016). ~~Lateral propagation of curved fault-tips and linkage by connecting faults are two of the mechanisms by which increasing displacement eventually produces the progressive evolution from the phase of fault overlap and relay zone stage to a fully breached fault (Ferrill et al., 1999; Peacock, 2002; Fossen and Rotevatn, 2016).~~ Recognition of linked en-échelon fault systems in the early stages of development is critical in seismic hazard assessment because seismic hazard analyses rely also on the ability to predict whether an earthquake will terminate at a fault tip or propagate onto adjacent faults (Ferrill et al., 1999; Wesnousky, 2008; Manighetti et al., 2009; Frinzi and Langer, 2012; Biasi and Wesnousky, 2016).

In moderately active intraplate areas, the historical seismic record is not long enough to include large earthquakes, owing to their large average recurrence intervals. In order to overcome this lack of information Therefore, to reconstruct the true seismic history of faults, and therefore to achieve realistic seismic hazard assessment, it is necessary to rely on paleoseismological studies (McCalpin, 1996; Pavlides et al., 1999; Caputo et al., 2008; Simón et al., 2016). Paleoseismology also provides additional information about fault kinematics: the pattern of incremental or 'infinitesimal' slip on individual faults, and hence the possibility of approaching the progressive bulk deformation of a tectonically active area.

This study assesses the state of geometric, kinematic and dynamic interaction of two neighbouring active faults, the Teruel and Concud faults, and discusses its influence on seismic hazard assessment for the region. These faults are located at the junction of the Teruel and Jiloca grabens (Fig. 1), which represent the largest Neogene-Quaternary extensional basins in the intraplate Iberian Chain (eastern Spain). This is an intraplate region containing several active extensional faults, though it shows low instrumental and historical seismicity. The west-dipping Concud and Teruel faults strike NW-SE and N-S, respectively, and show a right-stepping arrangement with a 1.3 km-wide relay zone (Fig. 2a). The Concud Fault, the best documented active structure in the region, is expressed in the relief by a prominent scarp. It is located in the southern sector of the Jiloca Graben, and shows paleoseismological evidence of recurrent activity during Late Pleistocene (Lafuente, 2011; Lafuente et al., 2011a, 2014; Simón et al., 2012, 2016).

While the paleoseismological behaviour of the Concud Fault is reasonably established, the seismogenic character and paleoearthquake history of the Teruel Fault remain almost unknown. Most of the Teruel Fault trace, somehow "invisible" through the local landscape, mainly crosses Neogene units, while Quaternary deposits along its trace are very scarce. Such differences between the Concud and Teruel faults are due to their distinct morpho-sedimentary setting during Pleistocene times. Sedimentary aggradation dominated at the hanging-wall block of the Concud Fault (alluvial fans making the piedmont of the Concud mountain front); on the contrary, downcutting of the drainage network (Alfambra and Turia rivers) in both the footwall and hanging-wall blocks of the Teruel Fault caused the lack of deposition. Therefore, the geological record of its Quaternary activity is expected to be much poorer than that of the Concud Fault.

Based on the proximity of the Teruel and Concud faults (Fig. 2a), Gutiérrez et al. (2012) have suggested that they make a single seismogenic structure (Concud-Teruel Fault), which would therefore involve the possibility of larger earthquakes than those generated by each separate structure. However, previous macro and mesostructural data indicate that they are independent structures from the geometric and kinematic point of view (Lafuente, 2011; Lafuente et al., 2011b), therefore our hypothesis is that they are also seismically independent. ~~Discerning between both possibilities is a critical issue for assessing seismic hazard in the region.~~

This paper presents the paleoseismological characterization of the Teruel Fault based on the results obtained in three trenches, together with a comprehensive structural study. The paleoseismic data will contribute both to evaluate seismic hazard and to discern the kinematic and kinematic relationships between the Concud and Teruel faults on short ~~('infinitesimal' from a geological perspective)~~ time scales. Our specific objectives are:

(1) Characterizing the structure and kinematics of the Teruel Fault, estimating its slip rates for different time intervals.

(2) Reconstructing the paleoseismological record of the Teruel Fault, and comparing it with that of the nearby Concud Fault. Additionally, analysing the representativeness of such paleoseismic record taking into account the morpho-sedimentary framework.

(3) Understanding the geometric, kinematic and dynamic interactions between the Concud and Teruel faults. In particular, examining their hypothetical structural linkage (and hence their potential joint activity as a single seismogenic structure) vs. hypothetical strain partitioning through independent, commonly alternating slip events on both of them.

(4) Discussing the implications for seismic hazard assessment.

2. Methodology

In order to evaluate Quaternary activity of the Teruel Fault, three explorative trenches were excavated across the fault. Ideal trench locations are those where recent sediments are affected by the fault, so that a geological record is present at least in the hanging-wall block enabling us to identify the sequence and timing of seismic events. Following a general survey of the fault, a study area (Pitraque-Valdelobos area; Fig. 2a) was selected in the central-southern sector, where the main fault splits into distinct branches. This area contains the only remnants of Quaternary sediments extending across the fault zone.

A detailed geological map of this area was made, based on field survey and orthoimage analysis, complemented with low-height aerial photographs taken from a drone. We also acquired topographic data: GPS coordinates (using a Garmin Oregon 450 device); height measurements for controlling the position of critical markers (Nikon hypsometer Forestry 550 pro); a laser-level (Leica Sprinter 100) profile along the Rambla de Valdelobos talweg across the Teruel fault zone, in order to check the hypothesis of a topographic drop.

Once selected the location of the trenches, we applied the classical methodology (e.g., McCalpin, 1996), which includes: excavating the trench; cleaning and gridding the selected walls; identifying, interpreting and marking sedimentary units and structures; taking a photograph and drawing a detailed log of each cell; analysing the relationship between units and faults to identify individual events; and collecting samples for absolute dating, especially those that pre- and post-date seismic events. Owing to clastic lithology of sediments, the dating method was that based on Optically Stimulated Luminescence (OSL); the samples were analysed in the Laboratorio de Datación y Radioquímica of Universidad Autónoma de Madrid (Spain).

3. Geological setting

The Neogene-Quaternary, NNW-SSE to NNE-SSW trending extensional basins of the eastern Iberian Chain (Fig. 1) cut in an oblique direction, and postdate the Alpine contractional structures (Vegas et al., 1979). The extensional faults represent the onshore deformation linked to rifting of the Valencia Trough, which is accommodated by a listric extensional fault system detached at a depth of 11-14 km (Roca and Guimerà, 1992). ~~Extension developed through two distinct rift episodes (Simón, 1982, 1983): the first one (Miocene) gave rise to the main NNE-SSW trending grabens (Teruel and Maestrazgo), and the second one (Late Pliocene-Quaternary) originated the NNW-SSE trending Jiloca Graben and reactivated the Teruel and Maestrazgo grabens.~~

The Teruel Basin, where the Teruel Fault is located, is a N-S to NNE-SSW trending half graben (Fig. 1). Its active, eastern boundary shows prominent mountain fronts separating the floor of the graben (usually at 800-1000 m a.s.l.) from El Pobo and

Javalambre massifs (around 1700 and 2000 m, respectively). The graben is filled with Neogene alluvial deposits that grade basinwards into lacustrine carbonates and evaporites. Several units based on either lithostratigraphy (Weerd, 1976; Godoy et al., 1983) or changes in allocyclic factors (Alcalá et al., 2000; Ezquerro et al., 2014) have been defined, their ages being constrained by mammal ages and magnetostratigraphy (Alcalá et al., 2000). The informal units proposed by Godoy et al. (1983) are commonly used in maps of the Neogene Teruel Basin: Rojo 1 (red clastics; Vallesian); Páramo 1 (white carbonates, Turolian); Rojo 2 (red lutites, Upper Turolian-Ruscinian); Páramo 2 (white carbonates, Ruscinian); and Rojo 3 (red lutites, Ruscinian-Villafranchian).

During the Late Pliocene-Quaternary the graben infill was excavated by the Alfambra and Turia rivers and their tributaries. ~~Quaternary sediments are linked to the fluvial network, in the form of stepped fluvial terraces and alluvial pediments.~~ Four main fluvial terrace levels developed (Peña, 1981; Godoy et al., 1983), some of them locally splitting into several sublevels (Sánchez Fabre, 1989; Moissenet, 1993; Simón et al., 2016).) Table 1 compiles the available information on the height and age of these terrace levels.

During graben development, ~~Teruel and Jiloca grabens developed under a~~ the tectonic stress field ~~that, through Neogene-Quaternary times,~~ evolved from: (i) triaxial extension with minimum stress (σ_3) trajectories oriented WNW-ESE, prevailing during the first, Late Miocene rift episode, to (ii) almost radial extension (σ_1 vertical, $\sigma_2 \approx \sigma_3$) with nearly WSW-ENE trending σ_3, prevailing during the second, Pliocene to Quaternary rift episode (Simón, 1982, 1989; ~~Cortés, 1999;~~ Capote et al., 2002; Arlegui et al., 2005). The latter has remained active up to the present-day (Herraiz et al., 2000), although both WSW-ENE and WNW-ESE σ_3 directions are recorded by fracture systems formed during the Pliocene and Quaternary. In summary, this regional 'multidirectional' extensional stress field has been partitioned (in the sense of Simón et al., 2008) into two stress systems, with S_{Hmax} (maximum horizontal stress axis) nearly parallel to trends of the Jiloca and Teruel grabens, respectively, and directly linked to the main tectonic stress sources during the Neogene-Quaternary in eastern Spain: the intraplate NNW-SSE compression produced by Africa-Iberia convergence, and the WNW-ESE extension induced by rifting at the Valencia trough (Simón, 1989; Herraiz et al., 2000; Capote et al., 2002; Arlegui et al., 2005). A similar 'time dissociation' of the overall stress field into distinct genetic stress systems (although in a compressional setting) has been described in the Italian Alps as *Twist Tectonics* by Caputo et al. (2010). Moreover, minor-order stress heterogeneities (deflection of stress trajectories, veering to become either parallel or perpendicular to major faults; swapping between σ_2 and σ_3 axes) are also frequent within this complex stress field (Simón, 1989; Arlegui et al., 2005, 2006).

The Concud Fault is a NW-SE trending, west-dipping fault, which shows an average transport direction N220ºE, has been active since the mid Pliocene, and totalizes a net slip of 255-300 m. Paleoseismological studies have been carried out on the Concud Fault based on analysis of five trenches ~~where a wide paleoseismic succession has been reconstructed~~ (Lafuente, 2011; Lafuente et al., 2011a, 2014; Simón et al., 2016). The results indicate that the fault underwent eleven events since ca. 74 ka BP, with an average recurrence period of 7.1 to 8.0 ka (according to different hypotheses on the age of the youngest recorded event; Simón et al., 2016). Timing of paleoearthquakes on the fault has been constrained by a total of 37 OSL ages. The net accumulated slip during this time interval was 20.5 m, with average coseismic slip of 1.9 m. The displacement pattern shows alternating ‘fast periods’ (up to 0.53 mm/a) and ‘slow periods’ (0.13 mm/a), resulting in an average slip rate of 0.29 mm/a. A potential moment magnitude up to Mw = 6.8 has been estimated by Lafuente et al. (2011a) based on the empirical correlation proposed by Wells and Coppersmith (1994), Stirling et al. (2002) and Pavlides and Caputo (2004). Recent calculations made by Ezquerro et al. (2015) using the equation by Hanks and Kanamori (1979), considering (i) a hypothetical rupture of the total length (14.2 km) up to a 14 km-deep detachment level with an assumed dip angle of 60º, and (ii) the average coseismic slip inferred from paleoseismological studies, renders Mw = 6.6.

Historic and instrumental seismicity of the Teruel Graben and the surrounding region is low to moderate. ~~Epicentres are concentrated in several areas (see e.g. Simón et al., 2016, fig. 2): Albarracín Massif, western margin of the Jiloca Graben, relay zone between the Concud and Sierra Palomera faults, northern Javalambre Massif, and southern sector of the Teruel Graben.~~ There exists a moderate epicentre clustering along the Teruel Fault (see e.g. Simón et al., 2016, fig. 2). Measured magnitudes (Mb) usually range from 1.5 to 3.5, with maximum Mb = 4.4 in the Teruel Graben (data from Instituto Geográfico Nacional, 2010). Before the instrumental period, intensities up to VIII were recorded in the Teruel Basin, ~~VI-VII in the Albarracín Massif,~~ and IV-V in the Jiloca Graben. Focal depths typically range from 5 to 15 km, at the brittle layer above the basal detachment level identified by Roca and Guimerà (1992). Most of the available focal mechanisms correspond to normal faults, and are consistent with the regional recent stress field (Herraiz et al., 2000).

4. Structure and kinematics

4.1. The Teruel Fault

The Teruel Fault is a N-S striking, 9.0 km-long normal fault that ~~extends from the north of Teruel city to the south of Villaspesa village,~~ offsets the Neogene infill of the Teruel basin (Fig. 2a). In detail, it shows a single, N170ºE trending trace in its northern sector, while southwards it branches into two main fault traces trending N-S and NNW-SSE, respectively. The latter, together with additional minor faults, progressively die out in the red lutites of Rojo 2 unit and the coeval Castralvo gypsum succession.

The hanging-wall block shows a rollover structure reflected by tilting of the Páramo 2 unit (Figs. 2b, 3a). This unit exhibits an average dip of 2ºE, its base decreasing in height from 1010 m a.s.l. at the highest point to less than 880 m a.s.l. west of Teruel city. In the footwall block, the base of the Páramo 2 unit lies at about 1130 m a.s.l., from which a cumulative throw of ca. 250 m can be estimated. This displacement has been partially accommodated by bending (perhaps, a monocline above a blind fault in a previous evolutionary stage), with dips up to 17º at the east of the Teruel city ~~and 30º at the southern tip of the fault~~. The combination of rollover and monocline gives rise to a synformal sag parallel to the fault (Figs. 2b, 3a,b).

Field measurements of rupture surfaces within the Teruel Fault show average strike close to N-S and dip ranging from 60º to 80º W (average: 68º; Fig. 2c,d). Striations observed on the main fault surfaces indicate an almost-pure normal movement with average transport direction towards N275ºE.

Considering (i) the above calculated throw, (ii) the average fault dip, and (iii) a pure normal movement, a net slip of ca. 270 m can be inferred for the base of the Páramo 2 unit. Given an age of ~ 3.6 Ma (latest Ruscinian, Godoy et al., 1983; Opdyke et al., 1997; Alcalá et al., 2000) for this stratigraphic marker, the long-term slip rate is ca. 0.075 mm/a.

~~On the other hand, remnants of the Upper Terrace of the Turia River have been mapped at an altitude of 970-980 m a.s.l. on the hanging-wall west of the Teruel Fault (La Muela site; Peña, 1981; Godoy et al., 1983). Moissenet (1983) identified the same level at a small outcrop east of Teruel city at 1017 m a.s.l., interpreting a vertical offset of the T3 terrace close to 40 m. Nevertheless, the age of this terrace remains unknown, so that no slip~~

rate could be calculated from these data. An independent estimation of the overall rate since the Late Pleistocene will be achieved at Puntal del Pitraque site, as explained below.

4.2. The relay zone between Teruel and Concud faults

Surface structural information, together with results of geophysical (magnetic, electromagnetic and georadar) surveys, suggest that the Teruel and Concud faults are geometrically and kinematically independent structures (Lafuente et al., 2011b). These faults do not show any evidence of a physical link: the northern tip of the Teruel Fault is located at a distance of 1.3 km from the Concud Fault (Fig. 2a), and both have distinct hanging-wall transport directions (N275ºE and N220ºE, respectively). They exhibit a right-stepping relay geometry, their displacement being transferred by means of a relay ramp dipping towards N or NNW, which can be clearly identified in Fig. 3a,b. Their displacement-length (D-L) profiles show high displacement gradients approaching the relay zone (Fig. 3c), indicating sharp slip transference between the faults. Further structural complexity at the relay zone occurs due to the presence of a transverse faulted syncline (Mansuetos-Valdecebro syncline; Fig. 2a, 3a,b).

Although the northern tip of the fault is apparently located to the north of Teruel city, there exist two sites aligned with the main trace where deformation structures affecting the fluvial terrace T2b are exposed. These could hypothetically reveal a prolongation of the Teruel Fault to the north, either at surface or as a blind fault (Figs. 2a, 3a). At Las Ramblillas site, T2b is offset by two synthetic faults (one of them with decametre-scale throw, and separated into two tilted blocks where bedding dips up to 10º E and 18º E, respectively (Fig. 4). The western synthetic fault has an average orientation 157, 48 W and striations that pitch 70ºS. The measured fault plane is nearly parallel to that of the southern Concud Fault, as well as to the northern Teruel Fault (Fig. 2a). Cuesta de la Bajada site shows two main rupture surfaces striking NNW-SSE, with minimum offsets of 7 m and 2.5 m, and associated rollover monoclines that tilt T2b beds up to 28º E and 10º E, respectively (Peiro, 2016). If the described deformation features actually represent the northwards propagation of the Teruel Fault parallel to the adjacent Concud Fault after the Middle Pleistocene, its total length would be more than 11 km.

The only misfit concerns the kinematics of Las Ramblillas faults. The transport direction (N 218ºE, inferred from a single striation measure) closely approaches the average calculated for the Concud Fault (N220ºE; Lafuente et al., 2011a,b), and clearly differs from that recorded for the entire Teruel Fault (N275ºE; Fig. 2e). Nevertheless, the possibility of occasional slip of one of these faults following the typical transport direction of the other fault cannot be ruled out. Indeed, Lafuente et al. (2014) describe striations recording two distinct movements along transport directions SW and WNW superposed on a single rupture plane of the Concud fault zone. This issue will be examined later when discussing strain partitioning between these structures.

5. Preliminary paleoseismological characterization of the Teruel Fault

Several empirical relationships allow the expected maximum moment magnitude (M_w) of a fault and its associated coseismic displacement to be estimated. Those proposed by Wells and Coppersmith (1994), Stirling et al. (2002), Pavlides and Caputo (2004), and Mohammadioun and Serva (2001) have been applied in this study. Considering a length of 9.0 km for the Teruel Fault and applying the mentioned relationships, values of M_w ranging from 6.1 to 6.6 are obtained (Table 2). For the coseismic displacement, ~~there is some disagreement between the results obtained from the different correlations.~~ Wells and Coppersmith (1994) and Pavlides and Caputo (2004) correlations yield values of 0.40 m and 0.65 m, respectively, while that by Stirling et al. (2002) attains 1.32 m (Table 2). These estimates will be later compared with real offsets measured in trenches. As mentioned above, there exists the possibility of a prolongation of the Teruel Fault to the north, reaching a total length of at least 11 km. If this length was considered, the inferred M_w values and coseismic displacements would be a little higher (Table 2).

Combining the potential coseismic displacement based on empirical relationships (0.37 m to 1.28 m, considering a 9 km-length fault) with the long-term slip rate calculated since mid Pliocene times (0.075 mm/a; only reliable rate available for the fault prior to the present research), a recurrence interval between 4.9 ka and 17.1 ka is tentatively approached. If the fault were 11 km long, the recurrence periods would slightly increase (5.3-17.6 ka).

6. Detailed structure of the Pitraque-Valdelobos area

In the Pitraque-Valdelobos area the Teruel Fault cuts Quaternary deposits, so it has been selected for trenching study. Puntal del Pitraque is a conical hill located 1.2 km south of Teruel city, in the area where the Teruel Fault splits southwards into several synthetic fault branches (M, N, P, Q, R, S in Fig. 5a; see location in Fig. 2a). A remnant of the lower sublevel of the Middle Terrace (T2a) occupies the top of the hill. A larger remnant of the same terrace appears on a horizontal platform some 100 m westwards. T2a unconformably overlies Neogene units (Rojo 2 and Páramo 2), and had previously provided an OSL age of 76.0 ± 5.0 ka (Simón et al., 2012). The Rambla de Valdelobos is a gully oriented transverse to the Teruel Fault that drains westwards into the Turia River, south of Puntal de Pitraque and shows a relatively wide bottom filled with Holocene clastic sediments, where the gully is slightly incised.

The main Teruel Fault branch (M) crops out north of Puntal del Pitraque site (Fig. 5b), where it has an average strike N033ºE and juxtaposes the Páramo 2 (hanging-wall block) and Rojo 2 (footwall block) units. The other macro-scale faults are also clustered around NNE-SSW (N024ºE in average from outcrop measures) and show westwards dip ranging from 52º to 84º (68ºW in average) (Fig. 5c,d). Each individual fault offsets several metres to several tens of metres the Neogene beds. Together with the main fault and the monocline visible at the footwall block, the total displacement accommodated across this transect is estimated at 190 m (Figs. 2b, 3a).

The top of Middle Terrace (T2a) at Puntal del Pitraque lies 8.2 m higher than that at the western, horizontal platform (Fig. 5e). Such a height difference can be attributed to displacement on fault branches M and N. The corresponding net slip, assuming the average dip of the rupture surface (68º) and the inferred transport direction (N275ºE), is ca. 8.8 m. Using the previously available OSL age at the base of the terrace deposits (76.0 ± 5.0 ka), Simón et al. (2012) calculated a minimum slip rate of 0.12 ± 0.01 mm/a since ca.76 ka. Taking into account that the marker where that offset was measured is the terrace top, and hence If the younger OSL age provided in the present work (46.5 ± 3.2 ka; Table 3) is assigned to the terrace top, a more realistic slip rate of 0.19 ± 0.01 mm/a is obtained for the Late Pleistocene-Holocene. Moreover, Since the displacement is only recorded at two (among five) synthetic branches within the fault zone, the total slip rate for the overall structure should exceed this value. The absence of Quaternary deposits displaced by the eastern branches of the fault makes impossible to test such hypothesis.

The primary target for our paleoseismological study was the M fault branch west of Puntal del Pitraque, where the initial field survey revealed small, decimetre-scale offset of the fluvial terrace T2a. Two paleoseismological trenches (Pitraque 1 and Pitraque 2) were excavated at this site, exposing Neogene lacustrine limestones and lutites unconformably overlain by the Pleistocene materials. Detailed inspection after trench digging showed that, within the M branch, the main observed fault surface (Fμ), locally striking N020ºE to

N030ºE, is cut by a second fault (Fα) striking N050ºE, which is exposed in Pitraque 2 trench and apparently extends below Pitraque 1 (Fig. 6a). In addition, a third fault striking N019ºE is exposed in Pitraque 2 (Fβ) as well as at the natural terrace scarp. Fβ constitutes the prolongation of Fμ, but their physical linkage could not be observed in the field. The described structural relationships suggest local segmentation of the main NNE-SSW fault surfaces, these being articulated with (and their displacement being locally transferred to) NE-SW striking faults. Fracture patterns observed at a mesostructural scale, both in trenches and on natural outcrops (Fig. 6b,c,d,e), are consistent with the general structure of the Pitraque-Valdelobos area, although the range of strike values (from NNE-SSW to ENE-WSW) is wider than that expressed at macroscale (Fig. 5d)~~, owing to juxtaposition of that second fracture set around N050ºE to the main, N020ºE to N030ºE striking set. Further geometric description and kinematic interpretation of the fracture systems will be provided while analysing each individual trench~~.

7. Trench study at the Pitraque-Valdelobos area

7.1. Pitraque 1 trench

The Pitraque 1 trench was excavated for studying deformation associated to the main branch of the Teruel fault zone (M in Fig. 5a,c). This trench trends N148ºE, is 12.5 m long and 4.5 m deep; its western wall was selected for detailed logging and analysis (Fig. 7a). Neogene sedimentary units (Rojo 2 and Páramo 2) crop out in the lower part of the trench, overlain by Pleistocene coarse clastic~~, generally well-cemented~~ materials that have been subdivided into six units (1 to 6 in Fig. 7a; see ~~detailed~~ description in Appendix 1).

The largest deformation structure exposed in this trench is a gentle bending fold that occupies most of the logged section shown in Fig. 7a. The geometry of the fold is continuous along both the Pliocene and Pleistocene beds (units 2 to 5), which suggests that ~~most of~~ folding essentially occurred after sedimentation of unit 5. ~~Perhaps this fold had already deformed the Pliocene units before Pleistocene sedimentation, but~~ The boundary between both lithological successions ~~essentially~~ represents an erosional discontinuity, not an angular unconformity.

The Páramo 2 unit is also deformed by a number of normal, NE-SW striking faults (domain 4 in Fig. 7a) that make a rough conjugate system ~~with a dominant strike close to NE-SW~~ (Fig. 7e). The overlying Pleistocene units in the northwestern sector are affected by numerous fractures also with an average NE-SW strike (domain 2; Fig. 7a,c). These fractures include a few small faults with centimetre-scale offsets, small closed joints, and a large tensile crack filled with carbonate (C1 in Fig. 7a) that attains about 2 m in length and 20 cm in thickness. The fracture systems affecting domains 2 and 4 are disconnected from each other; indeed, the only Pleistocene fracture that could be rooted in a Neogene fault does not clearly show any physical linkage with it (see cell 10c in Fig. 7a). Domain 1 shows the same types of faults and fractures as in domain 2 (although in domain 1 these are mostly close to vertical; Fig. 7b), as well as a second large open crack filled with carbonate ~~appears within this domain~~ (C2 in Fig. 7a)~~, showing even more walls than C1~~. Finally, domain 3 contains a number of small faults close to the Neogene-Pleistocene boundary. One of them (Fγ), ~~is~~ oriented NE-SW, produces an offset of about 0.1 m ~~on it~~ and propagates within the lower part of Unit 2. The others are oriented NNW-SSE (Fig. 7d) and do not produce any visible displacement.

Most fractures in the lower structural domains (3 and 4) express the prevailing extensional fracture pattern in the region, represented by sets oriented NNW-SSE and NNE-SSW~~, i.e. parallel to macroscale faults of the Jiloca and Teruel grabens, respectively~~. In contrast, most fractures within domains 1 and 2 seem to be induced by local deformation conditions, i.e. the bending fold. This interpretation is based on two pieces of evidence: (i) most of the fractures are concentrated within the outer arc at the hinge zone (cells 9d and 10d in Fig. 7a); (ii) the movement plane of the bending fold, as defined by poles of bedding (Fig. 7f), is nearly orthogonal to NE-SW fractures of domains 1 and 2 (including cracks C1 and C2, which accommodate an important part of stretching affecting units 3, 4 and 5 in the outer arc). Although at present most of these fractures dip towards SE, they probably originated as nearly vertical fractures, as can be inferred by restoring bed tilting. The genetic dependence of these fractures with respect to local bending, as well as the rheological contrast between Pleistocene cemented clastic deposits and Neogene carbonates, could explain why the fracture systems affecting domains 2 and 4 appear to be independent from each other. Bending, and hence the associated tensional fractures, could be related to movement on ~~either an adjacent fault cutting Pliocene units (tentatively, Fδ in Fig. 7a, striking N 030º E) or~~ an underlying blind fault.

Considering the structural relationships between faults and sedimentary units, as well as their OSL ages (Fig. 7a; Table 3), three paleoseimic events have been identified:

- Event(s) X_{P1}. Interpreted by the rupture and displacement (not quantified) of Neogene materials along fault Fα, and maybe other faults in domain 4, prior to local sedimentation of the Pleistocene terrace. More than one paleoearthquake could have resulted in such faulting, but they cannot be distinguished. This event (or events) occurred before 70.7 ± 5.3 ka BP (earliest OSL age obtained in the lower part of Unit 1). From the geologic record in the trench, it is not possible to estimate the associated displacement.

- Event Y_{P1}. Interpreted by the rupture along a small fault (Fγ), which produces a throw of 0.1 m at the base of the Pleistocene Unit 2. Predated by the upper part of Unit 1 (OSL age of 70.7 ± 5.3 ka BP) and postdated by overlying materials of Unit 2 (OSL age of 71.8 ± 5.1 ka BP).

- Event Z_{P1}. Represented by bending of Neogene (R2, P2) and Pleistocene (2, 3, 4, 5) units and development of associated tensional fractures, including opening of cracks (C1 and C2) subsequently filled with carbonate. ~~All fractures would be hypothetically related to movement of either fault Fδ or an underlying blind fault.~~ This event is predated by the youngest available OSL age (48.5 ± 3.8 ka BP; middle-upper part of Unit 5), and postdated by the regolith (Unit 4, probably Holocene in age). Considering the amplitude of the bending fold, a mimimum coseismic throw of 1.0 m is estimated on a hypothetical underlying, blind fault (coseismic net slip >1.1 m for a 70º dipping plane).

7.2. Pitraque 2 trench

Pitraque 2 trench also exposes the main branch of the Teruel fault zone (M in Fig. 5a,c). It trends N133ºE, is 7.5 m long and 2.5 m deep, the southwest wall being selected for study (Fig. 8a). ~~Neogene sediments similar to those described~~ As in Pitraque 1 trench, Rojo 2 and Páramo 2 Pliocene units underlie Pleistocene conglomerates and sandstones, which have been subdivided into four units (1 to 4 in Fig. 8a); see ~~detailed~~ description in Appendix 1).

Two main normal faults are exposed in Pitraque 2 trench. To the northwest, fault Fα (domain 2; Fig. 8a,d), locally striking N035ºE, offsets the Neogene units sinking its NW block and being responsible for erosion of Páramo 2 unit at the SE one; then Fα is overlain by non-affected Pleistocene deposits. To the southeast, Fβ (N019ºE) offsets Pleistocene units 1, 2 and 3, producing the same throw (0,5 m) on each of them, and splits upwards into several splay faults (domain 1, Fig. 8a,b,c). The association of splay faults to the main fault makes a *horse tail* structure (as defined by Granier, 1985), which is interpreted to be the product of local stretching close to the fault tip while fault Fβ was activated and propagated through the overlying Pleistocene deposits. This fracture system is also exposed on the opposite trench wall, with the same NNE-SSW to NE-SW strike and exhibiting pure-normal striations on the main fault Fβ (Fig. 8e). Finally, a tensile crack filled with carbonate (C3), similar to C1 and C2 of Pitraque 1 trench, overprints this system of splay faults. Although included within the main fault zone, C3 represents a kinematically distinct deformation pattern. Its opening vectors, with homogeneous length about 2-3 cm, are nearly orthogonal to the crack walls (Fig. 8a,b). Such a displacement pattern does not fit slip parallel to fault Fβ, and instead is consistent with tangential stretching at the outer arc of an accommodation monocline.

Three paleoseismic events have been interpreted (Fig. 8a; Table 3):

Event(s) X_{P2}. As in the case of Event $X_{P1,}$ deformation previous to deposition of the observed Pleistocene units is attributed to a first local event, although it may represent more than one paleoearthquake. Two inferred fault movements can be assigned to such a ‘composite’ X_{P2} event: (i) movement of Fβ that cut the Neogene Rojo 2 unit previously to deposition of Unit 1, therefore before 78.3 ± 5.2 ka BP; its associated *horse tail* structure (a fracture pattern typically found at extensional fault tips) involves activation of a blind, pre-existent fault through the overlying Pleistocene deposits; (ii) rupture and displacement of Rojo 2 and Páramo 2 units along fault Fα, as well as northwards tilting, previous to 50.0 ± 3.4 ka BP (age of the base of Unit 2, not affected). Since Fα is also exposed in Pitraque 1 trench, where it is postdated by OSL 70.7 ± 5.3 ka BP, we can assume this time constrain for it. These two fault movements cannot be chronologically distinguished and their associated displacements remain unknown.

Event Y_{P2}. Rupture and displacement of Pleistocene units 1, 2, and 3 along fault Fβ and its associated splay faults. Predated by the youngest OSL age available in the trench, at the base of Unit 3 (46.5 ± 3.1 ka). The associated coseismic slip along fault Fβ can be estimated at 0.5 m.

Event Z_{P2}. Represented by opening of tensile crack C3, which was subsequently filled with carbonate. As with the previous event, this one is predated by the youngest available OSL age (46.5 ± 3.1 ka), and postdated by the regolith (Unit 4, probably Holocene in age). We infer that the Z_{P2} event is distinct from the former event based on the kinematic differences between the tensile crack and the structures linked to Event Y_{P2}. The geometry of deformation does not permit measurement of coseismic slip.

7.3. Valdelobos trench

This N100ºE trending trench was excavated in the T0 terrace of Rambla de Valdelobos ~~some 0.4 km~~ south of Puntal del Pitraque, where the gully apparently crosses the fault branch P (Fig. 5a), and its talweg exhibits a discrete gradient anomaly inferred from the laser-levelling profile (Fig. 5f). An exposure of around 5 m long and 2.5 m deep along the southern wall of the trench was studied in detail. The trench shows massive red Neogene lutites (Rojo 2) at its base, which are covered by Quaternary clastic deposits subdivided into five units (1 to 5 in Fig. 9; see ~~detailed~~ description in Appendix 1).

The Neogene materials ~~exposed at the trench bottom~~ are displaced by a normal fault (Fε) striking N155ºE (Fig. 9). This fault also affects the lowermost Quaternary deposits (Units 1 and 2), and is covered by Unit 3. The minimum fault throw is 0.3 m, but it could be much larger since the fault scarp was eroded below the base of Unit 2. A single event has been interpreted in this case, referred to as **Event Z_{VL}**, ~~this event~~ occurred between 26.7 ± 1.9 ka BP (age of Unit 2) and 9.9 ± 0.7 ka BP (age of Unit 3).

8. Interpretation and discussion

8.1. Paleoseismic record of the Teruel Fault: correlation of events

Correlation of events between the Pitraque and Rambla de Valdelobos trenches (Table 4; Fig. 10) has been accomplished on the basis of geological judgement and OSL ages. It can be conventionally assumed that Event(s) X is common to both Pitraque 1 and Pitraque 2 trenches and inferred to be the same event (now renamed as Event 0): this event only affects Neogene materials, exhibiting upper time limits 70.7 ± 5.3 and 78.3 ± 5.2 ka BP, respectively, for each trench. We are aware that this event could actually represent a succession of several seismic episodes, either Pleistocene or even Pliocene in age. Considering the OSL ages that constrain their timing, Y_{P1} and Y_{P2} are interpreted as being two independent events: Event 1, with absolute time brackets 76.0 and 66.7 ka BP (central, most probable age: 70-71 ka BP), and Event 2, younger than 49.6 ka BP. Z_{P1} and Z_{P2} are interpreted as a single event (renamed Event 3, younger than 49.6 ka BP), taking into account their postdating OSL ages, the style of deformation (crack opening, subsequent carbonate filling) and the orientation of coseismic fractures (around NE-SW in both cases). Finally, Event Z_{VL}, only recorded at the Rambla de Valdelobos trench and therefore at a different fault branch, represents the youngest event (renamed Event 4, with absolute time brackets 28.6 and 9.2 ka BP).

In summary, the trench study has yielded ~~at least five independent events:~~ one (or several) uncertain event prior to 73.1 ka BP, and four events occurred between 76.0-66.7 ka and 28.6-9.2 ka BP. This four-event-succession yields an average recurrence period in the range of 9.5-16.7 ka. Nevertheless, the individual interseismic periods remain unknown, as only the timing of events 1 and 4 are constrained (quite widely in the case of the second one)~~, while the timing of Events 2 and 3 is unconstrained (only with a single, shared predatum)~~.

8.2. Representativeness of the paleoseismic record of the Teruel Fault

Events 1, 2 and 3 occurred on the western, main branch (M) of the Teruel Fault, while Event 4 occurred on a minor branch (P; see map in Fig. 5a). Events 1, 2 and 3 represent a minimum accumulated net slip of 1.7 m on branch M. The average coseismic slip for these three events (0.57 m) lies close to the estimates made from the empirical correlations of Wells and Coppersmith (1994) and Pavlides and Caputo (2004)~~: 0.40 m and 0.65 m, respectively~~ (see section 5 and Table 2). This suggests that (i) these correlation models better describes our data than that of Stirling et al. (2002)~~, which yields a value of 1.32 m~~, and (ii) the recorded paleoseismic single event displacements approach the *characteristic earthquake* of the Teruel Fault (in the sense of Schwartz and Coppersmith, 1984). If Event 4 is incorporated, the results do not change substantially: minimum net slip on branches M+P (as recorded in trenches) will attain 2.0 m, with average coseismic slip of 0.50 m, and local slip rate of 0.04 ± 0.01 mm/a (~~estimate from hypothetical ages of the four events within their respective time constraints;~~ Fig. 11d).

This paleoseismic succession only represents a fraction of the total activity on the western branches of the fault system during the sampled time interval. It should be reminded that the total offset of the fluvial terrace T2a represents a net slip of 8.8 m, with slip rate = 0.19 ± 0.01 mm/a for the last 46.5 ± 3.2 ka (Fig. 11d; see Section 6 and Table 5). Therefore, only a small part of the paleoseismic history of the Teruel Fault during the studied time window has been recorded in the studied trenches, and the calculated average recurrence period (9.5 to 16.7 ka) has little meaning. Assuming the average coseismic slip of 0.57 m and the accumulated net slip of 8.8 m, the total number of paleoseismic events on branches M+N since 76.0 ± 5.0 ka BP could attain fifteen, with a shorter average recurrence period of 5.1 ± 0.3 ka (close to the minimum estimated from empirical correlation, 4.9 ka). ~~Unfortunately, no other site apart from Pitraque and Rambla de Villalobos is available for trenching syntectonic Quaternary sediments across the fault, so improving the present paleoseismic record will be difficult.~~

8.3. Comparison with the paleoseismic record of the Concud Fault

The paleoseismic results for the Teruel Fault can be compared with those previously obtained on the neighbouring Concud Fault (Lafuente, 2011; Lafuente et al., 2011a, 2014; Simón et al., 2016) in order to analyse the seismogenic dependence or independence between them. At first glance, the recorded paleoseismic activity of the Teruel Fault seems significantly lower than that of the Concud Fault during a similar time period (76 ka vs. 74 ka BP; Fig. 10; Table 5): four events with average coseismic slip of ca. 0.6 m vs. eleven events with average coseismic slip of 1.9 m. Nevertheless, we should remind that the paleoseismic record obtained for the Teruel fault zone ~~should be considered: it~~ only includes the seismic events occurred on two fault branches (M and P)~~, which represent just a fraction of the total activity at the Teruel Fault zone~~. With this respect, it would be more realistic a comparison with the paleoseismic record obtained at a single fault branch in the the central sector of the Concud Fault (Fig. 11b,d; Table 5). Two trenches excavated across its southern branch (El Hocino site) ~~could be studied,~~ provided a sequence of five events occurred since 74 ka BP, with an accumulated net displacement of 3.9 m, average coseismic slip close to 0.8 m, and slip rate of 0.05 mm/a (Fig. 11b) (Lafuente et al., 2014). These results are closer to those obtained for the Teruel Fault in the present work, which allows us to estimate that the likely degree of activity of both faults has been similar. Unfortunately, due to the poor time constraint on individual events interpreted for the Teruel Fault, comparing and correlating events recorded on the Teruel and Concud faults is impractical (Fig. 10).

8.4. Structural and seismotectonic relationships between the Teruel and Concud faults

As stated above, surface and shallow subsoil information does not support the hypothesis of full structural link between the Teruel and Concud faults (hard linkage in the sense of Walsh and Watterson, 1991). Moreover, their distinct transport directions (N275ºE vs. N220ºE) indicate that they behave as two independent structures from the kinematic point of view. Their separate displacement-length profiles at the relay zone (Fig. 3c) are also consistent with such independence, although the sharp gradients of these profiles close to the fault tips suggest some dynamic interaction between them.

Our paleoseismological study provides further evidence for autonomous activity on each fault. Time constraints of events in the Teruel Fault do not allow us to either confirm or disprove that some events ruptured both faults (Fig. 10). Nevertheless, coseismic displacements observed at the Teruel Fault helps us to suggest that the Teruel and Concud faults behave as two independent seismogenic sources instead of as a single seismogenic structure. Displacement values of the Teruel Fault (0.1 to 1.1 m; average = 0.5-0.57 m): (i) are consistent with those expected for a 9.0 km-long fault according to empirical correlation; (ii) are significantly smaller than those actually recorded on the 14.2 km-long Concud Fault (1.9 m, in average); and (iii) are less consistent with a hypothetically joint Concud-Teruel, 23 km-long fault (expected coseismic slip ranging from 0.7 m to 2.4 m, according to empirical correlation; see section 5 and Table 2). Moreover, the difference between their prevailing transport directions, previously noticed from overall kinematic data at both faults, has been confirmed from faults exposed in paleoseismological trenches (Fig. 11a,c).

Another different issue concerns the location of the true northern tip, and hence the true length of the Teruel Fault and its distance to the Concud Fault. Faults and associated tilted beds observed in Middle Pleistocene deposits at two sites (Cuesta de la Bajada and Las Ramblillas; see location in Fig. 2a) suggest a prolongation of the Teruel Fault some 2 km northwards from the mapped tip point located north of Teruel city. As in the case of the Concud Fault, no trace can be identified through the flood plain of the Alfambra River (Holocene, T0 terrace), but the Teruel Fault could cut the underlying Neogene and Pleistocene units. ~~Future research in this area, including geophysical surveys of the Alfambra flood plain, may clarify this issue.~~

The transport direction inferred at Las Ramblillas (N218ºE) differs from that of the Teruel Fault (N275ºE) and is approximately parallel to that of the Concud Fault (N220ºE). This anomalous observation plays somehow against the full connection of the Las Ramblillas structure to the Teruel Fault, and points to two alternative hypothesis: (i) the outcropping Las Ramblillas fault is a smaller, recent synthetic rupture kinematically associated with the Concud Fault, although it could play a role within an eventual linkage process with the Teruel Fault; (ii) the striation measured on the Las Ramblillas fault is not representative of its prevailing transport direction: in the same way that a second striation exists on the Concud Fault surface at El Hocino site, oriented towards NW and overprinting the SW-oriented prevailing striation (Fig. 11a; Lafuente et al., 2014), an ‘anomalous’ movement towards SW could have been recorded on the Teruel Fault.

In any case, the tentative propagation and linkage of the Teruel Fault with the Las Ramblillas structure would represent a recent, incipient process, as suggested by the pronounced bell-shape of its D-L profile. In this profile a high D-L gradient at the relay zone (around the abscise 14 km in Fig. 3c) is followed by a sharp reduction of the gradient near the northern tip (frictional breakdown zone; Cowie and Sholz, 1992; Cowie and Shipton, 1998).

8.5. Dynamic interaction and future linkage?

Although the Teruel and Concud faults remain two independent structures, future linkage is possible, as proposed by Ezquerro et al. (2012) and Lafuente et al. (2012). Linkage would be consistent with the mechanical state inferred for the relay zone. ~~In spite of their geometric and kinematic independence,~~ The steep gradients of their displacement-length (D-L) profiles in the relay zone indicate that both faults undergo dynamic interaction, according to theoretical models. The elastic strain fields of two adjacent faults interfere close to their tip lines, which tends to hinder propagation while displacement increases, resulting in anomalously high displacement gradients (Huggins et al., 1995; Nicol et al., 1996; Cartwright and Mansfield, 1998; Gupta y Scholz, 2000; Peacock, 2002).

According to this hypothesis, the relay zone between the Teruel and Concud faults is in a transient stage from independence to linkage. It cannot be anticipated how such full connection would happen. The coalescence of Las Ramblillas fault with both the Teruel and Concud faults could be the most probable one, the southernmost, NNW-SSE trending segment of the Concud Fault probably remaining as an inactive splay fault (Childs et al., 1995). Alternatively, transverse faults of the Mansuetos-Valdecebro structure could cut the relay ramp, resulting in ~~a transfer fault zone (~~hard linkage. ~~Walsh and Watterson, 1991).~~

8.6. A scenario of strain and stress partitioning at the scale of the seismic cycle

Owing to their dynamic interaction, it is expected that displacement on one fault results in stress perturbation of the rock volume surrounding the other fault, and vice versa. At the scale of individual earthquakes, static Coulomb stress changes could trigger seismic events on segments of the other fault that were approaching critical conditions for rupture (Freed, 2005; King et al.,1994).

This suggests a scenario of slip on both structures taking place in a broadly alternating manner: stress release on one fault after a seismic event, and stress instability induced in the surrounding volume, will favour the next event to occur in the other fault (Fig. 12). Indeed, the average recurrence period may be similar for both structures during the Late Pleistocene times, with 7.1 ± 3.5 to 8.0 ± 3.3 ka on the Concud fault (Simón et al., 2016), and 10-15 ka on the Teruel Fault, as estimated from empirical correlation proposed by Villamor and Berryman (1999) using the average slip rate. This scenario involves local strain partitioning between the Teruel and Concud faults at the scale of the seismic cycle, representing a small incremental deformation episode within overall strain partitioning between NNW-SSE and NNE-SSW normal faults.

It is known that conjugate fault systems formed according to Mohr-Coulomb's failure criterium only accommodate plane strain ($\lambda_2 = 1$). In order to accommodate 3D finite strain, movement on multiple-set fault patterns (such as those typically made of four sets with orthorhombic symmetry) is necessary (Reches, 1978; Krantz, 1989; Nieto-Samaniego, 1999). Therefore, the biaxial extensional deformation that characterizes the recent tectonic setting of eastern Iberian Chain (Simón, 1982, 1989; Capote et al., 2002) could not be accommodated by a single fault set, or by a single conjugate normal fault system; progressive slip on diversely orientated fault planes and along diverse transport directions is needed.

However, this does not occur as a linear, steady process, but as a non-linear sequence of rupture episodes, during discontinuous deformation. The bulk 3D deformation is partitioned into a number of slip events on individual faults, which in their turn involve a sequence of episodic, systematic (not chaotic) stress changes that Simón et al. (2008) define as *stress partitioning*. Each failure event is compatible with stress-based models, while the finite 3-D strain fits kinematic boundary conditions.

The described process can occur at any spatial scale between e.g. tensile joints up to intraplate regions, and also at a wide range of time scales. In our study region, the long-term, Neogene-Quaternary tectonic evolution of eastern Iberia is characterized by both spatial transition and time shifting between regional stress systems with NNW-SSE and NNE-SSW S_{Hmax} trajectories, coexisting with local switching to orthogonal, either ENE-WSW or ESE-WNW trending ones (Simón, 1989; Cortés et al., 1996; Herraiz et al., 2000; Arlegui et al., 2005). At a much shorter time scale, it is known that earthquake focal mechanisms frequently reveal stress instabilities during aftershock sequences, some fault mechanisms being representative of the regional stress field while others represent second-order stresses including episodes of stress axis swapping (Mercier et al., 1989; Bowman et al., 2003;

Caputo, 2005). Similar outcomes arise from laboratory experiments carried out by Reches and Dieterich (1983), which describe how fracture patterns made of four sets with orthorhombic symmetry (needed for accommodating 3D finite strain) developed through two yielding events with swapping of the two major stress axes between them.

Our hypothesis is that strain/stress partitioning also occurs at an intermediate time scale, i.e. the scale of seismic cycle (as postulated as well for the notion of *Twist Tectonics* by Caputo et al., 2010) giving rise to ~~the above postulated scenario of~~ broadly alternating slip on the Teruel and Concud faults. Dynamic interaction between neighbouring faults (described in the previous section) provides the way for that process to come about. In this way, our scenario: (i) is consistent with the structural and dynamic relationships between faults, (ii) is consistent with the intrinsic stress changes in the complex regional stress field, and (iii) allows accommodation of bulk biaxial extension in the Teruel region.

8.7. Implications for seismic hazard assessment

The ~~type of~~ relationship interpreted for the Teruel and Concud faults has undeniable implications for seismic hazard assessment of the Teruel region. In general, an intermediate, transient stage (structural decoupling but dynamic interaction) implies a different seismic hazard level than that involved by the alternative, extreme options: (i) full independence, or (ii) linkage.

A hypothetically linked Concud-Teruel fault, with a total length of 23 km, would represent a seismogenic structure able to produce larger earthquakes than those generated by each separate structure. Their characteristic earthquake would show maximum moment magnitude Mw ≈ 6.6-7.0, while Mw ≈ 6.1-6.6 and Mw ≈ 6.6-6.8 for the single Teruel and Concud faults, respectively (Table 2). In the case of two independent seismic sources, with each having a similar recurrence period to that of the hypothetical linked structure, the probability of occurrence of such characteristic earthquakes in a given term would be significantly increased.

On the other hand, dynamic interaction between both faults involves shortening of the seismic cycle. Local stress perturbations induced by movement on one fault can trigger movement on the other one, which is found to be most evident within short distances (up to ≈ 5 km), although only for events that are relatively late in their respective earthquake cycle (Chen et al., 2010).

9. Conclusions

(1) Surface and shallow subsoil information indicates that the Teruel and Concud faults are not structurally linked. They also behave as kinematically independent structures, with distinct transport directions: N275ºE and N220ºE, respectively.

(2) The Pleistocene paleoseismic record of the Teruel Fault includes four events. One of them (Event 0, probably representing a succession of several seismic episodes indeed) is prior to 73.1 ka BP, and the other four (Events 1, 2, 3, and 4) occurred between 76.0 and 9.2 ka BP (Table 4, Fig. 10). Since timing of individual events is poorly constrained, the duration of interseismic periods remains unknown. The recorded paleoseismic activity only represents a limited succession of slip events in two fault branches (therefore far from embodying the total activity of the Teruel fault zone).

(3) This paleoseismic record is significantly lower than that of the overall Concud Fault during a similar studied time lapse (76 ka BP vs. 74 ka), but comparable to that obtained in the southern branch of the Concud Fault at its central sector (Fig. 11). Hence we estimate that the overall degree of activity of both faults could be similar. The most representative slip rates obtained from morpho-sedimentary markers (see Table 5) are ≈ 0.075 mm/a for the last ~ 3.6 Ma on the overall Teruel fault zone, and 0.19 ± 0.01 mm/a for the last 46.5 ± 3.2 ka on two branches at Pitraque site. Strictly considering the events recorded at trenches, such slip rate is reduced to 0.04 ± 0.01 mm/a. These values are comparable to those previously obtained at the Concud Fault: 0.07-0.08 mm/a for the last ~ 3.6 Ma, and 0.29 mm/a since ~74 ka BP on the entire fault zone; 0.05 mm/a since ~74 ka BP on a single branch (Lafuente, 2011; Lafuente et al., 2011a, 2014; Simón et al., 2016).

(4) Owing to the poorly constrained timing of events identified at the Teruel Fault, comparing and correlating them with those on the Concud Fault is not feasible, neither Therefore, our results are not conclusive in order discerning whether some rupture event have simultaneously occurred on both faults. Nevertheless, the observed coseismic displacements on the 9.0 km-long Teruel Fault (average = 0.5-0.57 m) are consistently smaller than those previously measured on the 14.2 km-long Concud Fault (average = 1.9 m), and unsuitable for a hypothetically joint Concud-Teruel, 23 km-long fault. We therefore interpret that the Teruel and Concud faults behave as two independent seismogenic sources.

(5) In spite of their geometric and kinematic independence, both structures undergo dynamic interaction (i.e. stress perturbation at the rock volume surrounding one fault subsequent to activation of the other one). This could have induced broadly alternating slip

on both faults along their distinctive transport directions, which would involve a certain type of strain partitioning at the scale of the seismic cycle (Fig. 12): combining multiple slip events on both fault surfaces would allow accommodation of bulk 3D deformation in the Teruel region, within the framework of a biaxial extensional stress regime. The described scenario represents a transient stage from independence to linkage; future connection (probably through coalescence with an intermediate fault, Las Ramblillas fault) is a potential process.

(6) Structural relationships between the Teruel and Concud faults clearly influences seismic hazard ~~of the studied region~~. Two independent seismic sources will produce smaller, although more frequent earthquakes than those generated by a hypothetically linked Concud-Teruel fault. Dynamic interaction between both faults probably involves shortening of the seismic cycle, therefore increasing the probability of seism occurrence, but distributing the total released energy into smaller events.

Acknowledgements

The research has been financed by project CGL2012-35662 of Spanish Ministerio de Economía y Competitividad-FEDER, as well as by the Aragón regional government (E27, Geotransfer research group). L. Ezquerro benefited from a FPI grant (BES-2010-031339) of Spanish Ministerio de Economía y Competitividad. We thank Laboratorio de Datación y Radioquímica de la Universidad Autónoma de Madrid for OSL dating, and Gabinete Geológico de la Diputación Provincial de Teruel for technical assistence in trenching works. I. Casado, A. Peiro and G. Simón helped us in field surveys.

References

Alcalá, L., Alonso-Zarza, A.M., Álvarez, M.A., Azanza, B., Calvo, J.P., Cañaveras, J.C., van Dam, J.A., Garcés, M., Krijgsman, W., van der Meulen, A.J., Morales, J., Peláez, P., Pérez-González, A., Sánchez, S., Sancho, R., Sanz, E., 2000. El registro sedimentario y faunístico de las cuencas de Calatayud-Daroca y Teruel. Evolución paleoambiental y paleoclimática durante el Neógeno. Revista de la Sociedad Geológica de España 13, 323-343.

Arlegui, L.E., Simón, J.L., Lisle, R.J., Orife, T., 2005. Late Pliocene-Pleistocene stress field in the Teruel and Jiloca grabens (eastern Spain): contribution of a new method of stress inversion. Journal of Structural Geology 27, 693-705.

Arlegui, L.E., Simón, J.L., Lisle, R.J., Orife, T., 2006. Analysis of non-striated faults in a recent extensional setting: the Plio-Pleistocene Concud fault (Jiloca graben, eastern Spain). Journal of Structural Geology 28, 1019-1027.

Biasi, G.P, Wesnousky, S.G., 2016. Steps and Gaps in Ground Ruptures: Empirical Bounds on Rupture Propagation. Bulletin of the Seismological Society of America 106, 1110-1124.

Bowman, D., King, G., Tapponnier, P., 2003. Slip partitioning by elastoplastic propagation of oblique slip at depth. Science 300, 1121-1123.

Capote, R., Muñoz, J.A., Simón, J.L., Liesa, C.L., Arlegui, L.E., 2002. Alpine tectonics I: The Alpine system north of the Betic Cordillera. In: Gibbons, W., Moreno, T. (Eds), Geology of Spain. The Geological Society, London, 367-400.

Caputo, R., 2005. Stress variability and brittle tectonic structures. Earth Sciences Reviews 70, 103-127.

Caputo, R., Mucciarelli, M., Pavlides, S., 2008. Magnitude distribution of linear morphogenic earthquakes in the Mediterranean region: Insights from paleoseismological and historical data. Geophysical Journal International 174, 930-940.

Caputo, R., Poli, M.E., Zanferrari, A. 2010. Neogene-Quaternary tectonic stratigraphy of the eastern Southern Alps, NE Italy. Journal of Structural Geology 32, 1009-1027.

Cartwright, J.A., Mansfield, C.S., 1998. Lateral displacement variation and lateral tip geometry of normal faults in the Canyonlands National Park, Utah. Journal of Structural Geology 20, 3-19.

Chen, K.H., Bürgmann, R., Nadeau, R.M., 2010. Triggering Effect of M 4–5 Earthquakes on the Earthquake Cycle of Repeating Events at Parkfield, California. Bulletin of the Seismological Society of America 100, 522–531.

Childs, C., Watterson, J., Walsh, J.J., 1995. Fault overlap zones within developing normal fault systems. Journal of the Geological Society, London 152, 535-549.

~~Cortés, A.L., 1999. Evolución tectónica reciente de la Cordillera Ibérica, Cuenca del Ebro y Pirineo centro-ocidental. Ph.D. thesis, Universidad de Zaragoza.~~

Cortés, A.L., Liesa, C.L., Simón, J.L., Casas. A.M., Maestro, A., Arlegui, L.E., 1996. El campo de esfuerzos compresivo neógeno en el NE de la Península Ibérica. Geogaceta 20, 806-809.

Cowie, P.A., Scholz, C.H., 1992. Physical explanation for the displacement-length relationship of faults using a post-yield fracture mechanics model. Journal of Structural Geology 14, 1133-1148.

Cowie, P.A., Shipton, Z.K., 1998. Fault tip displacement gradients and process zone dimensions. Journal of Structural Geology 20, 983-997.

Ezquerro, L,. Lafuente, P., Pesquero, M.D., Alcalá, L., Arlegui, L.E., Liesa, C.L., Luque, L., Rodríguez-Pascua, M.A., Simón, J.L., 2012. Una cubeta endorreica residual del Pleistoceno inferior en la zona de relevo entre las fallas neógenas de Concud y Teruel, Cordillera Ibérica: implicaciones paleogeográficas. Revista de la Sociedad Geológica de España 25, 157-175.

Ezquerro, L., Luzón, A., Navarro, M., Liesa, C.L., Simón, J.L., 2014. Climatic vs. tectonic signal in the Neogene extensional Teruel basin (NE Spain), based on stable isotope (δ18O) and megasequential evolution. Terranova 26, 337-346.

Ezquerro, L., Moretti, M., Liesa, C.L, Luzón, A., Simón, J.L., 2015. Seismites from a well core of palustrine deposits as a tool for reconstructing the palaeoseismic record of a fault. Tectonophysics 655, 191–205.

~~Faulds, J.E., Geissman, J.W., Mawer, C.K., 1990. Structural development of a major extensional accommodation zone in the Basin and Range Province, northwestern Arizona and southern Nevada; implications for kinematic models of continental extension. In: Wernicke, B.P. (Ed.), Basin and Range Extensional Tectonics near the Latitude of Las Vegas, Nevada Geological Society of America Memoir 176, Boulder, Colorado, pp. 37–76.~~

Ferrill, A.D., Stamatakos, J.A., Sims, D., 1999. Normal fault corrugation: implications for growth ans seismicity of active normal faults. Journal of Structural Geology 21, 1027-1038.

Fossen, H., Rotevatn, A., 2016. Fault linkage and relay structures in extensional settings–A review. Earth Science Reviews 154, 14-28.

Freed, A.M., 2005. Earthquake triggering by static, dynamic, and postseismic stress transfer. Annual Review of Earth and Planetary Sciences 33, 335–367.

~~Frinzi, Y., Langer, S., 2012. Damage in step-overs may enable large cascading earthquakes. Geophys. Res. Lett. 39(16), L16303, doi:10.1029/2012GL052436~~

Gibbs, A.D., 1984. Structural evolution of extensional basin margins. Journal of the Geological Society, London 141, 609–620.

Godoy, A., Ramírez, J.I., Olivé, A., Moissenet, E., Aznar, J.M., Aragonés, E., Aguilar, M.J., Ramírez del Pozo, J., Leal, M.C., Jerez-Mir, L., Adrover, R., Goy, A., Comas, M.J., Alberdi, M.T., Giner, J., Gutiérrez-Elorza, M., Portero, J.M., Gabaldón, V., 1983. Mapa Geológico Nacional 1:50.000, hoja 567 (Teruel). Instituto Geológico y Minero, Madrid.

Granier, T., 1985. Origin, damping, and pattern of development of faults in granite. Tectonics 4, 721-737.

Gupta, S., Scholz, C.H., 2000. A model of normal fault interaction based on observations and theory. Journal of Structural Geology 22, 865-880.

Gutiérrez, F., Gutiérrez, M., Gracia, F.J., McCalpin, J.P., Lucha, P., Guerrero, J., 2008. Plio-Quaternary extensional seismotectonics and drainage network development in the central sector of the Iberian Range (NE Spain). Geomorphology 102, 21-42.

Gutiérrez, F., Gracia, F.J., Gutiérrez, M., Lucha, P., Guerrero, J., Carbonel, D., Galve, J.P., 2012. A review on Quaternary tectonic and nontectonic faults in the central sector of the Iberian Chain, NE Spain. Journal of Iberian Geology 38, 145-160.

Hanks, T.C., Kanamori, H., 1979. A moment magnitude scale. Journal of Geophysical Research 84, 2348-2350.

Herraiz, M., De Vicente, G., Lindo-Ñaupari, R., Giner, J., Simón, J.L., González-Casado, J.M., Vadillo, O., Rodríguez-Pascua, M.A., Cicuéndez, J.I., Casas, A., Cabañas, L., Rincón, P., Cortés, A.L., Ramírez, M., Lucini, M., 2000. The recent (upper Miocene to Quaternary) and present tectonic stress distributions in the Iberian Peninsula. Tectonics 19, 762-786.

Huggins, P., Watterson, J., Walsh, J.J., Childs, C., 1995. Relay zone geometry and displacement transfer between normal faults recorded in coal-mine plans. Journal of Structural Geology 12, 1741-1755.

Instituto Geográfico Nacional, 2010. Servicio de Información Símica del Instituto Geográfico Nacional. http://www.ign.es/ign/es/IGN/SisCatalogo.jsp. Accessed December 2010.

King, G.C.P., Stein, R.S., Lin, J., 1994. Static stress changes and the triggering of earthquakes. Bulletin of the Seismological Society of America 84, 935–953.

Krantz R.W., 1989. Orthorhombic fault patterns: the odd axis model and slip vector orientations. Tectonics 8, 483-495.

Lafuente, P., 2011. Tectónica activa y paleosismicidad de la falla de Concud (Cordillera Ibérica central). Ph.D. thesis, Universidad de Zaragoza.

Lafuente, P., Rodríguez-Pascua, M.A., Simón, J.L., Arlegui, L.E., Liesa, C.L., 2008. Sismitas en depósitos pliocenos y pleistocenos de la fosa de Teruel. Revista de la Sociedad Geológica de España 21, 133-149.

Lafuente, P., Arlegui, L.E., Liesa, C.L., Simón, J.L., 2011a. Paleoseismological analysis of an intraplate extensional structure: the Concud fault (Iberian Chain, Spain). International Journal of Earth Sciences 100, 1713-1732.

Lafuente, P,. Arlegui, L.E.,, Casado, I., Ezquerro, L., Liesa, C.L., Pueyo, Ó., Simón, J.L., 2011b. Geometría y cinemática de la zona de relevo entre las fallas neógeno-cuaternarias de Concud y Teruel (Cordillera Ibérica). Revista de la Sociedad Geológica de España 24, 117-132.

Lafuente, P., Arlegui, L.E., Liesa, C.L., Pueyo, Ó., Simón, J.L., 2014. Spatial and temporal variation of paleoseismic activity at an intraplate, historically quiescent structure: the Concud fault (Iberian Chain, Spain). Tectonophysics 632, 167-187.

~~Manighetti, I., D. Zigone, M. Campillo, F. Cotton, 2009. Self-similarity of the largest-scale segmentation of the faults: Implications for earthquake behavior, Earth Planet. Sci. Lett., 288(3–4), 370–381, doi:10.1016/j.epsl.2009.09.040.~~

McCalpin, J.P., 1996. Paleoseismology. Academic Press, San Diego.

Mercier, J.L., Carey-Gailhardis, E., 1989. Regional state of stress and characteristic fault kinematics instabilities sown by aftershock sequences: the aftershock sequences of the 1978 Thessaloniki (Greece) and 1980 Campania-Lucania (Italia) earthquakes as examples. Earth and Planetary Science Letters 92, 247-264.

Mohammadioun, B., Serva, L., 2001. Stress drop, slip type, earthquake magnitude, and seismic hazard. Bulletin of the Seismological Society of America 91, 694-707.

~~Moissenet, E., 1983. Aspectos de la neotectónica en la fosa de Teruel. In: Comba, J.A. (Ed.), Geología de España, Libro Jubilar J.M. Ríos, Vol. II. Instituto Geológico y Minero de España, Madrid, 427-446.~~

Moissenet, E., 1993. L’age et les déformations des terrases alluviales du Fossé de Teruel. In: El Cuaternario de España y Portugal, Vol. I. Instituto Geológico y Minero de España-AEQUA, Madrid, 267-279

Nicol, A., Watterson, J., Walsh, J.J., Childs, C., 1996. The shapes, major axis orientations and displacement patterns of fault surfaces. Journal of Structural Geology 18, 235-248.

Nieto-Samaniego, A.F., 1999. Stress, strain and fault patterns. Journal of Structural Geology 21, 1065-1070.

Opdyke, N., Mein, P., Lindsay, E., Pérez-González, A., Moissenet, E., Norton, V.L., 1997. Continental deposits, magnetostratigraphy and vertebrate paleontology, late Neogene of Eastern Spain. Palaeogeography, Palaeoclimatology, Palaeoecology 133, 129-148.

Pavlides, S., Caputo, R., 2004. Magnitude versus faults´ surface parameters: quantitative relationships from the Aegean Region. Tectonophysics 380, 159-188.

~~Pavlides S.B., Zhang P., Pantosti D. (eds), 1999. Earthquakes, active faulting, and paleoseismological studies for the reconstruction of the seismic history of faults, Tectonophysics, 308 (1–2), 1–298.~~

Peacock, D.C.P., 2002. Propagation, interaction and linkage in normal fault systems. Earth-Science Reviews 58, 121-142.

Peiro, A. (2016). Una posible prolongación septentrional de la Falla de Teruel y su interacción con la Falla de Concud. Trabajo Fin de Grado, Universidad de Zaragoza.

Peña, J.L., 1981. Las acumulaciones cuaternarias de la confluencia de los ríos Alfambra y Guadalaviar, en las cercanías de Teruel. En: Actas VII Coloquio de Geografía, Pamplona, 255-259.

Reches, Z., 1978. Analysis of faulting in three-dimensional strain fields. Tectonophysics 47, 109-129.

Reches, Z., Dieterich, J.H., 1983. Faulting of rocks in three-dimensional strain fields. I. Failure of rocks in polyaxial, servo-control experiments. Tectonophysics 95, 111-132.

Roca, E., Guimerà, J., 1992. The Neogene structure of the eastern Iberian margin: structural constraints on the crustal evolution of the Valencia trough (western Mediterranean). Tectonophys 203, 203-218.

Sánchez Fabre, M., 1989. Estudio geomorfológico de la Depresión de Alfambra-Teruel-Landete y sus rebordes montañosos. Ph.D. thesis, Universidad de Zaragoza.

Simón, J.L., 1982. Compresión y distensión alpinas en la Cadena Ibérica Oriental. Ph.D. thesis, Universidad de Zaragoza.

Simón, J.L., 1983. Tectónica y neotectónica del sistema de fosas de Teruel. Teruel 69, 21-97.

Simón, J.L., 1989. Late Cenozoic stress field and fracturing in the Iberian Chain and Ebro Basin (Spain). Journal of Structural Geology 11, 285-294.

Simón, J.L., Arlegui, L.E., Liesa, C.L., 2008. Stress partitioning: a practical concept for analysing boundary conditions of brittle deformation. Geodinamica Acta 53, 1057-1065.

Simón, J.L., Arlegui, L.E., Lafuente, P., Liesa, C.L., 2012. Active extensional faults in the central-eastern Iberian Chain, Spain. Journal of Iberian Geology 38, 127-144.

Simón, J.L., Arlegui, L.E., Ezquerro, L., Lafuente, P., Liesa, C.L., Luzón, A., 2016. Enhaced paleoseismic succession at the Concud Fault (Iberian Chain, Spain): new insights for seismic hazard assessment. Natural Hazards 80, 1967-1993.

Stirling, M., Rhoades, D., Berryman, K., 2002. Comparison of Earthquake Scaling Relations Derived from Data of the Instrumental and Preinstrumental Era. Bulletin of the Seismological Society of America 92, 812-830.

Schwartz, D.P., Coppersmith, K.J., 1984. Fault behaviour and characteristic earthquakes: Examples form the Wasatch and San Andreas Faults, Journal of Geophysical Research 89, 5681-5698.

Vegas, R., Fontboté, J.M., Banda, E., 1979. Widespread Neogene rifting superimposed on alpine regions of the Iberian Peninsula. In: Proceedings Symposium Evolution and Tectonics of the

Western Mediterranean and Surrounding Areas,Viena. Instituto Geográfico Nacional, Madrid, Special Publication 201, 109-128.

Villamor, P., Berryman, K.R., 1999. La tasa de desplazamiento de una falla como aproximación de primer orden en las estimaciones de peligrosidad sísmica. I Congreso Nacional de Ingeniería Sismica, Asociación Española de Ingeniería Sísmica, Abstracts, 1.

Walsh, J.J., Bailey, W.R., Childs, C., Nicol, A., Bonson, C.G., 2003. Formation of segmented normal faults: a 3-D perspective. Journal of Structural Geology 25, 1251–1262.

Walsh, J.J., Watterson, J., 1991. Geometric and kinematic coherence and scale effects in normal fault systems. In: Roberts, A.M., Yielding, G., Freeman, B. (Eds.), The Geometry of Normal Faults, Geological Society Special Publication No 56, 193-203.

Weerd, A. van de, 1976. Rodent faunas of the Mio-Pliocene continental sediments of the Teruel-Alfambra region, Spain. Utrecht Micropaleontology Bulletin, Special Publication 2, 1-185.

Wells, D.L., Coppersmith, K.J., 1994. New Empirical Relationships among Magnitude, Rupture Length, Rupture Width, Rupture Area, and Surface Displacement. Bulletin of the Seismological Society of America 84, 974-1002.

Wesnousky, S.G., 2008. Displacement and Geometrical Characteristics of Earthquake Surface Ruptures: Issues and Implications for Seismic-Hazard Analysis and the Process of Earthquake Rupture. Bulletin of the Seismological Society of America 98,1609-1632.

FIGURE CAPTIONS

Fig. 1. Location of the Teruel Fault within the Teruel Graben system, eastern Spain. Inset: sketch of the main Alpine chains within the Iberian Peninsula.

Fig. 2. Structure of the Teruel Fault. (a) Geological map. MVS: Mansuetos-Valdecebro syncline. (b) Cross section (see location in a). (c) Partial outcrop view of the main fault zone cutting the Rojo 2 unit within the Teruel urban area (see location in a). (d) Equal-area plot (lower hemisphere) showing orientations of measured planes and striations along the main fault. Black: data from central and southern sectors, showing an overall transport direction (red dot) towards N275ºE. Grey: Las Ramblillas fault.

Fig. 3. (a) Structural contour map of the base of Páramo 2 (youngest pre-rift unit relative to the Late Pliocene-Quaternary extensional period) at the relay zone between the Teruel and Concud faults. (b) 3D scheme of the relay structure reconstructed from the previous map. (c) Distribution of vertical displacement (throw) along fault length (D-L profiles) for the Concud and Teruel faults, obtained from the structural contour map. Modified from Lafuente et al. (2011b).

Fig. 4. Deformation at Las Ramblillas site, revealing hypothetic prolongation of the Teruel Fault. (a) Panoramic view. (b) Interpretation sketch. V: Villafranchian pediment; T2b: Middle Terrace of Alfambra River; T0: Holocene terrace; Qa: Quaternary alluvial pediment.

Fig. 5. Aspects of local geology of the Pitraque-Valdelobos area. (a) Detailed geological map (see location in Fig. 2a). (b) Outcrop view of the main Teruel Fault branch (M) north of Puntal del Pitraque (see location in Fig. 2a). (c) Overall field view. (d) Equal-area plot (lower hemisphere) of the main macroscale fault planes, and one observed striation. (e) Schematic cross section showing offset of the Middle Terrace T2a (see location on Fig. 5a). (f) Laser-

levelling profile along the talweg of Valdelobos gully (sector shown in map a), showing the location chosen for the Valdelobos trench. M, N, P, Q, R, S: fault branches referred to in the text; R1, R2, and P2: Rojo 1, Rojo 2, and Páramo 2 units, respectively; T2a: Middle Terrace of the Turia River; T0: Holocene terrace; QA: Holocene alluvium and colluvium.

Fig. 6. Meso-scale fracturing at the Pitraque 1 and Pitraque 2 site (equal-area plots, lower hemisphere). (a) Vertical, low height aerial photograph with structural sketch. (b) Fault planes and striations observed on the natural terrace scarp. (c) Idem in Pitraque 1 trench. (d) Idem in Pitraque 2 trench. (e) Synthetic rose diagram of fault strikes measured in the whole site. Fμ, Fδ, Fα, Fβ: faults referred to in the text; R2: Rojo 2 unit; P2: Páramo 2 unit; T2a: Middle Terrace of the Turia River.

Fig. 7. (a) Detailed cross section of Pitraque 1 trench. R2: Rojo 2 unit; P2: Páramo 2 unit; 1, 2, 3, 4, 5, 6: Pleistocene units described in the text; light-grey stripes: carbonate; Fγ, Fα, Fδ: faults referred to in the text; location (asterisks) and age of samples dated by OSL is indicated. (b) (c) (d) (e) Stereoplots (equal-area, lower hemisphere; symbols as in Fig. 6) of meso-scale fractures measured in domains 1, 2, 3 and 4, respectively. (f) Poles to bedding measured in all sedimentary units, and inferred movement plane (M).

Fig. 8. (a) Detailed cross section of trench Pitraque 2. R2: Rojo 2 unit; P2: Páramo 2 unit; 1, 2, 3, 4: Pleistocene units described in the text; light-grey stripes: carbonate; Fβ, Fα: faults referred to in the text; location (asterisks) and age of samples dated by OSL is indicated. (b) Detail photograph of domain 1 in (a). (c) (d) Stereoplots (equal-area, lower hemisphere; symbols as in Fig. 6) of meso-scale fractures measured in domains 1 and 2, respectively. (e) Idem in the opposite, not logged trench wall.

Fig. 9. Detailed cross section of Valdelobos trench. R2: Rojo 2 unit; 1, 2, 3, 4, 5: Quaternary units described in the text; Fε: active fault; location (asterisks) and age of samples dated by OSL is indicated.

Fig. 10. Chronological sketch of paleoseismic events recorded at the overall Concud Fault (complete paleoseismic succession reconstructed by Simón et al., 2016), its southern branch (El Hocino trenches; Lafuente et al., 2104), and the Teruel Fault (this work).

Fig. 11. Comparison between seismic succession reconstructed for the southern branch of the Concud Fault (Lafuente et al., 2014) and for the Teruel Fault (M and P branches, present work). (a) Kinematic data for the southern branch of the Concud Fault at El Hocino site: equal-area, lower hemisphere stereoplot of fault planes and striations, and prevailing transport direction. (b) Slip history of the southern branch of the Concud Fault, as inferred from the palaeosesimic succession at El Hocino trenches; slip rates inferred from that succession and from offset of a morpho-sedimentary marker (pediment cover) are expressed as dotted lines. (c) and (d): Idem as a and b, respectively, for the western branches of the Teruel Fault at Pitraque-Valdelobos site (offset marker in this case: top of fluvial terrace T2a).

Fig. 12. Proposed model of stress/strain partitioning at the scale of seismic cycle for the activity of the Teruel and Concud faults. (a) (b) (c) (d) Sketches of succesive, alternating slip on both faults favoured by stress release on each fault after a seismic event (see explanation in text); large arrows: transport directions; stereoplots: active fault (plane and prevailing striation) for each seismic event, and oriention of stress axes (σ_1, σ_2 and σ_3) of the most representative stress systems ~~responsible for such movements~~ (according to palaeostress analysis by Lafuente, 2011). (e) Simplified model for the overall fracture systems in the Teruel area, and kinematic interpretation according to the model proposed by Reches (1978); X, Y, Z: virtual strain axes representing the bulk finite deformation. ~~achieved by accumulating the variety of incremental fault slips.~~

TABLE 1:

Level	Age	Sublevel	Height above talweg (m)	Numerical age	Dating method	References
Upper	Early Pleistocene (?)	T3	85-90	Unknown		
Middel	Middle Pleistocene	T2b	45-65	250 (± 32) to 116 (± 4) ka	U/Th	Arlegui et al. (2005); Gutiérrez et al. (2008)
		T2a	40-45	90.5 (± 5.3) to 76.0 (± 5.0) ka	OSL	Lafuente et al. (2008); Simón et al. (2012)
Lower	Late Pleistocene	T1c	20-30	22.0 (± 1.6) ka	OSL	Lafuente (2011)
		T1b	15-20	14.9 (± 1.0) to 15.6 (± 1.3) ka	OSL	Lafuente et al. (2008); Gutiérrez et al. (2008)
		T1a	10-15	Unknown		
Subactual	Holocene	T0	3-5	3.4 (± 0.7) ka	OSL	Lafuente (2011)

Table 1. Levels of fluvial terraces defined in the Teruel area (Alfambra and Turia rivers).

TABLE 2:

Scenario Paleoseismic parameters		Wells & Coppersmith (1994)	Stirling *et al.* (2002)	Pavlides & Caputo (2004) (*) (**)	Mohammadioun & Serva (2001) (*) (***)	
Length of 9 km					100 bar	30 bar
Moment magnitude (M_w)		6.12	6.64	6.35	6.26	5.73
Coseismic slip (m)	Vertical	-	-	0.55	-	-
	Net	0.37	1.28	0.59	-	-
Length of 11 km						
Moment magnitude (M_w)		6.23	6.71	6.41	6.39	5.87
Coseismic slip (m)	Vertical	-	-	0.60	-	-
	Net	0.40	1.32	0.65	-	-
Length of 23 km (linked Concud and Teruel faults)						
Moment magnitude (M_w)		6.66	6.96	6.62	6.88	6.36
Coseismic slip (m)	Vertical	-	-	0.66	-	-
	Net	1.19	2.43	0.71	-	-

Table 2. Moment magnitude and coseismic slip for the Teruel Fault estimated from empirical relationships for three different scenarios. ([a]) Obtained M_s values have been transformed to M_w by applying the relationship of Konstantinou et al. (2005): $M_w = 0.76\ M_s + 1.53$. ([b]) Vertical displacement initially yielded by this correlation has been translated into net displacement considering an average dip of 68º and a pure normal movement of the Teruel Fault. ([c]) Moment magnitudes according to Mohammadioun and Serva (2001) have been calculated for stress drop scenarios of 100 and 30 bar.

TABLE 3:

Sample	Laboratory reference	Lithological unit	Equivalent dose (Gy)	Annual dose (mGy/yr)	Supralinearity (Gy)	K factor	OSL age (ka B.P.)
Trench: Pitraque 1							
P1-4	MAD-6076SDA	Fluvial terrace (Unit 1)	170.46	2.41	0	0.19	70.730 ± 5.259
P1-5	MAD-6077SDA	Fluvial terrace (Unit 2)	124.93	1.74	0	0.12	71.798 ± 5.059
P1-6	MAD-6078BIN	Fluvial terrace (Unit 5)	77.57	1.60	0	0.11	48.481 ± 3.801
Trench: Pitraque 2							
P2-1	MAD-6079SDA	Fluvial terrace (Unit 1)	130.05	1.66	0	0.14	78.343 ± 5.189
P2-7	MAD-6081BIN	Fluvial terrace (Unit 2)	91.95	1.84	0	0.11	49.972 ± 3.365
P2-5	MAD-6080SDA	Fluvial terrace (Unit 3)	127.80	2.75	0	0.14	46.472 ± 3.147
Trench: Valdelobos							
VL-C1	MAD-6073SDA	Fluvial terrace (Unit 2)	112.82	4.23	0	0.16	26.671 ± 1.912
VL-B2	MAD-6074SDA	Fluvial terrace (Unit 3)	16.97	1.71	0	0.23	9.923 ± 0.690

Table 3. OSL dating of samples collected from trenches at the Teruel fault.

TABLE 4:

Teruel Fault event (renamed)	Original event at individual trench	Predating OSL age (ka B.P.)	Postdating OSL age (ka B.P.)	Absolute age constraints (ka)	Coseismic net slip (m)
Event 0	XP1 XP2		70.7 ± 5.3 78.3 ± 5.2	Pre-73.1	?
Event 1	YP1	70.7 ± 5.3	71.8 ± 5.1	76.0 – 66.7	0.1
Event 2	YP2	46.5 ± 3.1		Post-49.6	0.5
Event 3	ZP1 ZP2	48.5 ± 3.8 46.5 ± 3.1		Post-49.6	> 1.1
Event 4	ZVL	26.7 ± 1.9	9.9 ± 0.7	28.6 – 9.2	> 0.3

Table 4. Summary of paleoseismic events of the Teruel Fault interpreted and correlated from the studied trenches: Pitraque 1 (P1), Pitraque 2 (P2) and Valdelobos (VL). Absolute age constraints take into account the error bar for each OSL age.

TABLE 5:

Marker / data source	Age / time window	Teruel Fault (this work)			Concud Fault (*)		
		Net slip (m)	Slip rate (mm/a)		Net slip (m) (**)	Slip rate (mm/a)	
			Overall	Partial (In 1-2 branches among 4-5)		Overall	Partial (In 1 branches among 2-3)
Trenching information							
Compilation of coseismic slip values	since 76.0 to 9.9 ka BP	1.7 - 2.0		0.03 – 0.05			
	since ca. 74 to 3.4 ka BP				20.5 (3.9)	0.29	0.05
Stratigraphic marker							
T2b terrace top	46.5 ± 3.2 ka	8.8		0.18 – 0.20			
T2a terrace top	282 – 112 ka				39	0.14 – 0.35	
Páramo 2 unit (Latest Ruscinian)	3.6 Ma	270	0.075		255 – 290	0.07 – 0.08	

Table 5. Summary of slip rates calculated for the Teruel and Concud faults from different markers and for different time windows. (*) Data for the Concud Fault are compiled from Gutiérrez et al. (2008), Lafuente (2011), Lafuente et al. (2011a, 2014), and Simón et al. (2016). (**) In parentheses, partial net displacement measured on one fault branch.

APPENDIX 1:

Description and age of sedimentary units exposed in trenches

Pitraque 1 trench

Neogene sediments comprise: (i) pedogenized massive brown lutites~~ with pedogenic features~~ (top of ~~the~~ Rojo 2 ~~clastic~~ unit); (ii) brecciated ~~and karstified~~ grey and white limestones ~~(mudstone or wackestone)~~ interbedding black and green marls with remains of gastropods and charophytes, representing ~~the~~ Páramo 2 carbonate unit. These materials correspond to the Genetic Unit 4 ~~Megasequence 3~~ of Ezquerro et al. (~~2014~~2017).

The Pleistocene succession has been subdivided into six units (1 to 6 in Fig. 7a):

Unit 1. Gravel ~~made of white~~ with Neogene limestone angular~~ to ~~-subrounded pebbles-~~ to ~~boulders and ~~brown and green~~ rip up clasts. It ~~Gravel ~~is grain-supported and crops out discontinuously below the erosive base of ~~the overlying~~ unit 2. Sample ~~A sample collected in this unit (~~P1-4~~; (~~see location in Fig. 7a) yielded an OSL age of 70.7 ± 5.3 ka (Table 2).

Unit 2. Greyish and yellowish gravel with interbedded brown, fine- to coarse-grained sand ~~levels~~. Gravel is grain-supported and ~~composed by~~ made of angular~~ to ~~-subangular carbonate and siliceous pebbles and cobbles up to 14 cm in diameter;~~.~~ ~~Internal erosive surfaces individualise~~ it shows trough cross-bedding ~~sets indicating paleocurrent towards SW~~. Sand forms ~~appears in~~ decimetre-scale, tabular levels with parallel and cross-lamination, and ripples. Sample P1-5 (see location in Fig. 7a) yielded an OSL age of 71.8 ± 5.1 ka (Table 2).

Unit 3. Grey gravel with encased brown medium-grained sand lenses with floating clasts up to 3 cm in diameter. Gravel is grain-supported and made of angular~~ to ~~-subrounded limestone and siliceous pebbles and cobbles up to 24 cm in diameter; it shows pebble-granule cycles and trough cross-bedding ~~in decametre-thick sets~~. ~~Sand is massive and contains floating clasts up to 3 cm in diameter.~~

Unit 4. Grey gravel with interbedded medium to coarse-grained brown sand. Gravel is grain-supported with ~~homometric,~~ subangular-~~ to ~~subrounded limestone clasts up to 8 cm in diameter and trough~~. Trough ~~cross-bedding ~~can be recognised indicating SW-directed paleocurrents~~. Sand makes laminated lensoid or tabular bodies ~~with horizontal lamination~~.

Unit 5. Grey gravel with encased coarse-grained brown sand. Gravel, grain-supported, is composed of ~~homometric~~, angular-~~ to-~~subangular clasts up to 6 cm in diameter. Horizontal bedding (pebble-granule cycles) ~~is evident and~~ merges laterally into ~~towards the SE into~~ trough cross-bedding sets. Sand makes tabular levels with parallel lamination~~,~~ and ~~contains~~ floating grey limestone clasts up to 1 cm in diameter. Sample P1-6 (see location in Fig. 7a) yielded an OSL age of 48.5 ± 3.8 ka (Table 2).

Unit 6. Regolith. ~~consisting of b~~Brown lutite with scattered centimetre-scale limestone clasts, carbonate nodules, and root traces.

Pitraque 2 trench

Neogene sediments are similar to those described in Pitraque 1 trench (Rojo 2 and Páramo 2 units). The overlying Pleistocene materials have been subdivided into four units (1 to 4 in Fig. 8a):

Unit 1. Grey and brown, grain-supported gravel with rare sand. Gravel is made of angular-~~ to-~~subangular limestone and siliceous-pebbles and cobbles up to 18 cm in diameter;~~.~~ ~~I~~it shows planar cross-stratification and interbbedded ~~coarse~~ sand levels in the lower part. Sample P2-1 ~~from this unit~~ (see location in Fig. 8a) has an OSL age of 78.3 ± 5.2 ka BP (Table 2).

Unit 2. Grey and brown gravel with intercalated brown very coarse-grained sand towards the top ~~of the unit~~. Gravel, ~~consists of angular limestone and siliceous pebbles and cobbles up to 16 cm in diameter, being~~ matrix-supported at the base and ~~turning into~~ grain-supported topwards, consists of angular limestone and siliceous pebbles and cobbles up to 16 cm in diameter and shows c~~. C~~ross-bedding ~~indicates SW-directed paleocurrents~~. Sand forms a slightly channelled body with angular, grey limestone floating clasts (up to 2 cm ~~in diameter~~), and armoured clay balls (up to 16 cm). Sample P2-7 ~~at the base of this unit~~ (Fig. 8a) yielded an OSL age of 50.0 ± 3.4 ka (Table 2).

Unit 3. Gravel with interbbeded centimetre-thick ~~scale~~ levels of fine- to coarse-grained sand. Gravel, ~~commonly~~ mainly grain-supported, is made of ~~homometric~~ angular limestone pebbles and cobbles, and forms ~~making~~ a tabular body in the lower part and a channel in the upper part. The channel is composed by larger clasts (up to 15 cm ~~in diameter~~) and shows planar cross-bedding ~~indicating SW paleocurrents~~. Sand makes irregular levels with horizontal and cross-lamination. Its base has an OSL age (sample P2-5) of 46.5 ± 3.1 ka (Table 2).

Unit 4. Regolith. ~~consisting of b~~Brown lutite with carbonate nodules, root traces and scattered centimetre-scale limestone clasts.

Valdelobos trench

Massive red Neogene lutites (Rojo 2) are covered by ~~a succession of~~ Quaternary ~~fluvial and~~ alluvial deposits in which five units have been distinguished (1 to 5 in Fig. 9):

Unit 1. Massive brown lutite with grey patches, carbonate nodules and interbedded fine- to medium-grained sand ~~that grades laterally into brown silt and includes~~ with carbonate granules ~~clasts up to 5 mm in diameter.~~ that grades laterally into brown silt ~~and includes~~.

Unit 2. Coarse-grained sand with white and grey carbonate and black quartzite granules~~.~~ in ~~It makes~~ a coarsening upward channelled body ~~with coarsening upwards evolution, preserved~~ close to a fault plane in the middle part of the trench. ~~A s~~Sample ~~(~~VL-C1)~~,~~ (Fig. 9) yielded an OSL age of 26.7 ± 1.9 ka BP (Table 2).

Unit 3**.** Channeled ~~body with~~ highly erosive body ~~base integrated by~~ with brown gravel in the lower part and medium-grained sand and lutites in the upper part. Gravel is made of subangular~~-to-~~ subrounded white carbonate (up to 8 cm in diameter) and brown and red siliceous clasts (up to 3 cm); it shows horizontal bedding and~~, as well as~~ imbricated clasts ~~broadly indicating a SW-directed paleocurrent~~. Sand forms tabular levels with parallel lamination and low angle cross-stratification. Some mud boulders have been recognized, up to ~~with~~ ~~a maximum diameter of~~ 88 cm exist. Sample VL-B2 ~~collected in this unit~~ (Fig. 9) yielded an OSL age of 9.9 ± 6.9 ka BP (Table 2).

Unit 4. Gravel (lower part) and coarse-grained sand (upper part) arranged in a dominantly red, tabular and fining-upwards ~~body with~~ erosive body with~~,~~ locally channelled~~,~~ base. Gravel, m~~M~~atrix-supported, ~~gravel~~ is made of white, subangular~~-to-~~subrounded carbonate clasts, up to 15 cm in diameter. Sand shows parallel lamination, ripples, scattered clasts and rare mud boulders.

Unit 5. Greyish grain-supported gravel in a tabular body with erosive base and horizontal stratification made of fining upwards sequences. It is ~~grain-supported,~~ composed by sugangular~~-to-~~ subrounded white carbonate clasts (up to 7 cm in diameter), subrounded orange siliceous clasts (up to 4 cm), and ~~locally~~ rare ~~some~~ mud boulders ~~broadly indicates paleocurrent towards SW~~. It supplied two fragments of clay teals (historical times, post-Middle Age). ~~have been found~~ ~~within this unit which indicates that it belongs to~~

***Figure**

Click here to download high resolution image

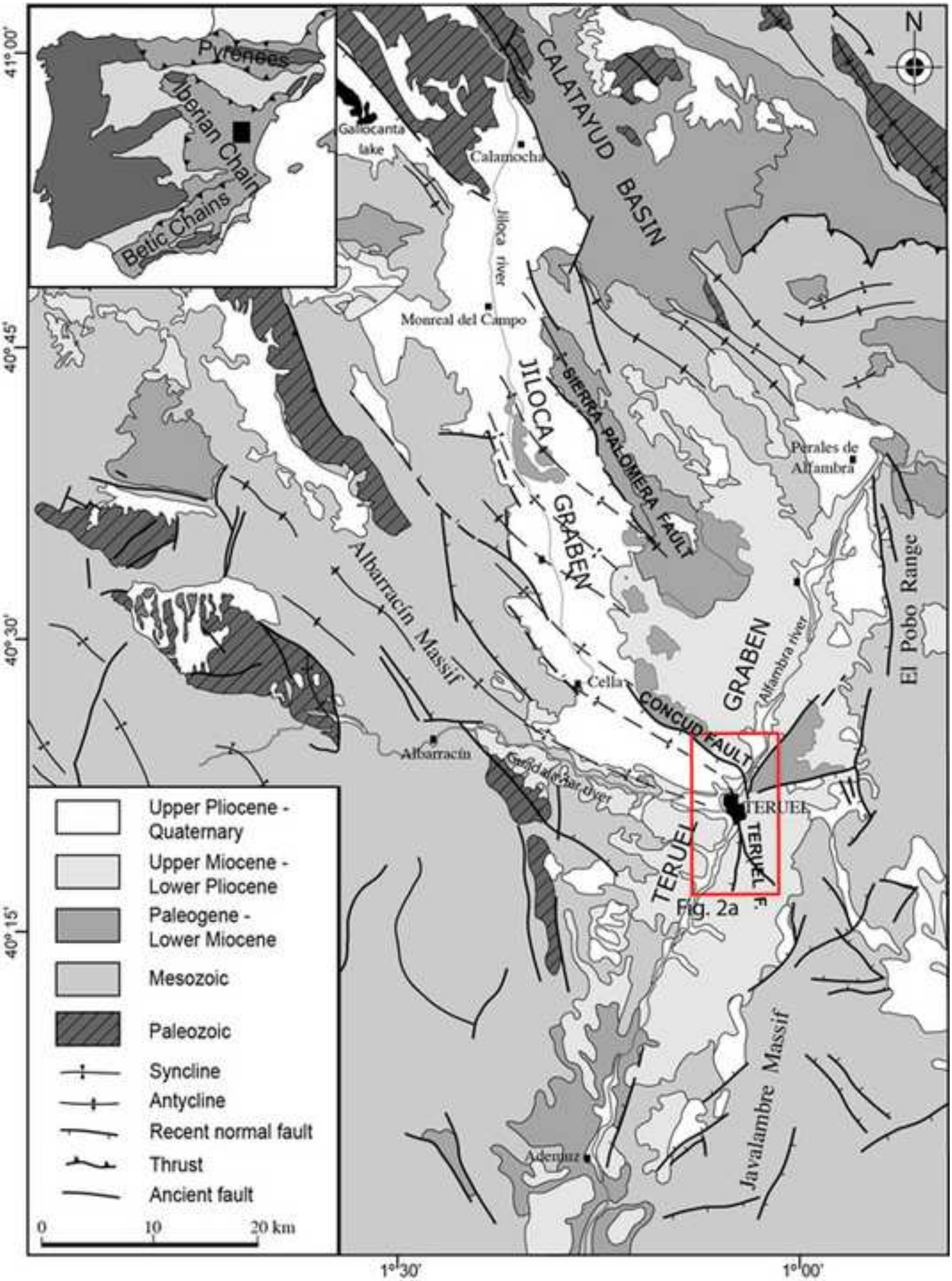

*Figure
Click here to download high resolution image

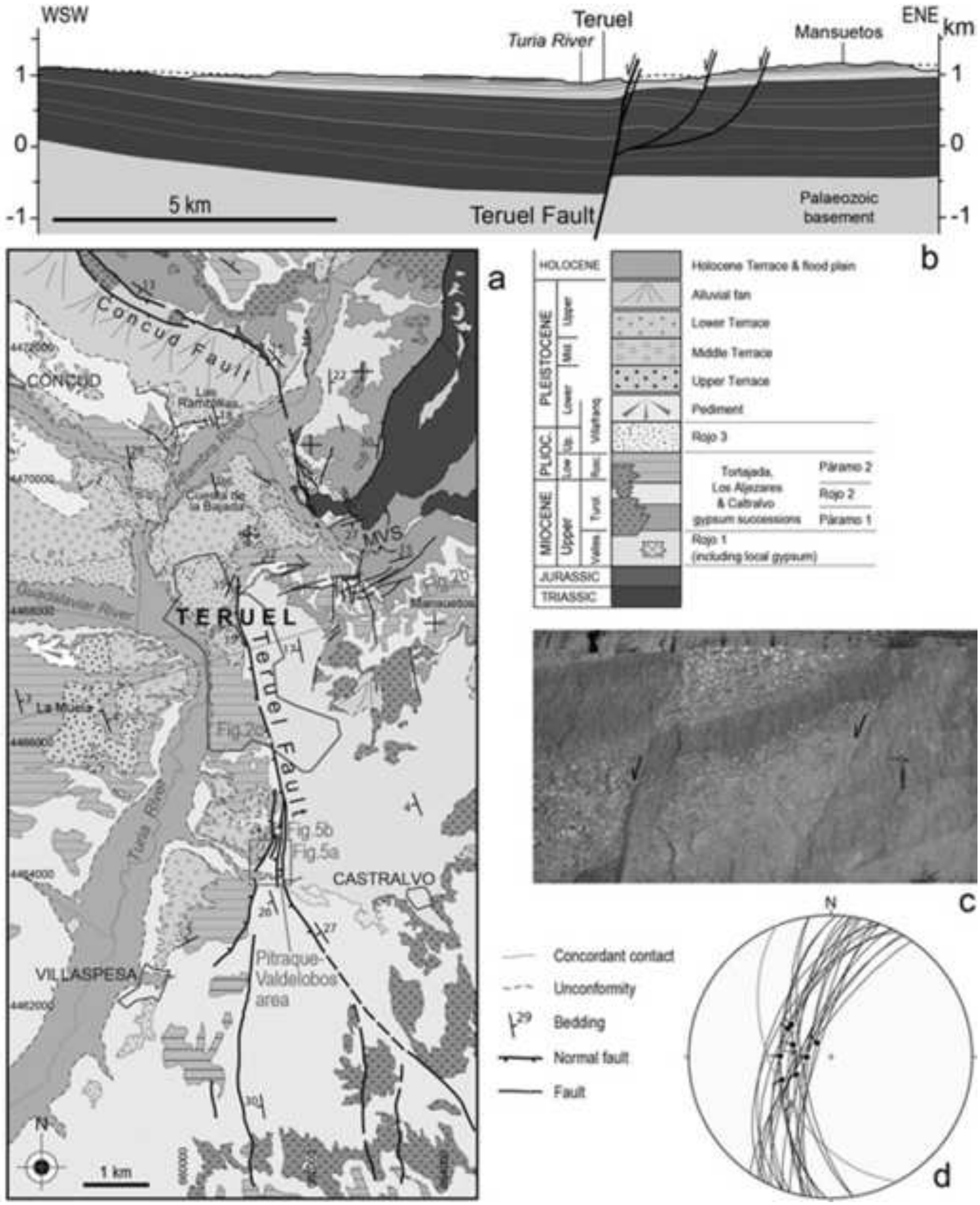

***Figure**

Click here to download high resolution image

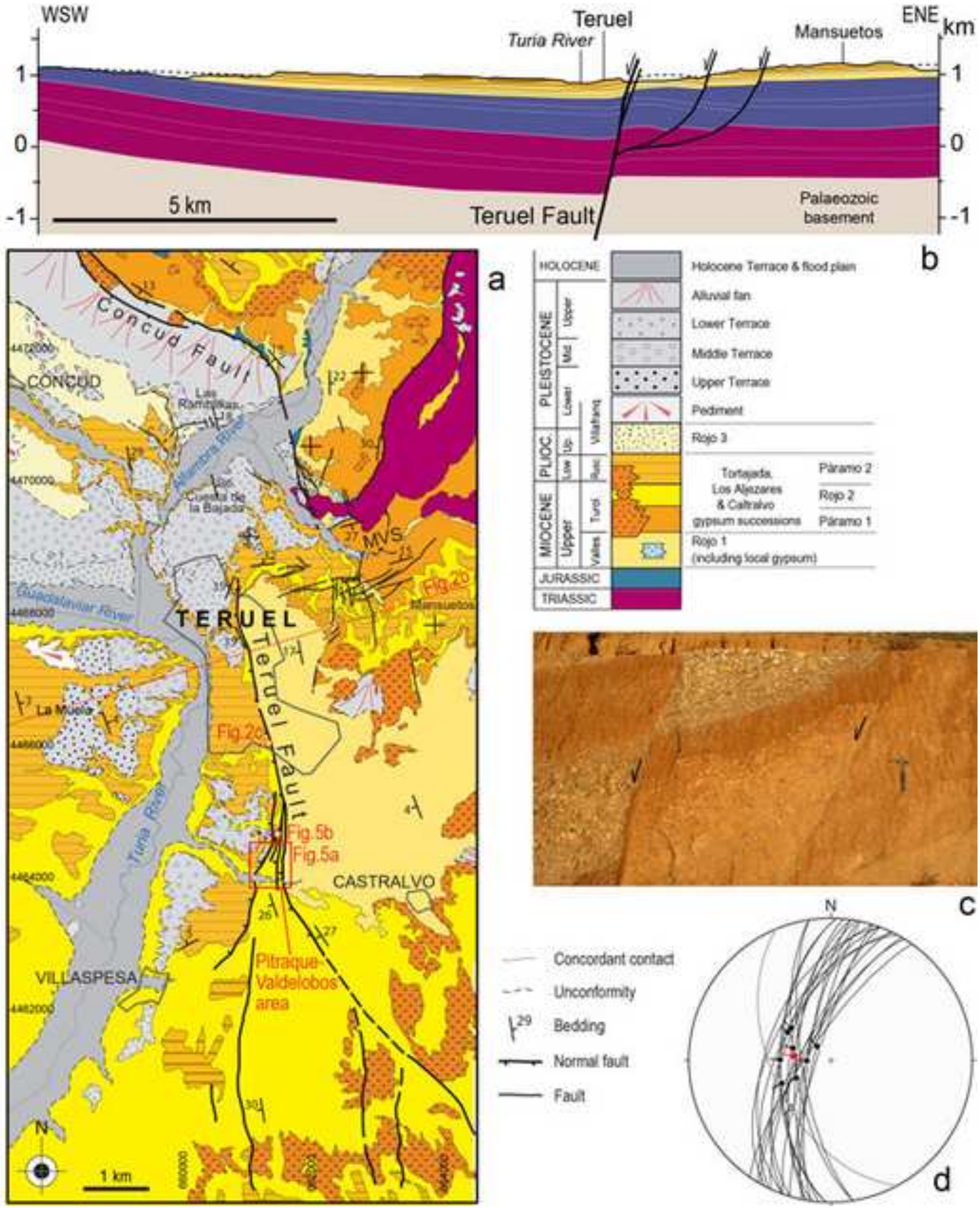

Figure

Click here to download high resolution image

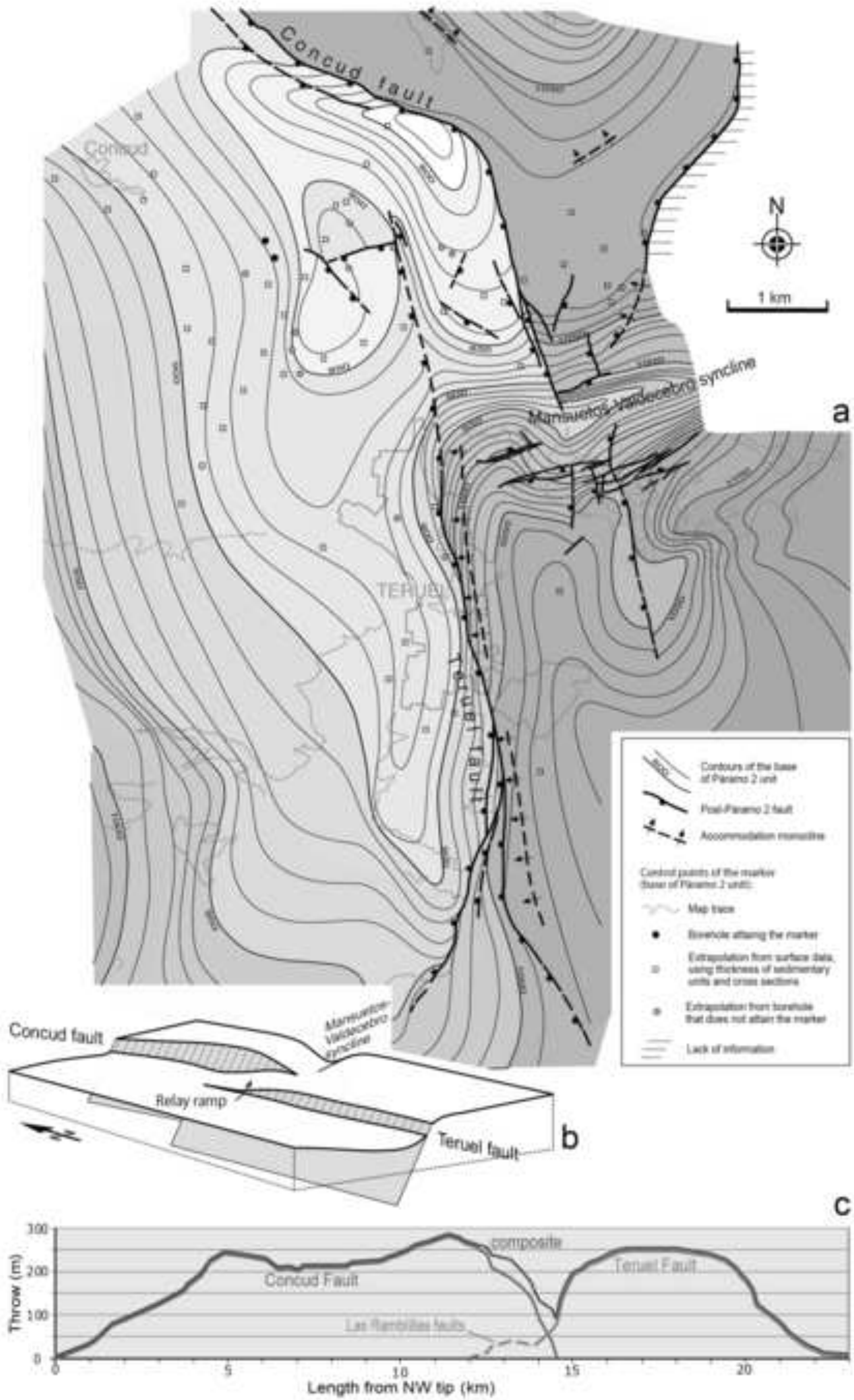

Figure
Click here to download high resolution image

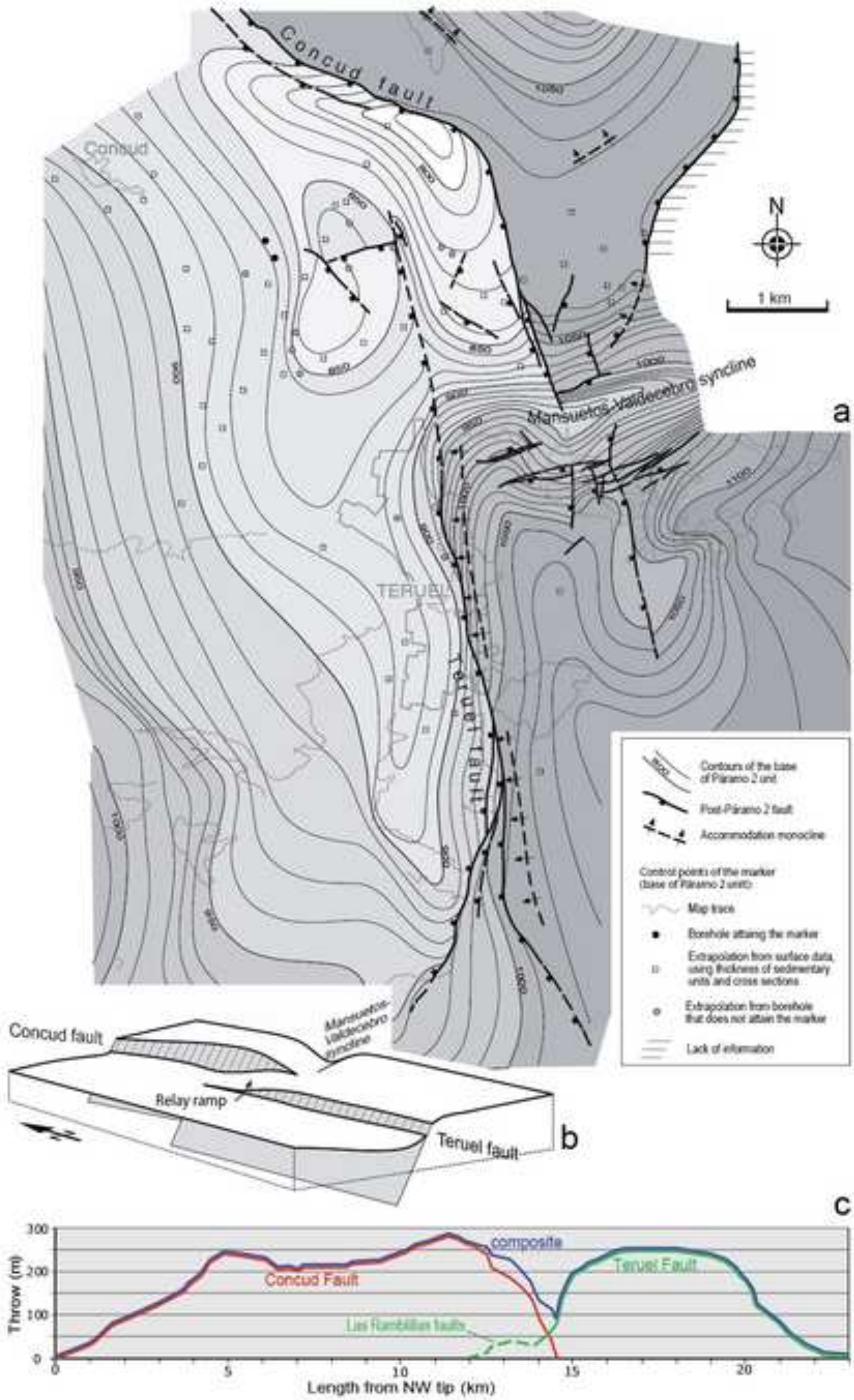

Figure
Click here to download high resolution image

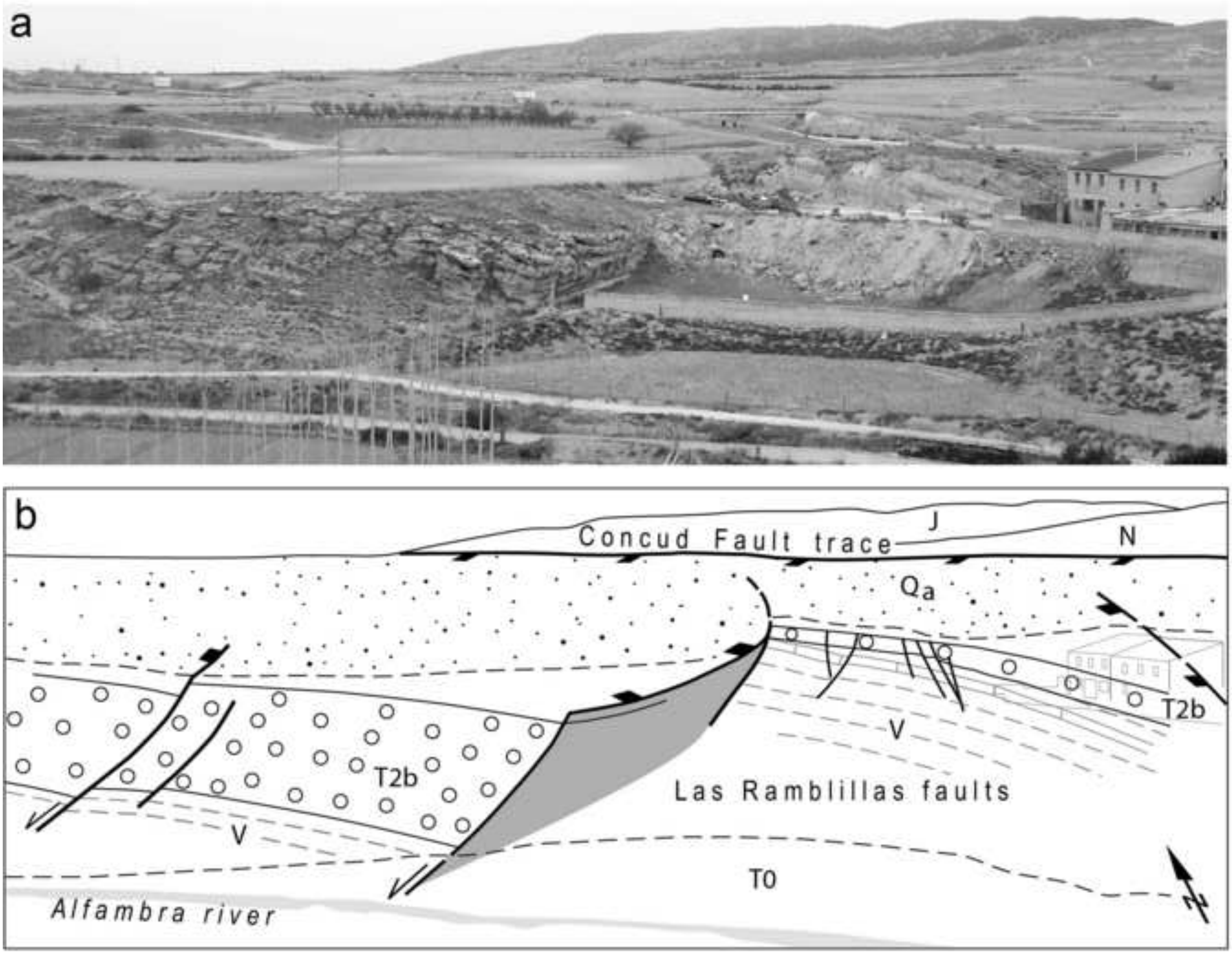

Figure

Click here to download high resolution image

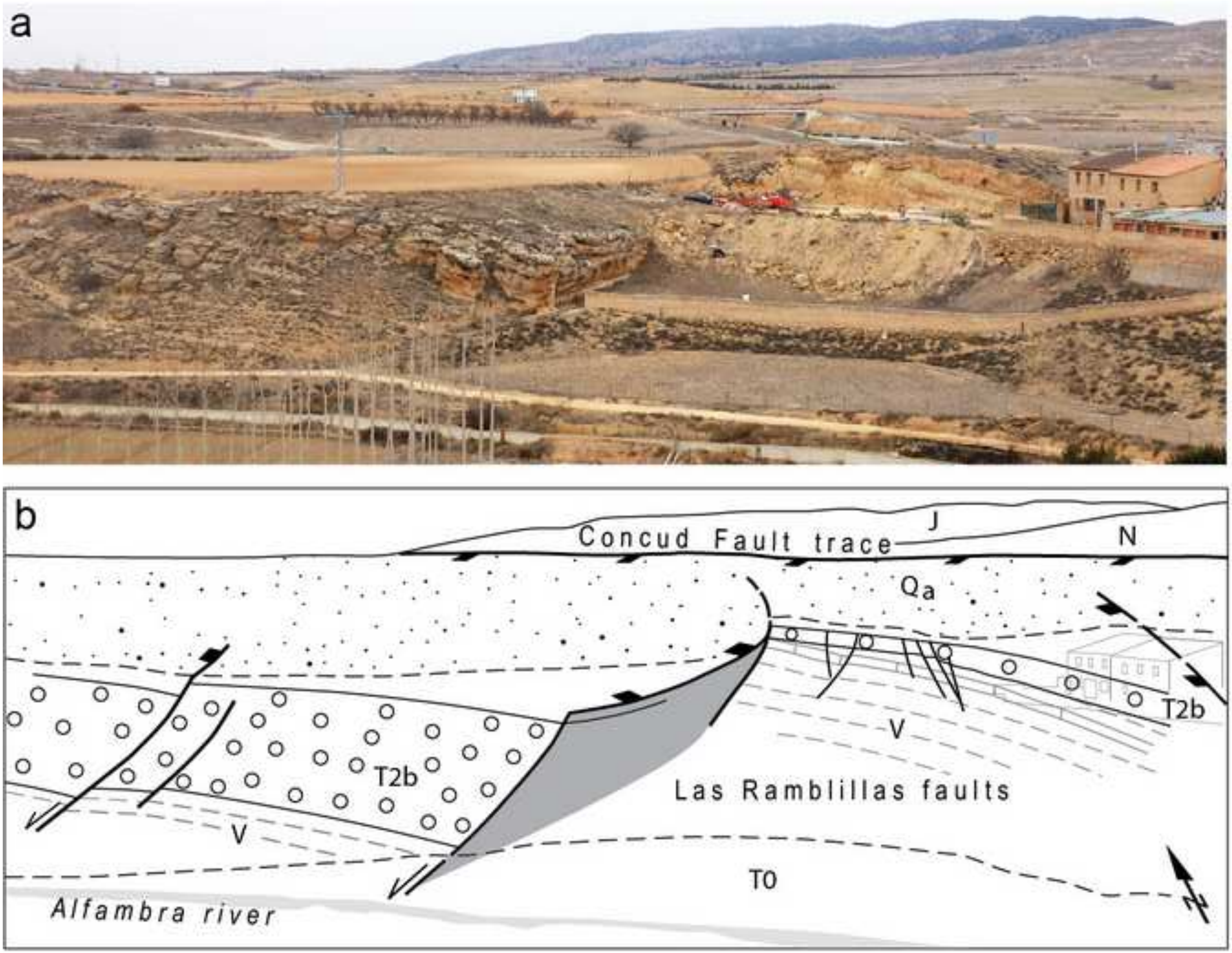

***Figure**

Click here to download high resolution image

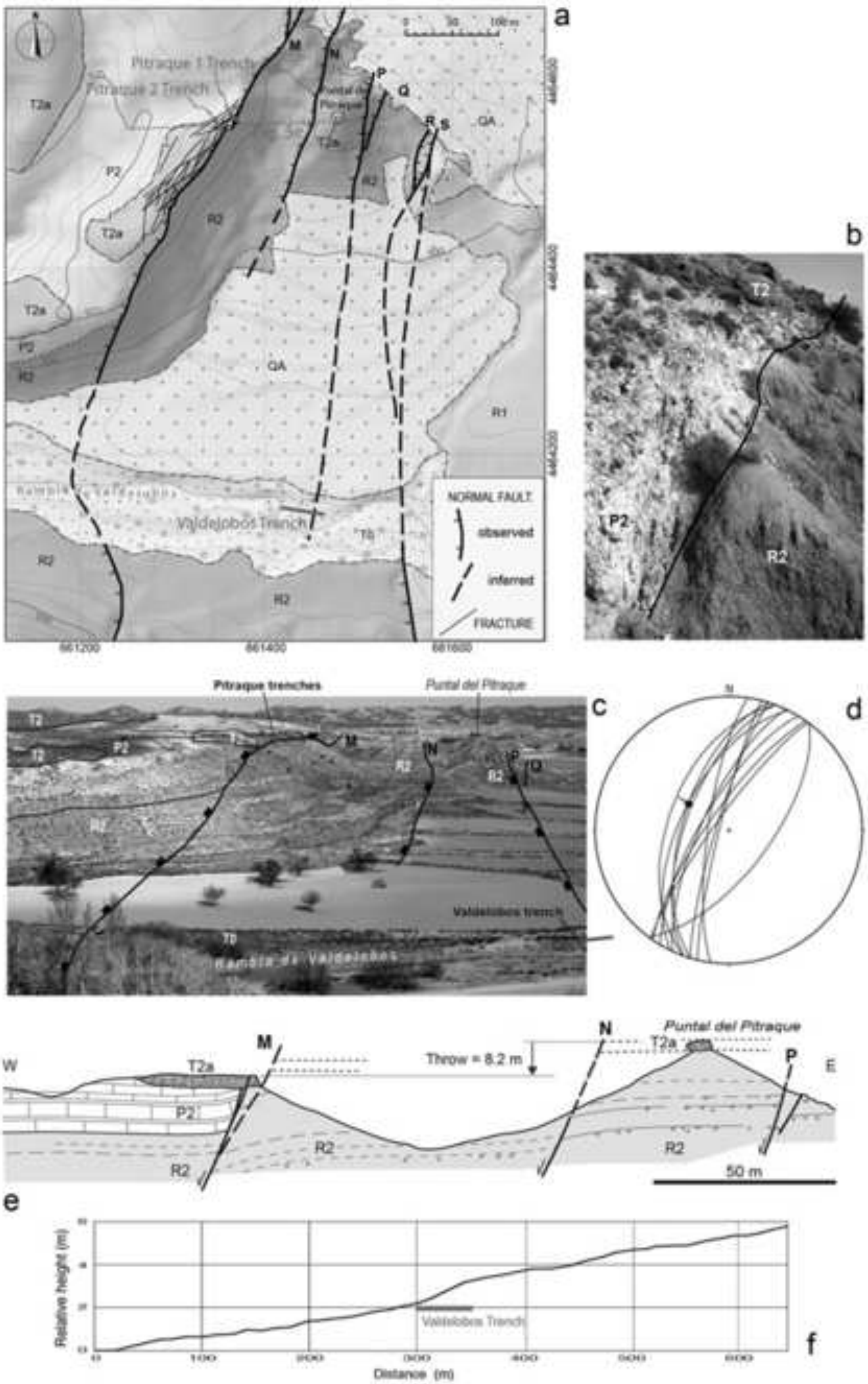

*Figure
Click here to download high resolution image

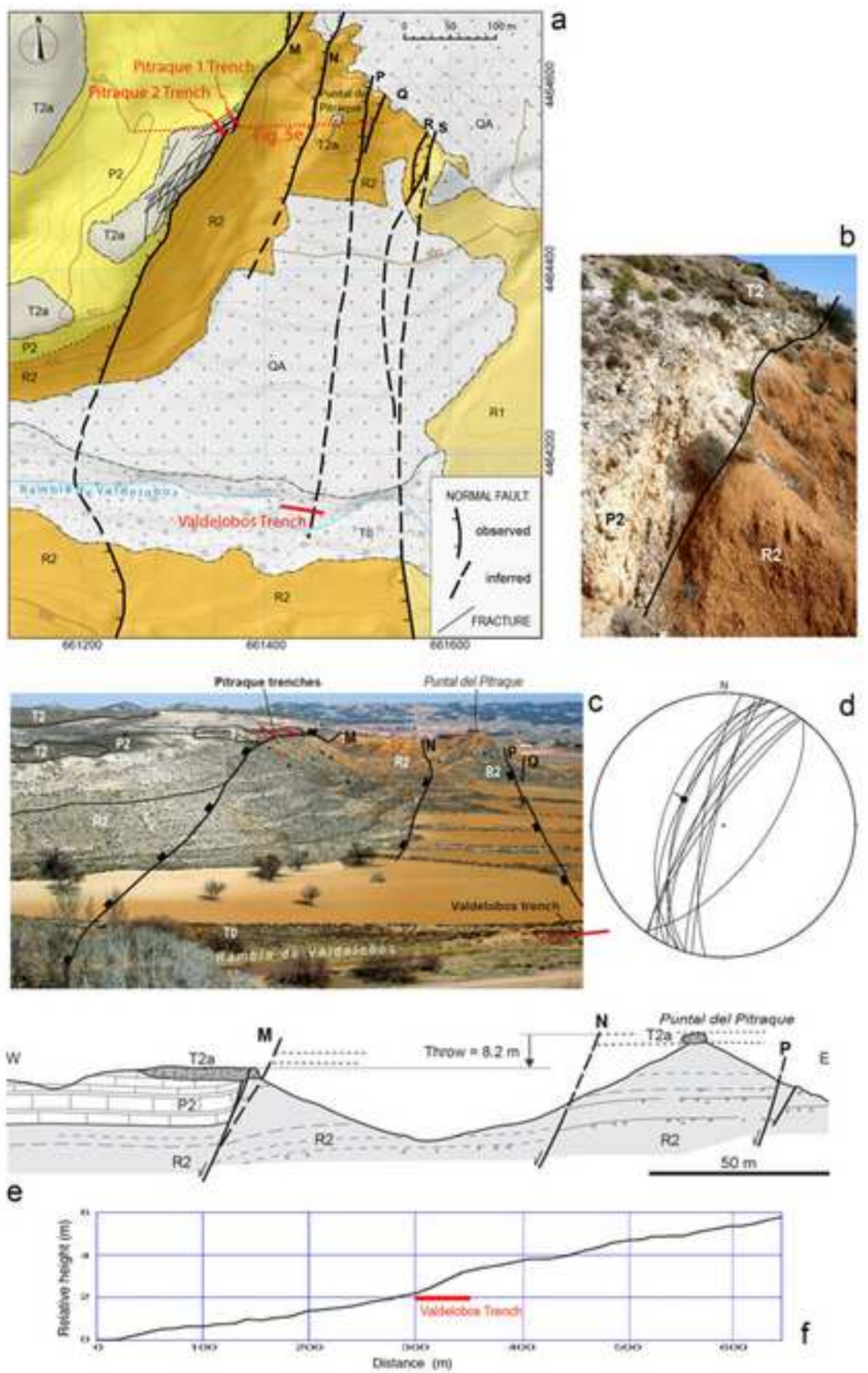

Figure
Click here to download high resolution image

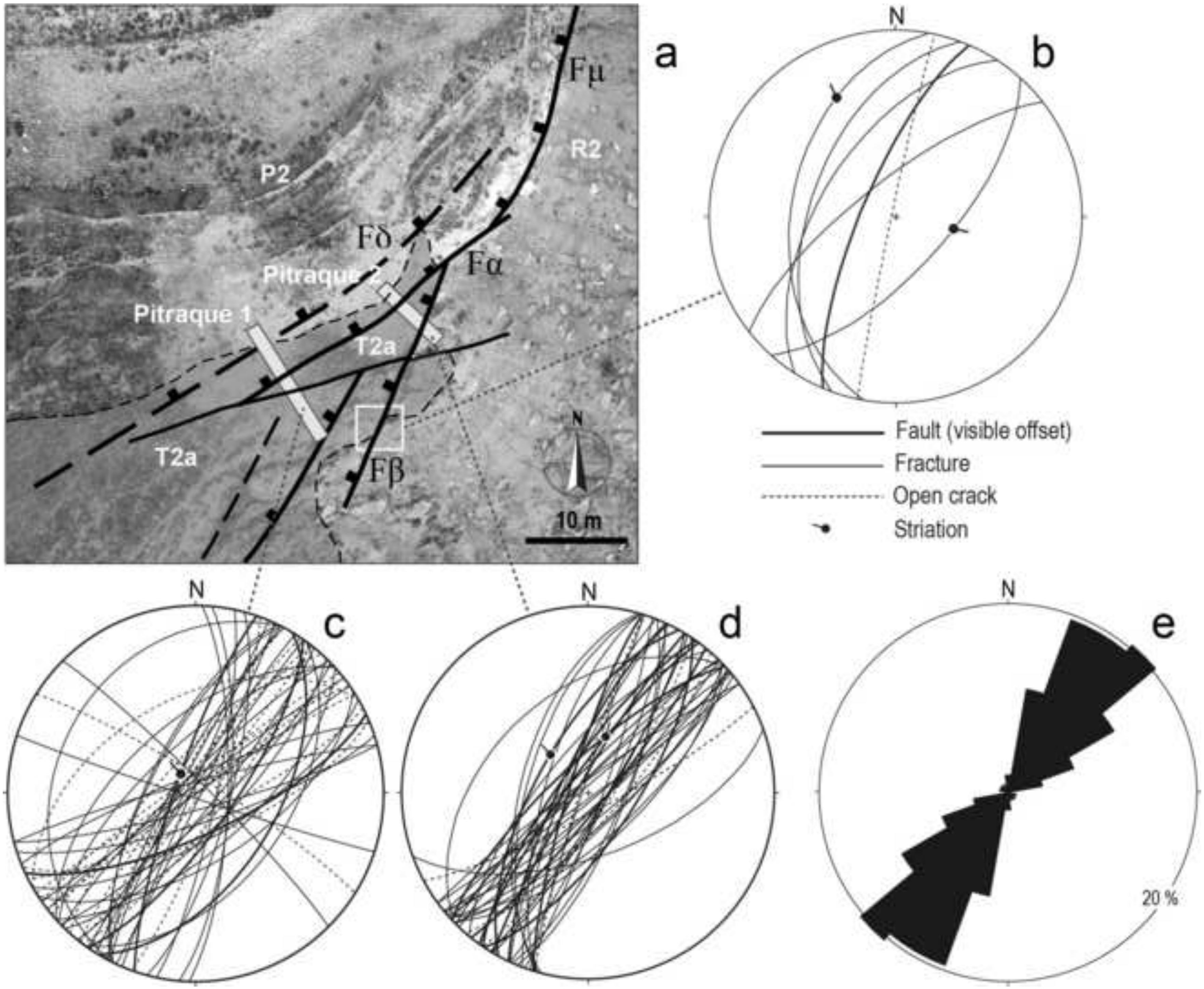

Figure
Click here to download high resolution image

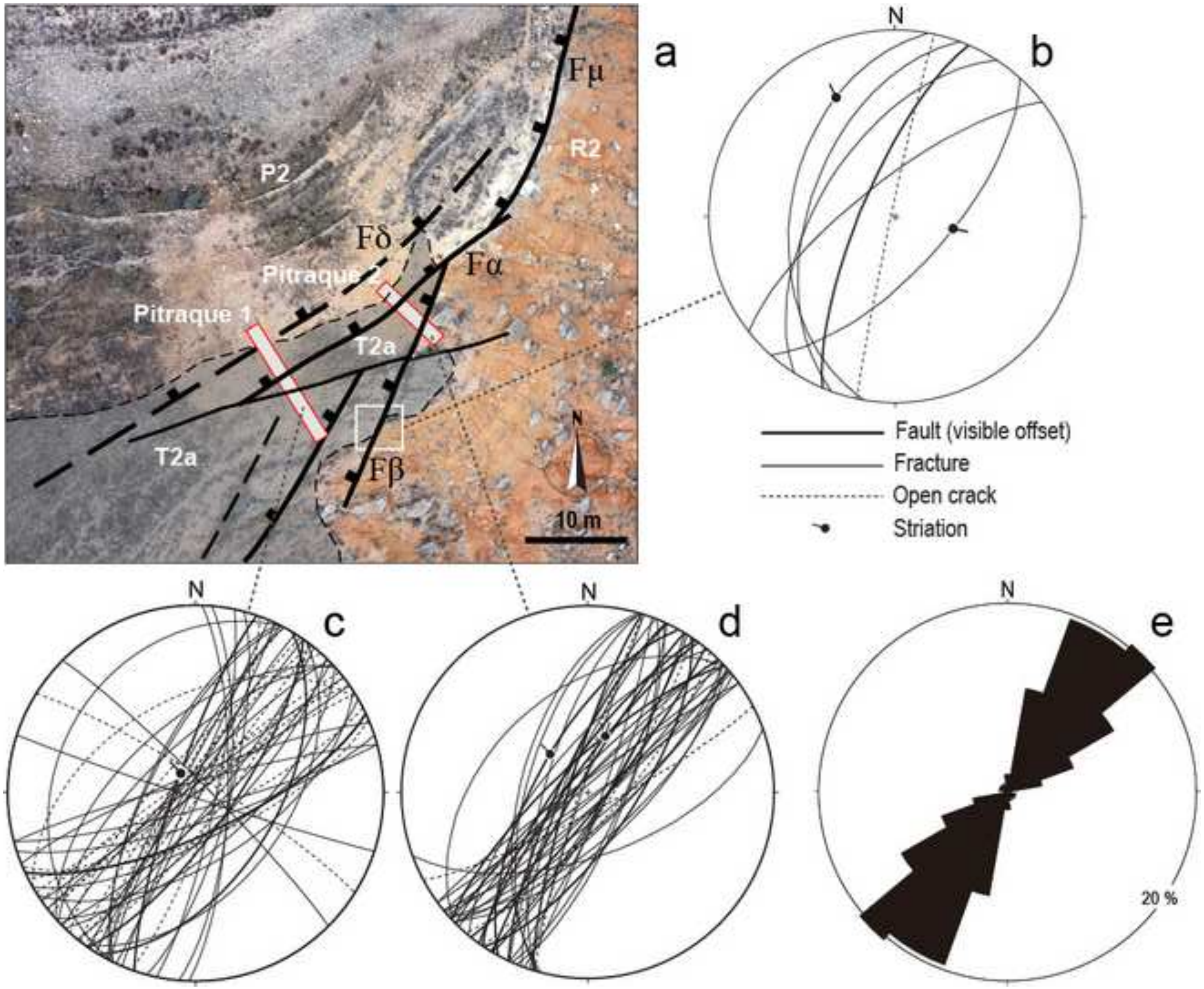

Figure
Click here to download high resolution image

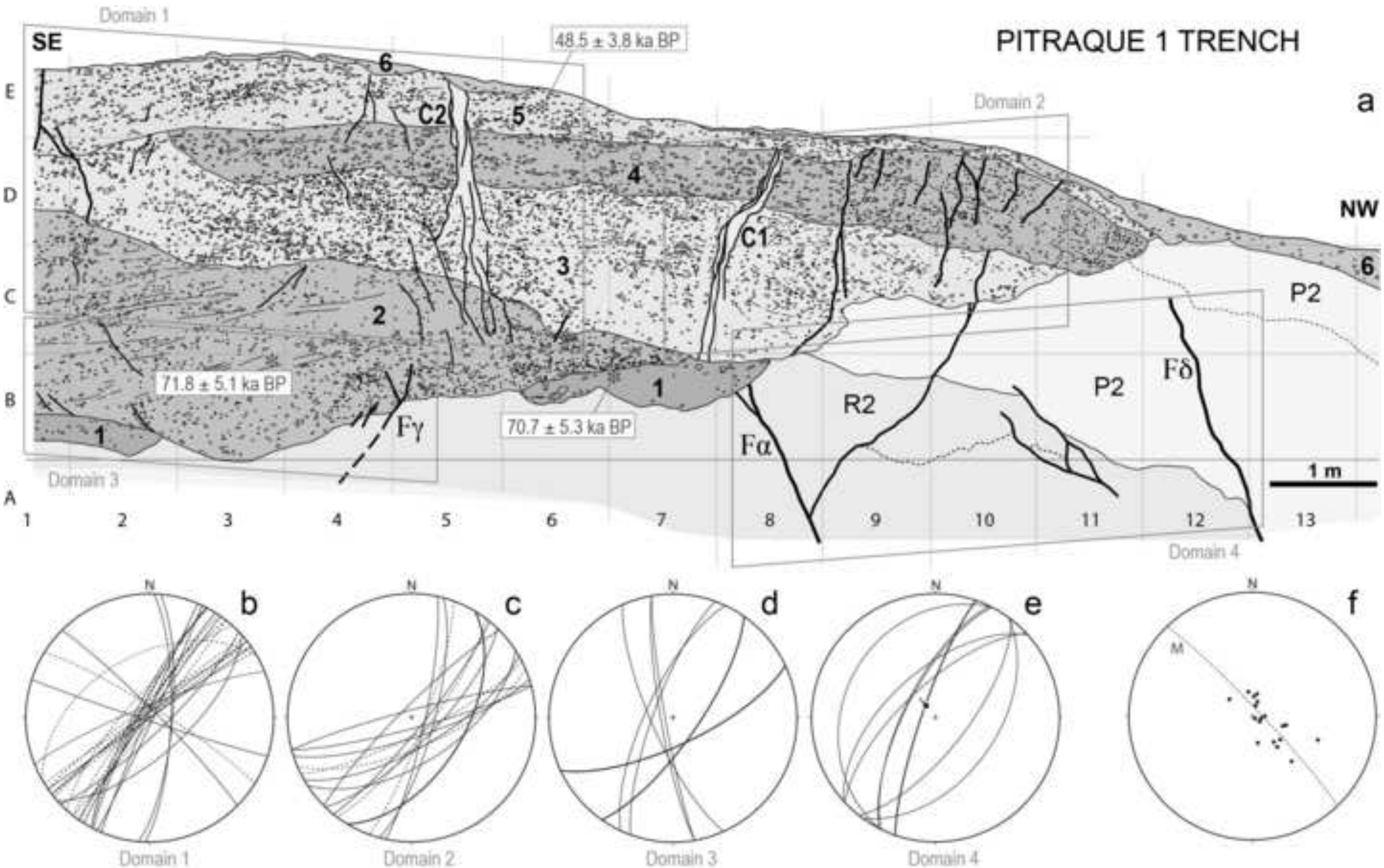

Figure
Click here to download high resolution image

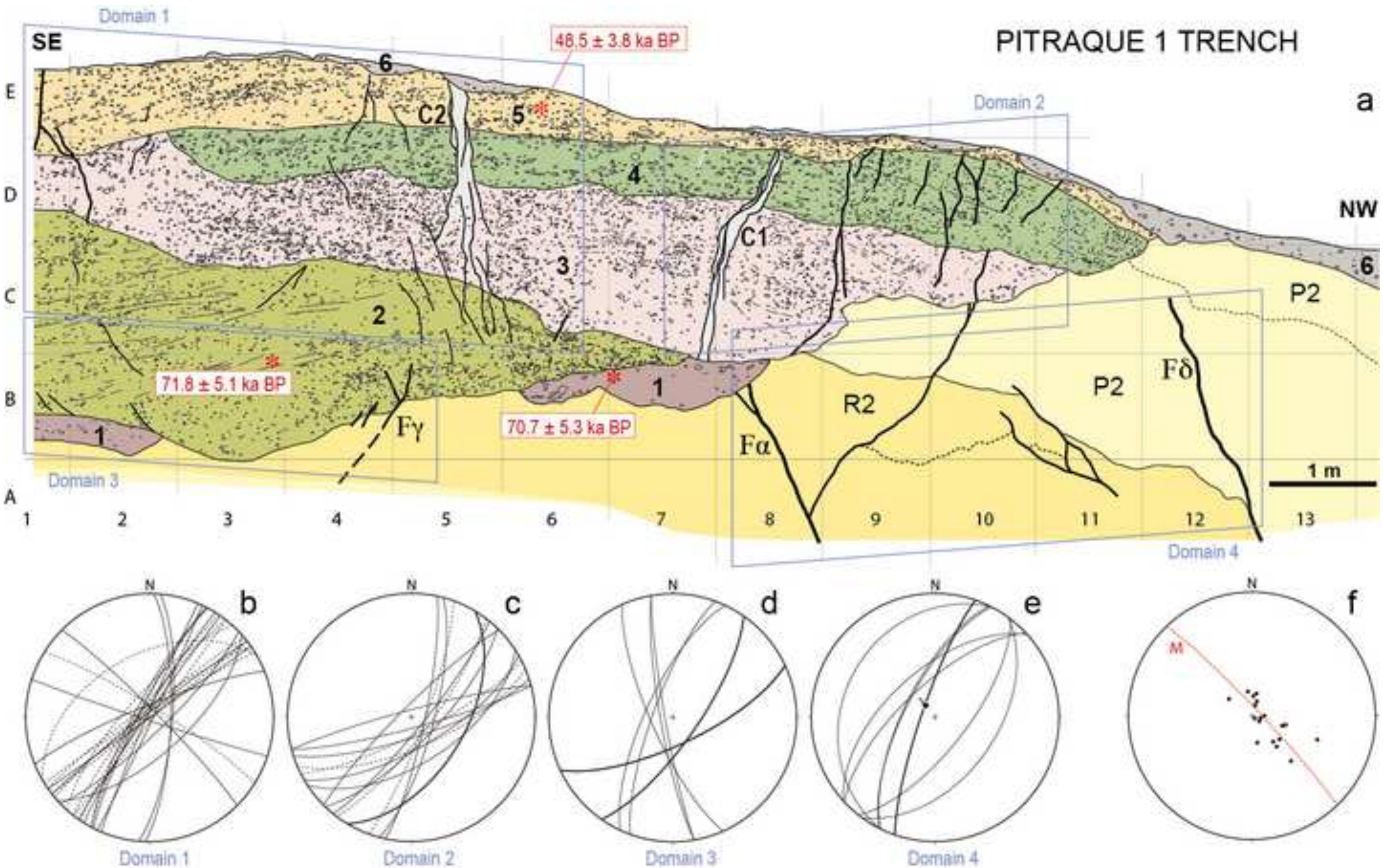

Figure
Click here to download high resolution image

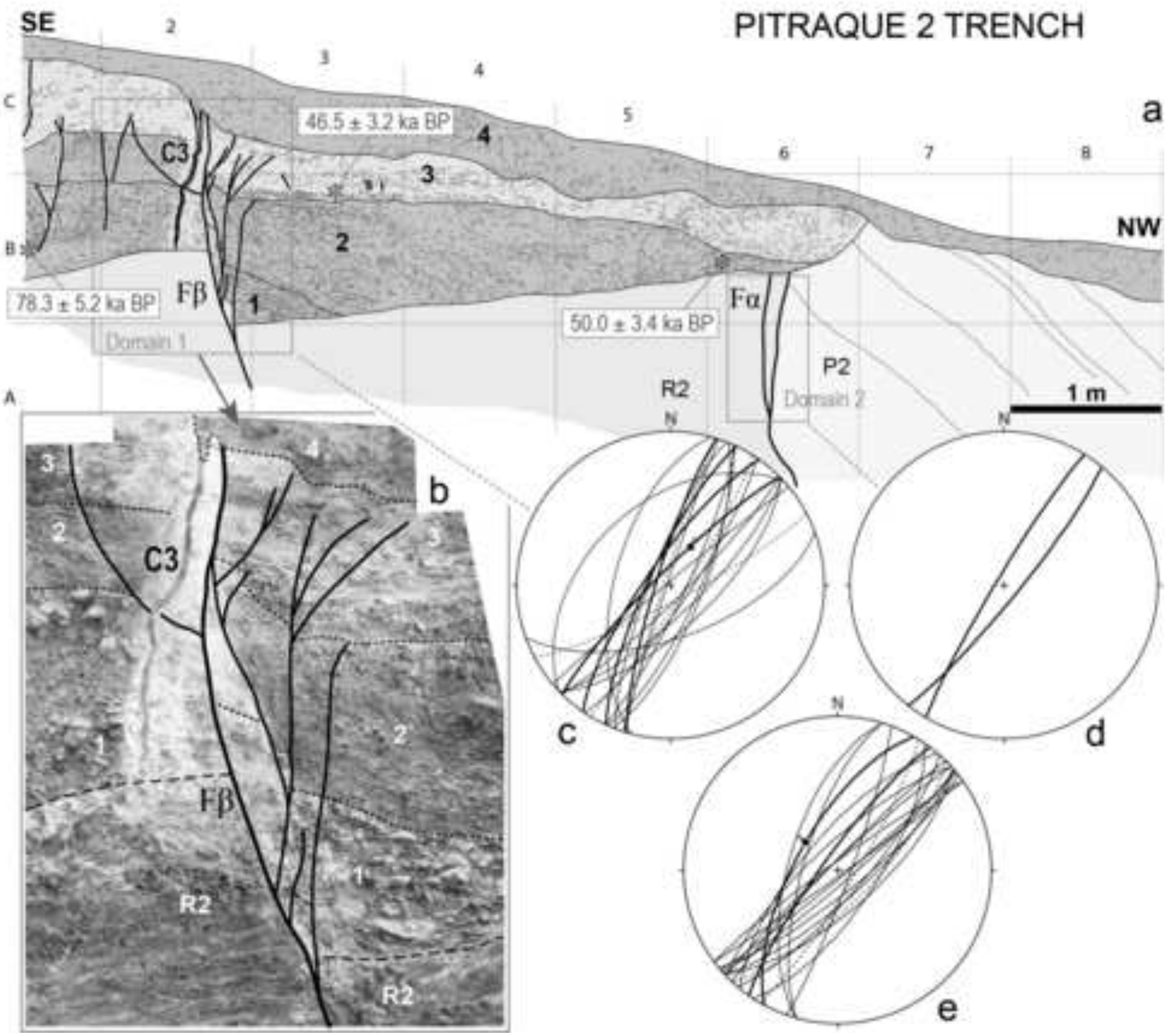

Figure
Click here to download high resolution image

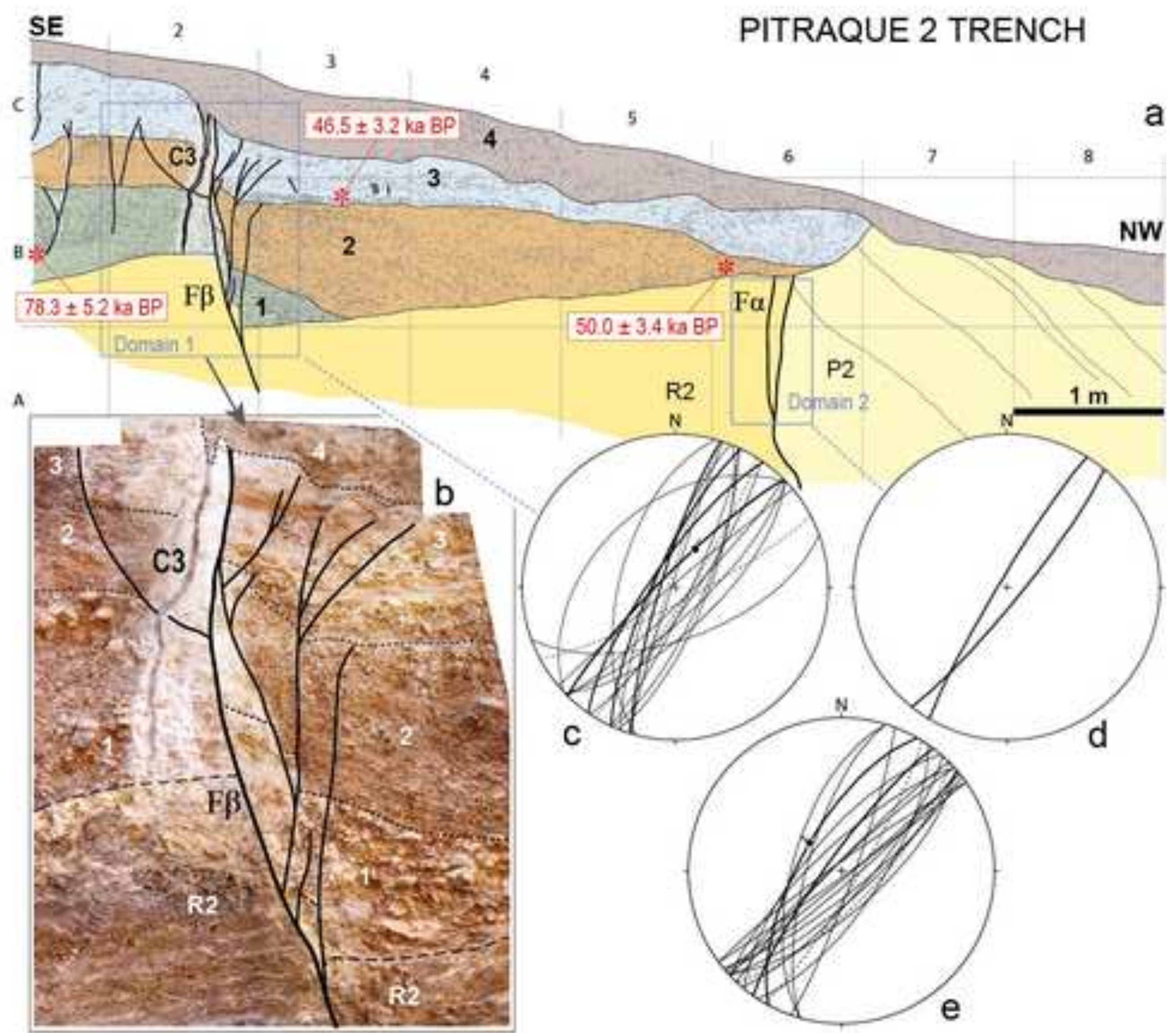

Figure
Click here to download high resolution image

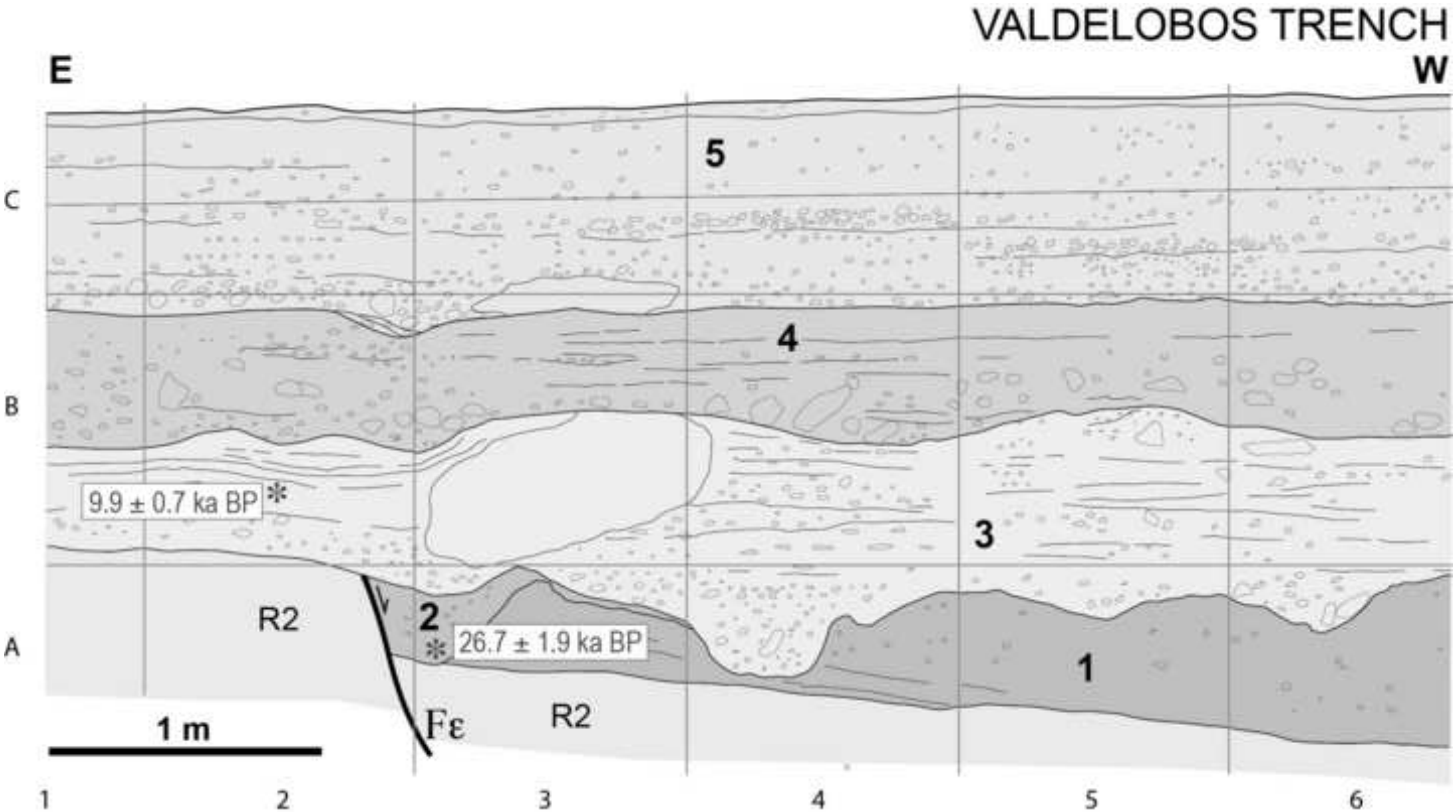

Figure
Click here to download high resolution image

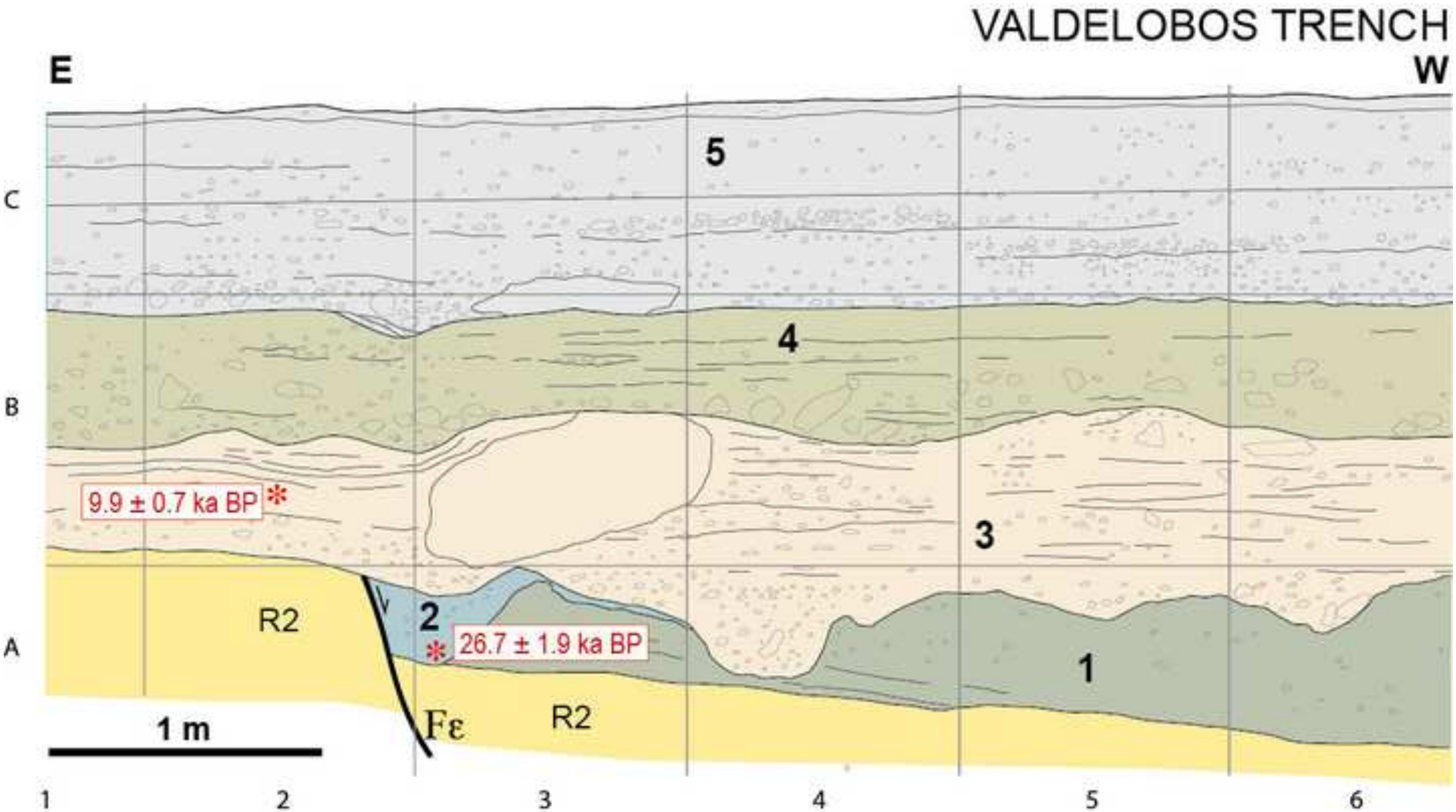

Figure

Click here to download high resolution image

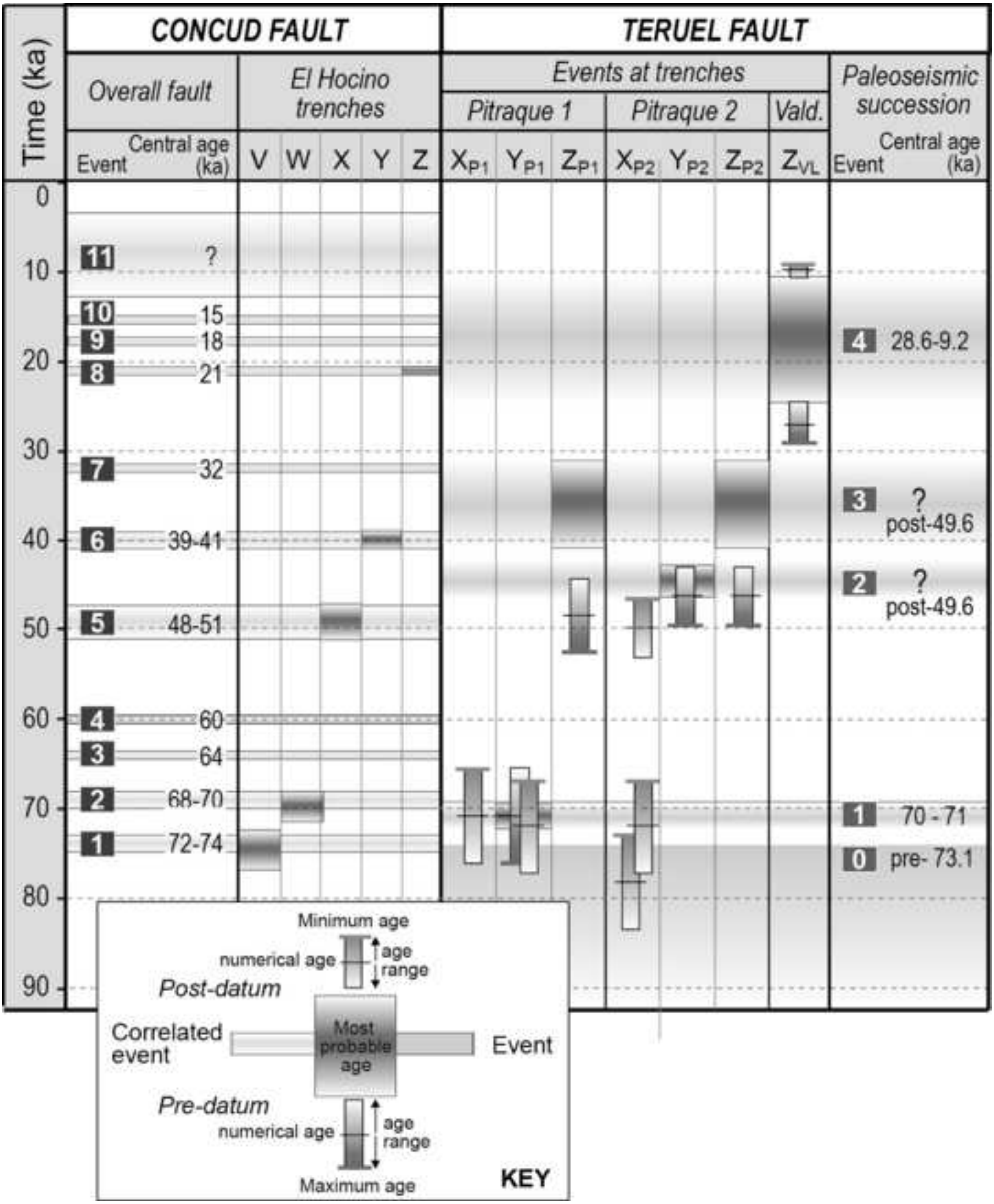

Figure

Click here to download high resolution image

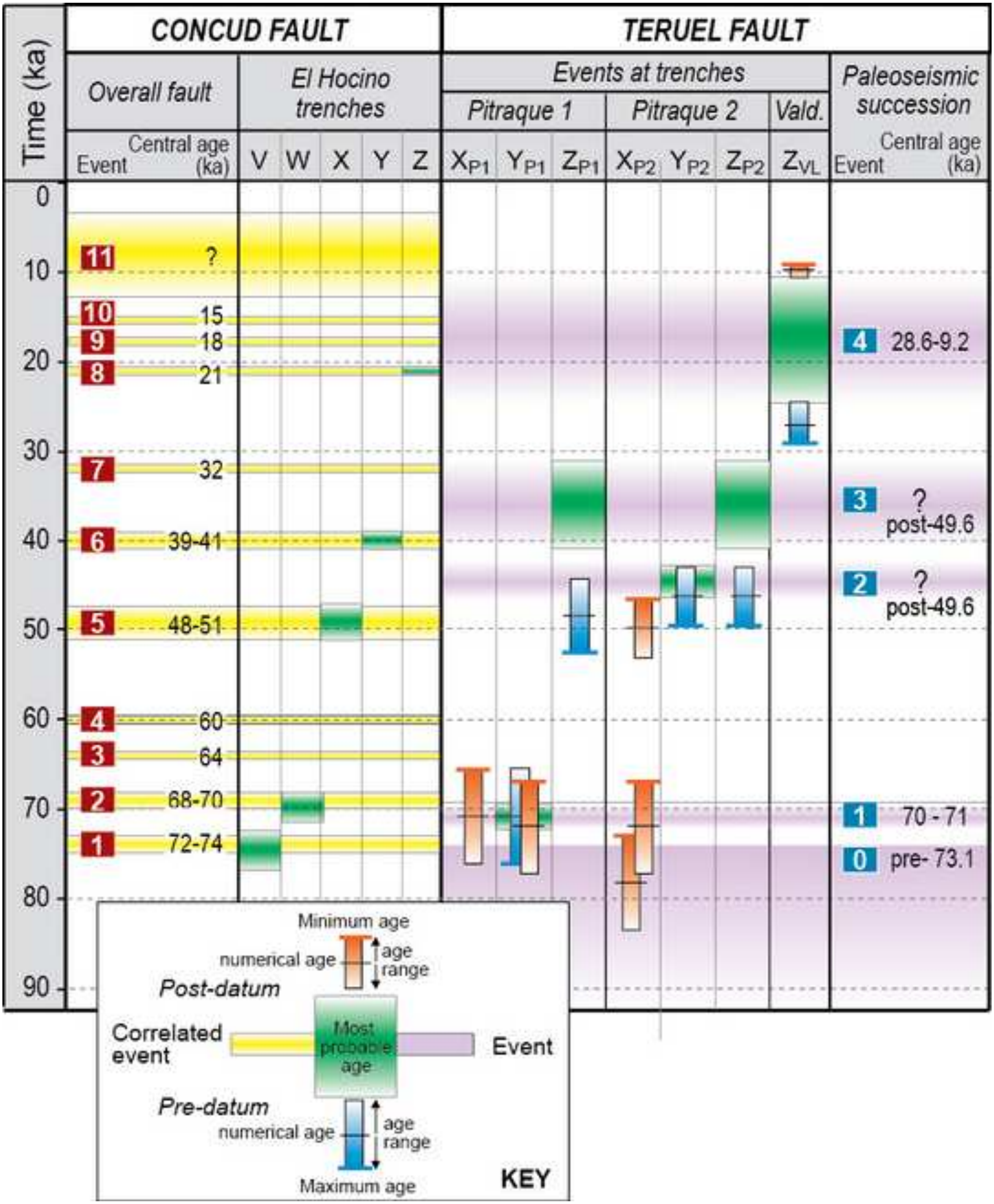

Figure

Click here to download high resolution image

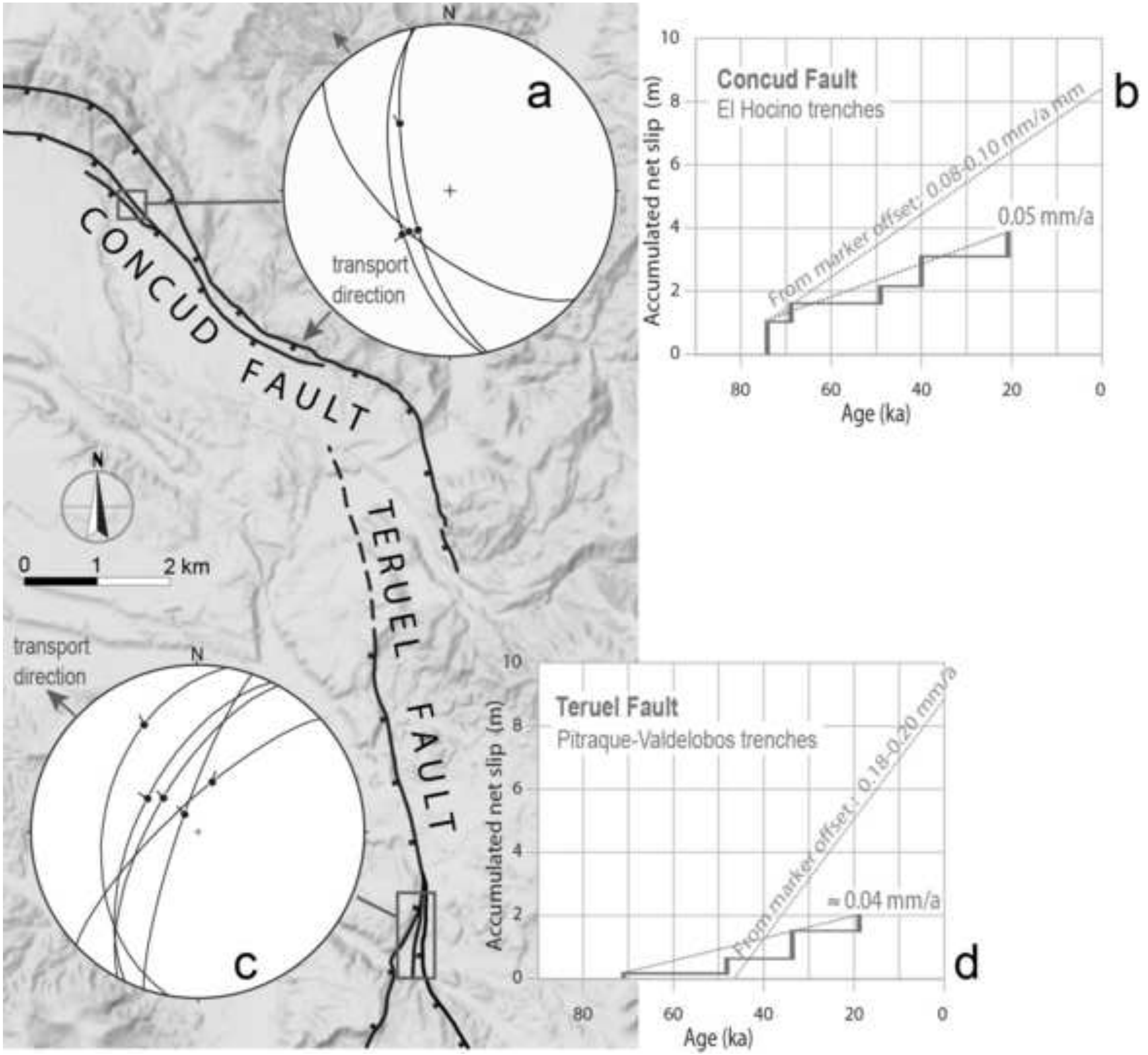

Figure

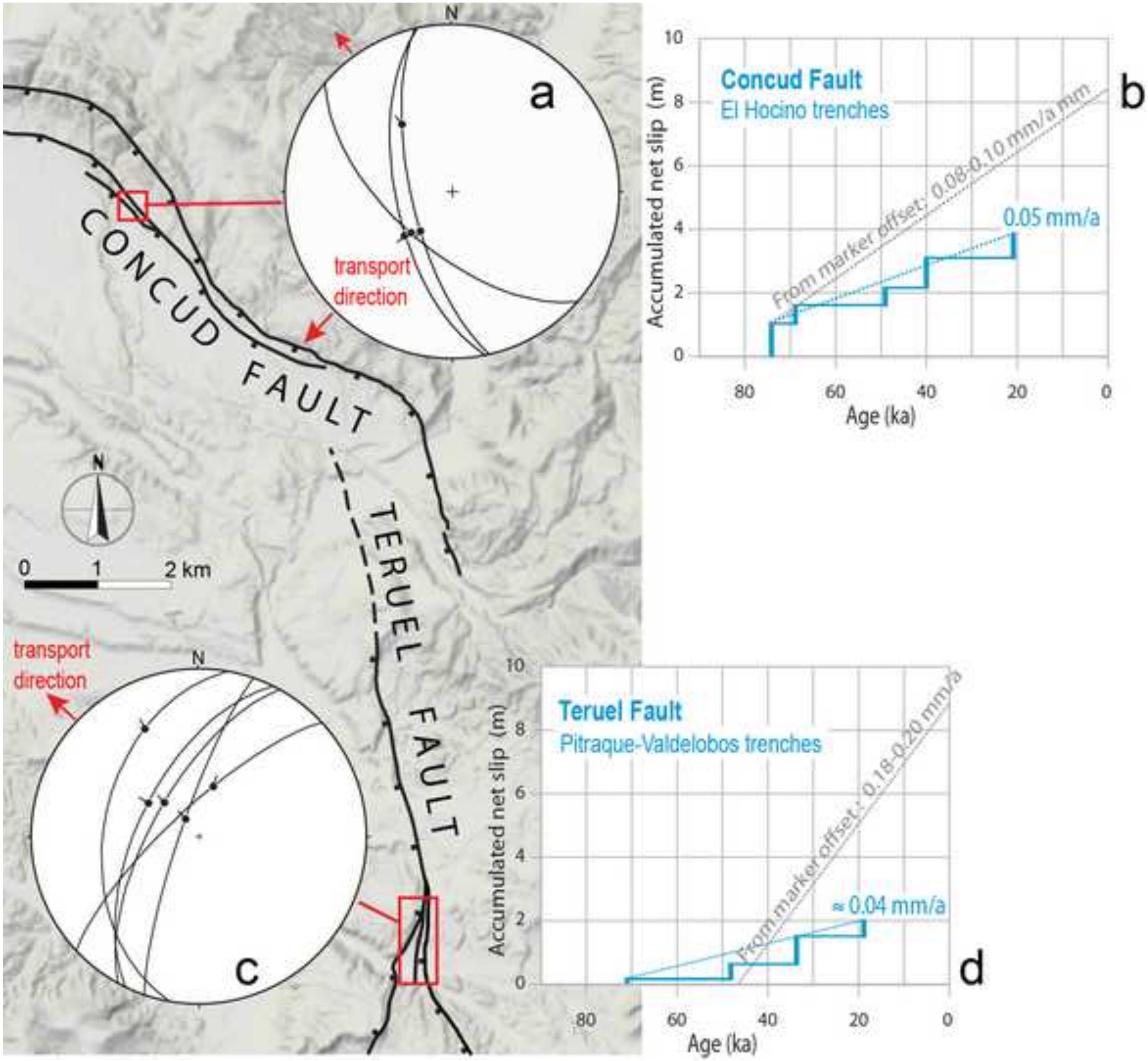
a
transport direction
CONCUD FAULT
TERUEL FAULT
N
0 1 2 km
transport direction
c
b
Concud Fault
El Hocino trenches
From marker offset: 0.08-0.10 mm/a mm
0.05 mm/a
Accumulated net slip (m)
Age (ka)
d
Teruel Fault
Pitraque-Valdelobos trenches
From marker offset: 0.18-0.20 mm/a
≈ 0.04 mm/a
Accumulated net slip (m)
Age (ka)

Figure
Click here to download high resolution image

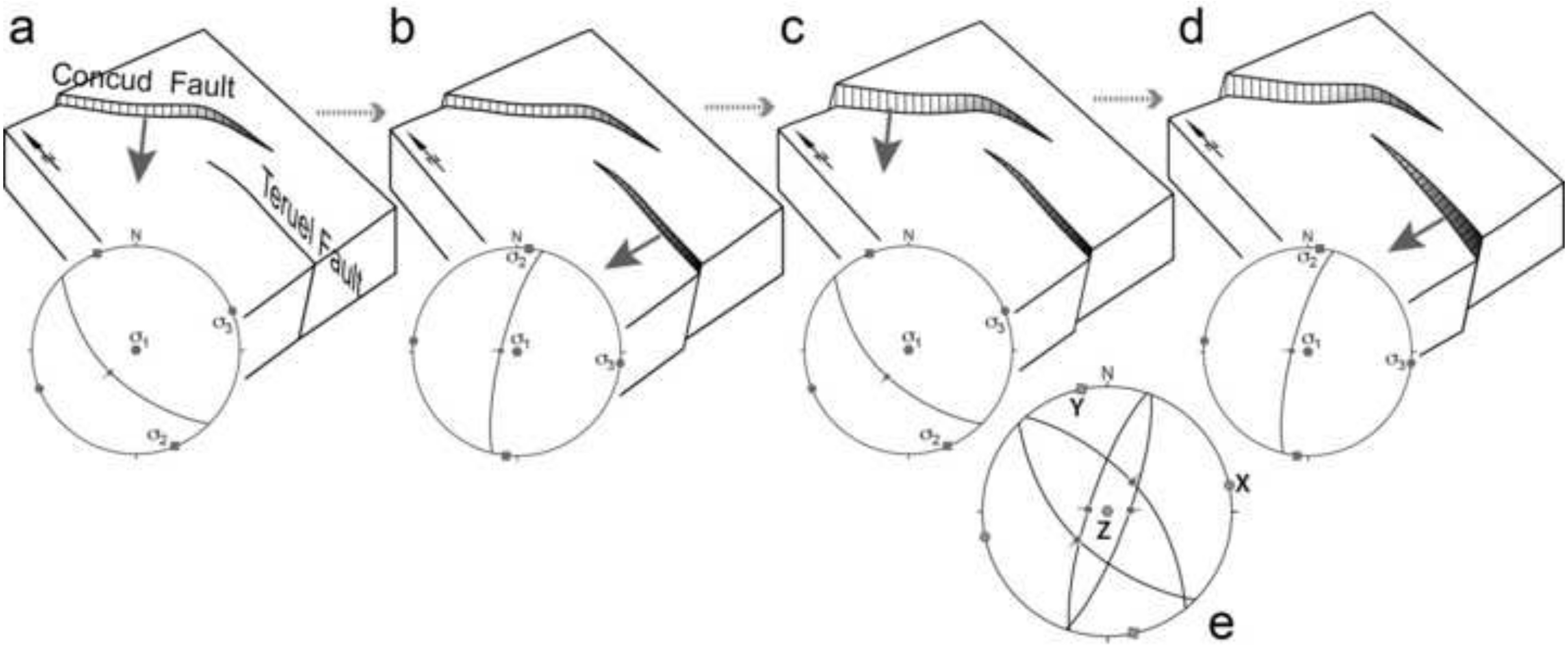

Figure

Click here to download high resolution image

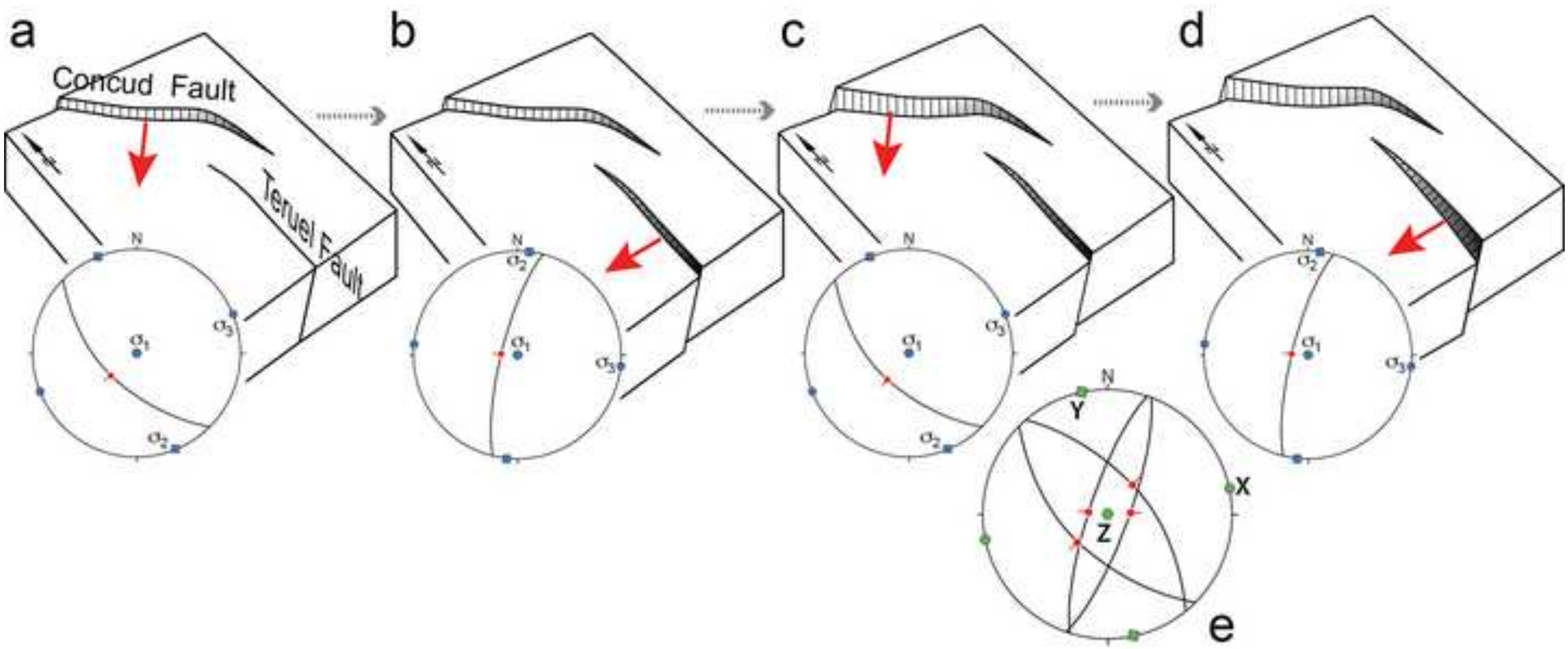

Table

Level	Age	Sublevel	Height above talweg (m)	Numerical age	Dating method	References
Upper	Early Pleistocene (?)	T3	85-90	Unknown		
Middel	Middle Pleistocene	T2b	45-65	250 (± 32) to 116 (± 4) ka	U/Th	Arlegui et al. (2005); Gutiérrez et al. (2008)
		T2a	40-45	90.5 (± 5.3) to 76.0 (± 5.0) ka	OSL	Lafuente et al. (2008); Simón et al. (2012)
Lower	Late Pleistocene	T1c	20-30	22.0 (± 1.6) ka	OSL	Lafuente (2011)
		T1b	15-20	14.9 (± 1.0) to 15.6 (± 1.3) ka	OSL	Lafuente et al. (2008); Gutiérrez et al. (2008)
		T1a	10-15	Unknown		
Subactual	Holocene	T0	3-5	3.4 (± 0.7) ka	OSL	Lafuente (2011)

Table 1. Levels of fluvial terraces defined in the Teruel area (Alfambra and Turia rivers).

Table

Scenario Paleoseismic parameters		**Wells & Coppersmith (1994)**	**Stirling *et al.* (2002)**	**Pavlides & Caputo (2004) (*) (**)**	**Mohammadioun & Serva (2001) (*) (***)**	
Length of 9 km					100 bar	30 bar
Moment magnitude (M_w)		6.12	6.64	6.35	6.26	5.73
Coseismic slip (m)	Vertical	-	-	0.55	-	-
	Net	0.37	1.28	0.59	-	-
Length of 11 km						
Moment magnitude (M_w)		6.23	6.71	6.41	6.39	5.87
Coseismic slip (m)	Vertical	-	-	0.60	-	-
	Net	0.40	1.32	0.65	-	-
Length of 23 km (linked Concud and Teruel faults)						
Moment magnitude (M_w)		6.66	6.96	6.62	6.88	6.36
Coseismic slip (m)	Vertical	-	-	0.66	-	-
	Net	1.19	2.43	0.71	-	-

Table 1. Moment magnitude and vertical and net coseismic slip for the Teruel Fault estimated from empirical relationships for three different scenarios (fault length of 9, 11 and 23 km). (*) Obtained M_s values have been transformed to M_w by applying the relationship of Konstantinou et al. (2005): $M_w = 0.76\ M_s + 1.53$. (**) Vertical displacement initially yielded by this correlation has been translated into net displacement considering an average dip of 68º and a pure normal movement of the Teruel Fault. (***) Moment magnitudes according to Mohammadioun and Serva (2001) have been calculated for stress drop scenarios of 100 and 30 bar.

Table

Sample	Laboratory reference	Lithological unit	Equivalent dose (Gy)	Annual dose (mGy/yr)	Supralinearity (Gy)	K factor	OSL age (ka B.P.)
Trench: Pitraque 1							
P1-4	MAD-6076SDA	Fluvial terrace (Unit 1)	170.46	2.41	0	0.19	70.730 ± 5.259
P1-5	MAD-6077SDA	Fluvial terrace (Unit 2)	124.93	1.74	0	0.12	71.798 ± 5.059
P1-6	MAD-6078BIN	Fluvial terrace (Unit 5)	77.57	1.60	0	0.11	48.481 ± 3.801
Trench: Pitraque 2							
P2-1	MAD-6079SDA	Fluvial terrace (Unit 1)	130.05	1.66	0	0.14	78.343 ± 5.189
P2-7	MAD-6081BIN	Fluvial terrace (Unit 2)	91.95	1.84	0	0.11	49.972 ± 3.365
P2-5	MAD-6080SDA	Fluvial terrace (Unit 3)	127.80	2.75	0	0.14	46.472 ± 3.147
Trench: Valdelobos							
VL-C1	MAD-6073SDA	Fluvial terrace (Unit 2)	112.82	4.23	0	0.16	26.671 ± 1.912
VL-B2	MAD-6074SDA	Fluvial terrace (Unit 3)	16.97	1.71	0	0.23	9.923 ± 0.690

Table 3. OSL dating of samples collected from trenches at the Teruel fault.

Table

Teruel Fault event (renamed)	Original event at individual trench	Predating OSL age (ka B.P.)	Postdating OSL age (ka B.P.)	Absolute age constraints (ka)	Coseismic net slip (m)
Event 0	X_{P1} X_{P2}		70.7 ± 5.3 78.3 ± 5.2	Pre-73.1	?
Event 1	Y_{P1}	70.7 ± 5.3	71.8 ± 5.1	76.0 – 66.7	0.1
Event 2	Y_{P2}	46.5 ± 3.1		Post-49.6	0.5
Event 3	Z_{P1} Z_{P2}	48.5 ± 3.8 46.5 ± 3.1		Post-49.6	> 1.1
Event 4	Z_{VL}	26.7 ± 1.9	9.9 ± 0.7	28.6 – 9.2	> 0.3

Table 4. Summary of paleoseismic events of the Teruel Fault interpreted and correlated from the studied trenches: Pitraque 1 (P1), Pitraque 2 (P2) and Valdelobos (VL). Absolute age constraints take into account the error bar for each OSL age.

Table

Marker / data source	Age / time window	**Teruel Fault** (this work)			**Concud Fault (*)**		
		Net slip (m)	**Slip rate (mm/a)**		**Net slip (m) (**)**	**Slip rate (mm/a)**	
			Overall	**Partial** (In 1-2 branches among 4-5)		**Overall**	**Partial** (In 1 branches among 2-3)
Trenching information							
Compilation of coseismic slip values	since 76.0 to 9.9 ka BP	1.7 - 2.0		0.03 – 0.05			
	since ca. 74 to 3.4 ka BP				20.5 (3.9)	0.29	0.05
Stratigraphic marker							
T2b terrace top	46.5 ± 3.2 ka	8.8		0.18 – 0.20			
T2a terrace top	282 – 112 ka				39	0.14 – 0.35	
Páramo 2 unit (Latest Ruscinian)	3.6 Ma	270	0.075		255 – 290	0.07 – 0.08	

Table 5. Summary of slip rates calculated for the Teruel and Concud faults from different markers and for different time windows. (*) Data for the Concud Fault are compiled from Gutiérrez et al. (2008), Lafuente (2011), Lafuente et al. (2011a, 2014), and Simón et al. (2016). (**) In parentheses, partial net displacement measured on one fault branch.